Development and Modelling of a High-Resolution Aquifer Analog in the Guarani Aquifer (Brazil)

Dissertation

der Mathematisch-Naturwissenschaftlichen Fakultät

der Eberhard Karls Universität Tübingen

zur Erlangung des Grades eines

Doktors der Naturwissenschaften

(Dr. rer. nat.)

vorgelegt von

Dominik Höyng

Bonn

Tübingen

2014

Tag der mündlichen Qualifikation:	21.07.2014
Dekan:	Prof. Dr. Wolfgang Rosenstiel
1. Berichterstatter:	Prof. Dr. Peter Grathwohl
2. Berichterstatter:	Prof. Dr. Holger Weiß

Table of Contents

Abstract

A comprehensive and detailed knowledge about the spatial distribution of physical and chemical properties in heterogeneous porous aquifers plays a decisive role for a realistic representation of governing parameters in mathematical models. Models allow the simulation, prediction and reproduction of subsurface flow and transport characteristics.

This work explains the identification, characterization and effects of small-scale aquifer heterogeneities in the Guarani Aquifer System (GAS) in São Paulo State (Brazil) and elaborates on the fate and transport of a hypothetical petroleum hydrocarbon contamination in the GAS. The GAS represents one of the biggest aquifers in the world and is the most relevant groundwater resource in South America. The leading questions behind this thesis are: (1) What is the hydraulic response characteristic for the sedimentary architecture of the Pirambóia Formation in the Guarani aquifer recharge area in São Paulo State (Brazil)? (2) How do the heterogeneously distributed Fe(III) oxides as solid state electron acceptors effect the natural attenuation potential in this hydrostratigraphic unit? (3) How well is Compound Specific Isotope Analysis (CSIA) suited for assessing the occurrence and extent of intrinsic biodegradation of contaminants in heterogeneous porous aquifers? In order to properly address these three lead questions, field and laboratory work as well as a series of reactive transport simulations have been performed. In an outcrop study the sedimentary heterogeneities in the upper part of the Pirambóia Formation have been investigated in regard to the distribution of lithofacies as well as determination of hydraulic properties and sedimentary Fe(III) content. The three-dimensional distribution of the local litho- and hydrofacies is described and presented in an aquifer analog model. The model depicts the variations of hydraulic conductivity (K), porosity (n), and sediment-bound ferric iron content resolved on the centimeter scale. The two-dimensional (2D) fields of hydraulic and chemical properties were transferred into a numerical model to study the effects of small-scale

heterogeneities on the flow and reactive transport of an oxidizable organic contaminant. Additional analog models have been applied in a numerical experiment to study the evolution of carbon isotope signatures during reactive transport of hydrocarbons in heterogeneous porous aquifers. Hereby, the performance of CSIA to quantify intrinsic biodegradation has been assessed.

The research project resulted in three main outcomes: (1) A quantitative description of the spatial distribution of hydraulic and chemical parameters in the Pirambóia Formation of the GAS and construction of an aquifer analog model; the identification of the most permeable units and determination of a higher mean K value than previously reported for this hydrostratigraphic unit. (2) The solid-phase ferric iron concentrations and hydraulic conductivity inversely correlate and consequently limit the natural attenuation potential at the investigated site. (3) The effects of small-scale physical aquifer heterogeneities strongly influence the degree of dilution/dispersion, which is highly site-specific and undergoes significant spatiotemporal variations. The findings indicate that if the degree of dilution/dispersion is not accurately accounted for - a difficult task at contaminated sites - correct quantification of CSIA based *in situ* biodegradation in heterogeneous porous aquifers remains hardly possible.

Kurzfassung

Ein umfassendes und detailliertes Verständnis über die räumliche Verteilung der physikalischen und chemischen Eigenschaften in heterogenen porösen Grundwasserleitern spielt eine entscheidende Rolle für eine realistische Darstellung der wichtigsten Parameter in mathematischen Modellen. Modelle ermöglichen die Simulation, Vorhersage und Wiedergabe von Strömungs- und Transportprozessen im Untergrund.

Diese Arbeit behandelt die Identifizierung, Charakterisierung und Auswirkungen von kleinskaligen Aquiferheterogenitäten im Guarani Aquifer System (GAS) im Bundesstaat São Paulo (Brasilien) und erläutert das Verhalten und den Verbleib einer hypothetischen Grundwasserverunreinigung durch Kohlenwasserstoffe im GAS. Der Guarani Aquifer ist eines der weltweit größten Grundwassersysteme und die wichtigste Grundwasserressource in Südamerika. Die Hauptfragestellungen dieser Arbeit sind: (1) Was sind die hydrogeologischen Eigenschaften der sedimentären Einheiten der Pirambóia Formation in Gebieten der Grundwasserneubildung im Bundesstaat São Paulo (Brasilien)? Wie beeinflusst die heterogene Verteilung von Eisen(III) als Festphasenelektronenakzeptor das natürliche Abbau- und Rückhaltepotential in dieser hydrostratigraphischen Einheit? (3) Wie geeignet ist die substanzspezifische Isotopenanalyse zur Bewertung des Auftretens und Bestimmung des Ausmaßes von mikrobiellem Abbau von Schadstoffen in heterogenen porösen Grundwasserleitern? Zur Beantwortung dieser drei Leitfragen wurden umfangreiche Feld- und Laborarbeiten sowie eine Reihe von numerischen reaktiven Transportsimulationen durchgeführt. In einer Feldstudie wurden an Aufschlusswänden die sedimentären Heterogenitätsmuster der oberen Pirambóia Formation hinsichtlich der Verteilung der Lithofaziestypen, deren hydraulischen Eigenschaften und sedimentäre Eisen(III)-Gehalte untersucht. Die dreidimensionale Verteilung der lokalen Litho- und Hydrofazies wird in einem Aquifer Analogmodell dargestellt. Das Model beschreibt die zentimeterskaligen

Variationen der hydraulischen Leitfähigkeiten (*K*), Porositäten (*n*) und sedimentären Eisen(III)-Gehalte. Digitalisierte Zeichnungen der zweidimensionalen (2D) Verteilung der hydraulischen und chemischen Eigenschaften wurden in ein numerisches Modell übersetzt. In Strömungs- und reaktiven Transportsimulationen wird die Auswirkung von kleinskaligen Aquiferheterogeneitäten auf Fliess- und Transportprozesse eines gelösten oxidierbaren organischen Schadstoffs untersucht. Desweiten wurden zusätzliche Analogmodelle in einem numerischen Experiment verwendet, um die Entwicklung von Kohlenstoffisotopensignaturen während des reaktiven Transports von Kohlenwasserstoffen in heterogen porösen Aquiferen zu untersuchen. Dabei wurde die Anwendbarkeit von substanzspezfischer Isotopenanalyse zur Beurteilung und Quantifizierung von biologischem Schadstoffabbau in heterogenen porösen Aquiferen beurteilt. Die Hauptergebnisse dieser Arbeit sind: (1) Eine quantitative und qualitative Beschreibung der räumlichen Verteilung der hydraulischen und chemischen Parameter der Pirambóia Formation im Guarani Aquifer und die Konstruktion eines Analogmodells; die Identifizierung der höchst permeablen Ablagerungselementen und die Bestimmung eines höheren gemittelten *K* Wertes als in vorhergehenden Studien für diese hydrostratigraphische Einheit. (2) Eisen(III) Festphasenelektronenakzeptoren korrelieren invers mit der hydraulischen Leitfähigkeit und begrenzen demnach das natürliche Abbau- und Rückhaltepotential am untersuchten Standort. (3) Kleinskalige physikalische Aquiferheterogenitäten beeinflussen stark das Ausmaß der Durchmischung und Verdünnung, welches stark standortspezifisch ist und erheblichen räumlichen und zeitlichen Variationen unterliegt. Die Ergebnisse zeigen, dass ohne eine genaue Bestimmung des Ausmaßes der Verdünnung – welches eine schwierige Aufgabe an kontaminierten Standorten ist – eine Quantifizierung von biologischem Schadstoffabbau auf der Basis substanzspezifischer Isotopenanalyse in heterogenen porösen Aquiferen kaum optimal möglich ist.

1 Introduction

1.1 Background and Motivation

Water is the most fundamental and indispensable resource for all forms of life. More specifically, groundwater is the primary source of drinking water for the vast majority of people on our planet (UN, 2009). Until the middle of the 20th century it was common sense, to value groundwater as a ubiquitous and lasting resource of high quality. However, within the past decades the scale and intensity of groundwater consumption and exploitation has rapidly increased driven by a global population and economic growth with the consequence of a surge for both, urbanization and industrialization (Puri et al., 2001). As a result, the continuing demand for fresh water has adversely impacted groundwater reservoirs and already led to water scarcity on a local, regional and even global scale. The processes that lead to aquifer degradation and groundwater deterioration are multifaceted and occur on different scales, such as over-abstraction, salinization, anthropogenic pollution associated with industrial point and diffusive sources as well as through extensive agricultural activities. Additionally, unreasonableness in groundwater quality management in "developed countries" often exacerbates the aforementioned concerns for an adequate quality water supply (Ronen et al., 2012). As a consequence, the increased stress on groundwater reservoirs as a protectable finite resource has negatively impacted social, economic and environmental systems that depend on groundwater (e.g., Puri et al., 2001). Making matters worse, due to the competition for adequate groundwater supply, it has become a strategic resource invoking political pressures and influencing geo-political decisions and realignments (e.g., Wolf, 2007). The pollution of groundwater often subsists for years, decades or even centuries attributed to the slow flow velocities in the subsurface environment and the persistence of many chemical substances. In contrast to surface water bodies, groundwater resides in the subsurface, and thus, makes it more difficult to access, characterize and control aquifer contamination.

Groundwater is often hosted in sedimentary aquifers, which are for instance in Central Europe among the most important aquifers (Bayer et al., 2011). Sedimentary aquifers are built up by non-uniform sequences of layers and are characterized by a wide variety of sedimentary heterogeneities that determine the hydraulic and geochemical properties (e.g., Bayer et al., 2011; Huggenberger and Aigner, 1999). The highly heterogeneous character and complexity of geological porous media and its variability of physical and chemical properties in space and time profoundly effects the transport and fate of groundwater contaminants (Dentz et al., 2011). Therefore, a detailed characterization of the subsurface structure and parameterization of its heterogeneously distributed properties is essential to understand and predict flow, transport and transformation processes. This type of analysis in turn becomes a measure of any successful groundwater remediation and risk assessment.

Tremendous efforts have been dedicated and various techniques employed to characterize subsurface reservoirs in order to resolve spatial parameter distribution on different scales. However, aquifer characterization is commonly based on sparse point data (well logs) not only because of cost reasons but also due to limited resolution of the most common reflection seismic tools, which are only suitable at a basin scale (Bersezio, 2007). Considering the limited spatial extent of data from boreholes and the resolution/detection constraints of seismic data, the reconstruction and interpretation of subsurface reservoirs can be greatly assisted by the study of analogous geological formations in surface outcrops. Such outcrops can provide an exact insight into natural heterogeneity at various scales and outcrops models are invaluable for establishing high-resolution subsurface models (Grammer et al., 2004). Analog studies were first established in the field of hydrocarbon exploration which realizes the concept of accompanying and improving reservoir characterization by detailed investigation of exposed corresponding or analogous geological formations of buried formations (Bersezio, 2007). In order to predict reservoir quality and its architecture it is essential to understand the

facies and their distribution since geology is a first order control on petrophysics (Pringle et al., 2006). Reservoir properties are a critical factor affecting hydrocarbon production and therefore the integration of a maximum amount of information on the subsurface including the utilization of outcrop analog studies are required to reduce reservoir uncertainties, mitigate interpretation ambiguities and optimize production.

Similar principles apply to groundwater reservoirs (Huggenberger and Aigner, 1999). The upsurge in pollution and degradation of aquifers has simultaneously increased the demand for evaluation and remediation of contaminated sites in combination with assessing the risk of waste disposals. As a consequence, the necessary analyses has shifted from the discipline of petroleum geology to hydrogeology (e.g., Bersezio, 2007; Huggenberger and Aigner, 1999). For more than two decades the investigation of surface outcrops, which give insight into geological formations that host groundwater at other locations, has played a vital role to capture and record the large spectrum of complex aquifer heterogeneities affecting hydraulic properties. As a result, the analysis of surface outcrops provided rich datasets for the development and construction of aquifer analog models (e.g., Anderson et al., 1999; Bayer et al., 2011; Bersezio et al., 1999; Bersezio et al., 2004; Felletti et al., 2006; Heinz et al., 2003; Hornung and Aigner, 1999; Kessler et al., 2013; Weissmann et al., 1999; Whittaker and Teutsch, 1999; Zappa et al., 2006).

Outcrops significantly support aquifer characterization on different scales, but they are in particular beneficial for identifying and resolving hydraulic features relevant for the migration and spreading of contaminants that are on sub-seismic scale, such as cm-dm scale sedimentary heterogeneities or fracture characteristics. In fact, the utilization of the aquifer analog concept turned out to be most applicable on the local scale (Bersezio, 2007). The recognition, mapping and modelling of facies and depositional elements identifies the volume and connectivity of the most permeable facies which is the most effective element of hetero-

geneity in regard to the transport of contaminants (Bersezio, 2007). Thus, the integration of sedimentary heterogeneities into models greatly improves to forecast preferential groundwater contaminant transport pathways (Huggenberger and Aigner, 1999). The detailed description of the heterogeneity of sedimentary structures from 2D vertical outcrop faces also greatly assist reservoir characterization by offering training images for stochastic methods to develop a volumetric three-dimensional reconstruction of heterogeneity (e.g., Comunian et al., 2011). However, at the scale of depositional systems to basin fills, the geological formations considerably vary dependent on the ancient depositional environment and deformation history. Consequently, hydrogeological parameters and its distribution derived from outcrops on a local scale cannot necessarily be up-scaled or extrapolated to medium or large scale projects (Bersezio, 2007). Still, detailed observations from surface outcrops provide valuable insight into geological structures that may occur in deeper parts of the reservoir. It also allows examining the role of geological structures on contaminant transport to complement generic process understanding and experience from field monitoring.

Mathematical modelling has become an increasingly important and powerful tool in promoting the understanding of a multitude of processes that occur in subsurface systems (Prommer et al., 2003b). Along with the development of high performance computing the numerical modelling capabilities have tremendously improved in the past and allow the integration of detailed and high-resolution field data. Therefore, outcrop-based hydrogeological and hydrochemical information in combination with numerical modelling enables to derive flow and transport characteristics of the subsurface, which is beneficial in a many respects and provides an ideal framework to address and answer both scientific questions and applied hydrogeological issues (e.g., Maier et al., 2005; Maji and Sudicky, 2008; Werth et al., 2006). For instance, aquifer analog models can support sound conceptual model development, assist proper site characterization and treatment of groundwater contamination, and aid risk assess-

ment for point or diffusive sources. Moreover, they can overcome the shortcomings of imprecise subsurface characterization in testing the applicability of remediation design and monitoring techniques for groundwater contaminants.

Aquifer analog studies are of particular interest for groundwater reservoirs, where recharge areas and urbanized/industrialized areas coexist. Aquifer vulnerability to contamination in such cases is extremely high and requires a detailed knowledge on the local reservoir heterogeneity. This is, for instance, the case for the Guarani Aquifer System (GAS) in South America which is essentially a confined or semi-confined aquifer with only 10% outcrop area, where recharge occurs (Rabelo and Wendland, 2009).

This Ph.D. research work focuses on the first application of the aquifer analog model approach in the fluvial-aeolian sediments of the Pirambóia Formation in the GAS in order to characterize the physical and chemical aquifer heterogeneities. The GAS is the world´s largest transboundary groundwater reservoir and beneath the Mercosul countries (Mercosul in Portuguese = *Mercado Comum do Sul - Southern Common Market)* Brazil, Argentina, Paraguay and Uruguay, and covers an area of approximately 1,200,000 km^2. About 70% (839,800 km^2) of the aquifer area is situated on Brazilian territory (OAS, 2009). The GAS is one of the most important Brazilian groundwater reservoirs and, therefore, a strategic resource for future demands (OAS, 2009). A considerable portion of the recharge area of the GAS on the Brazilian side is located in the State of São Paulo, the powerhouse of Brazilians thriving economy. The GAS has not only the capacity to guarantee the clean drinking water supply for about 360 Mio. people, but also provides water for industrial, agricultural and recreational activities (Campos, 2000). Due to intense urban build up and large scale agricultural activities in the State of São Paulo, the use of the GAS has increased dramatically over the past decades in the area (BMBF, 2010). Water conflicts have already occurred by reducing the groundwater levels and interferences among wells (BMBF, 2010). High levels of industrial and agro-

industrial (e.g., sugar and biofuel production) activities along with still insufficient environmental constraints pose an increasing threat to local groundwater.

Biological degradation processes play an essential role in groundwater systems. Dissolved organic groundwater contaminants can be broken down or transformed into innocuous by-products by microorganisms indigenous to the subsurface environment. Microorganisms use naturally occurring electron acceptors to metabolize organic contaminants including petroleum hydrocarbons (Wiedemeier et al., 1999). Oxygen is the preferred electron acceptor but rapidly consumed in contaminated aquifers. Instead, alternative electron acceptors are utilized, such as nitrate (NO_3^-), manganese (IV) (Mn^{4+-}), ferric iron (Fe^{3+}), sulfate (SO_4^{2-}), and carbon dioxide (CO_2). Therefore, a detailed knowledge and the spatial and temporal distribution of contaminants and electron acceptors is crucial to evaluate the extent of contaminant degradation in aquifers (e.g., Bombach et al., 2010). Due to the high costs and inefficiency of active remedial technologies to clean up contaminated aquifers in a reasonable time frame, monitored natural attenuation (MNA) has become a preferred remedy (Wiedemeier et al., 1999). The degradation of organic compounds is often accompanied by change of the ratio of stable isotopes resulting in an enrichment of the heavier isotopes (e.g., ^{13}C, ^{2}H) in the non-degraded residual fraction of the contaminant. The change in the ratio of stable isotopes (e.g., $\delta^{13}C$, $\delta^{2}H$) can be identified by Compound Specific Isotope Analysis (CSIA) and the extent of biodegradation is commonly quantified applying the Rayleigh equation (e.g., Blum et al., 2009; Elsner et al., 2005; Meckenstock et al., 2004; USEPA, 2008). The Rayleigh equation rests on the assumption of a fully mixed and closed system where degradation is the only concentration attenuating and isotope fractionating process. The transport and fate of a degradable compound is strongly affected by the physical heterogeneity of the aquifer and dilution/dispersion processes cause concentration changes alike (Mak et al., 2006). Thus, the criteria for the application of the Rayleigh equation are rarely ever met in field conditions and

the accumulated extent of biodegradation estimated by CSIA seems biased. This identifiable deficiency hence calls for an investigation of the bias induced by small-scale physical heterogeneities, which are ideally represented in high-resolution aquifer analogs. This Ph.D. research work also integrates multiple aquifer analogs in a numerical experiment to test the performance of the commonly applied Rayleigh equation as far as it applies for heterogeneous porous aquifers.

1.2 Research questions and objectives

The research presented in this thesis investigates the physical and chemical heterogeneities in the Pirambóia Formation of the Guarani aquifer in São Paulo State in a comprehensive field study. Based on this field investigation, an aquifer analog model was constructed and reactive transport simulations conducted in order to enhance the understanding of groundwater flow characteristics and contaminant transport in this segment of the Guarani aquifer. Further, the applicability of CSIA-based biodegradation estimates of groundwater contaminants was rigorously tested in a numerical experiment. This experiment includes the application of the constructed aquifer analog model from the GAS as well as four additional analog models constructed from aquifers in SW-Germany. The five aquifer analog models were utilized to cover a wide range of physical aquifer heterogeneities and to imitate and as much as possible realistic field conditions in order evaluate how reliable CSIA functions in complex geological conditions as a tool for assessing the occurrence and extent of biodegradation processes.

The specific objectives were as follows:

- To examine and describe on a cm-scale the physical heterogeneities and their three-dimensional distribution from vertical outcrop faces in the Pirambóia Formation in the Guarani aquifer recharge area in São Paulo State (Brazil). Investigations were aimed at recognizing and parameterizing potential preferential flow paths in this

aquifer portion. The formation has been seen so far as a relatively homogenous hydrostratigraphic unit.

- To resolve chemical heterogeneities, in particular sedimentary Fe(III) concentrations, which may have a relevant impact on the effective natural attenuation potential of the aquifer.
- To digitize the portrayals of litho- and hydrofacies for the construction of a quasi-three-dimensional aquifer analog model and to translate it into a numerical flow and transport model.
- To simulate in a 2D numerical reactive transport experiment a hypothetical petroleum hydrocarbon contamination in the Pirambóia Formation so that one understands the influence of small-scale physical and chemical heterogeneities on the transport and fate while focusing on the effectiveness of ferric iron as electron acceptor.
- To investigate the bias induced by small-scale physical aquifer heterogeneities on CSIA based biodegradation estimates in heterogeneous porous aquifers in a numerical reactive transport experiment using high-resolution aquifer analogs.

1.3 Thesis outline

The following thesis consists of this introduction, three consecutive chapters, the results and conclusion of the overall work, as well as supplementary information on one 3D realization of the aquifer analog as an appendix. The main research work is described in Chapters 2, 3, 4:

- The second chapter describes the field study in the recharge area of the Guarani aquifer in São Paulo State, in which three parallel sections of frontal outcrops and two parallel sections of lateral outcrops were carefully investigated to describe the local litho-

facies on a cm-scale and to translate them into hydrofacies types. Further, the second chapter describes the assessment of facies specific sedimentary Fe(III) content. The focus of this study was to recognize and parameterize potential preferential contaminant flow paths of this aquifer portion. An aquifer analog model was developed, the first of its kind in the Guarani aquifer, depicting the three-dimensional distribution of the variations of hydraulic conductivity, porosity and sedimentary Fe(III) content. This model, including physical and chemical properties, allowed (1) to recognize the most permeable facies and its connectivity, (2) to contrast the new findings against previously reported average hydraulic conductivities from Hirata et al. (2011) and Araújo et al. (1999) and to (3) relate hydraulic properties with facies based sedimentary Fe(III) content in the Guarani aquifer. The outcome of the detailed sedimentological, hydrogeological and hydrochemical investigations contribute to an improved reservoir understanding in the Guarani aquifer on a local scale.

- The study described in the third chapter investigates the influence of small-scale physical and chemical heterogeneities on the transport and fate of a hypothetical petroleum hydrocarbon contamination in the GAS. A high-resolution 2D aquifer cross-section from the constructed aquifer analog is utilized in a reactive transport modelling experiment. This study emphasizes the heterogeneous distribution of sediment bound Fe(III) as a solid-phase electron acceptor and elucidates the role for the effectiveness of the *in situ* bioremediation potential in the upper Pirambóia Formation of the Guarani aquifer. The model honors cm-scale variation in hydraulic properties, solid-phase Fe(III) concentrations based exclusively on hard data and dissolved electron acceptors of the ambient groundwater representing field conditions as realistic as possible. The findings of the reactive transport simulations envisions for the first time the degradation and geochemical evolution during a hypothetical petroleum hydrocarbon con-

tamination in the Guarani aquifer on the field scale. The result emphasizes the importance of hydrofacies related determination of immobile electron acceptors for reliable assessment of microbial natural attenuation potential in aquifers.

- The study described in the fourth chapter is motivated by the fact that the accurate determination of the extent of *in situ* biodegradation estimates based on CSIA data occurs often as problematic under realistic field-scale conditions (e.g., Van Keer et al., 2012). In a numerical reactive transport experiment high-resolution datasets were utilized from a variety of realistic heterogeneous aquifers. The goal of this study was to simulate the propagation of an oxidizable organic compound (toluene) and to thrice analyze: (1) the effects of physical aquifer heterogeneities on spatiotemporal patterns of contaminant concentrations and isotope signatures, and (2) the performance of the commonly applied Rayleigh equation, and (3) the applicability of an extension of the Rayleigh equation for complex hydrogeological conditions. The study also investigates the influence of low/high resolution data samples on the assessment of *in situ* biodegradation in heterogeneous porous aquifers. The findings elucidate that dilution/dispersion is highly site-specific and undergoes significant spatiotemporal variations even for aquifers with moderate physical heterogeneities. Biodegradation estimates using the conventional Rayleigh equation are highly uncertain if the bias induced by dilution/dispersion is not appropriately considered during the estimation of field-derived enrichment factors. Furthermore, the investigations demonstrate that aquifer analogs in combination with reactive transport models significantly improve generic process understanding to evaluate monitoring and quantification strategies for complex hydraulic environments.

2 Construction of a high-resolution aquifer analog model[1]

2.1 Guarani aquifer system

Progressive increase in groundwater resource development and depletion, along with strong urban development, has been placing stress on the transboundary Guarani aquifer system (GAS), which underlies the countries of Brazil, Argentina, Paraguay and Uruguay in South America (Figure 2.1).

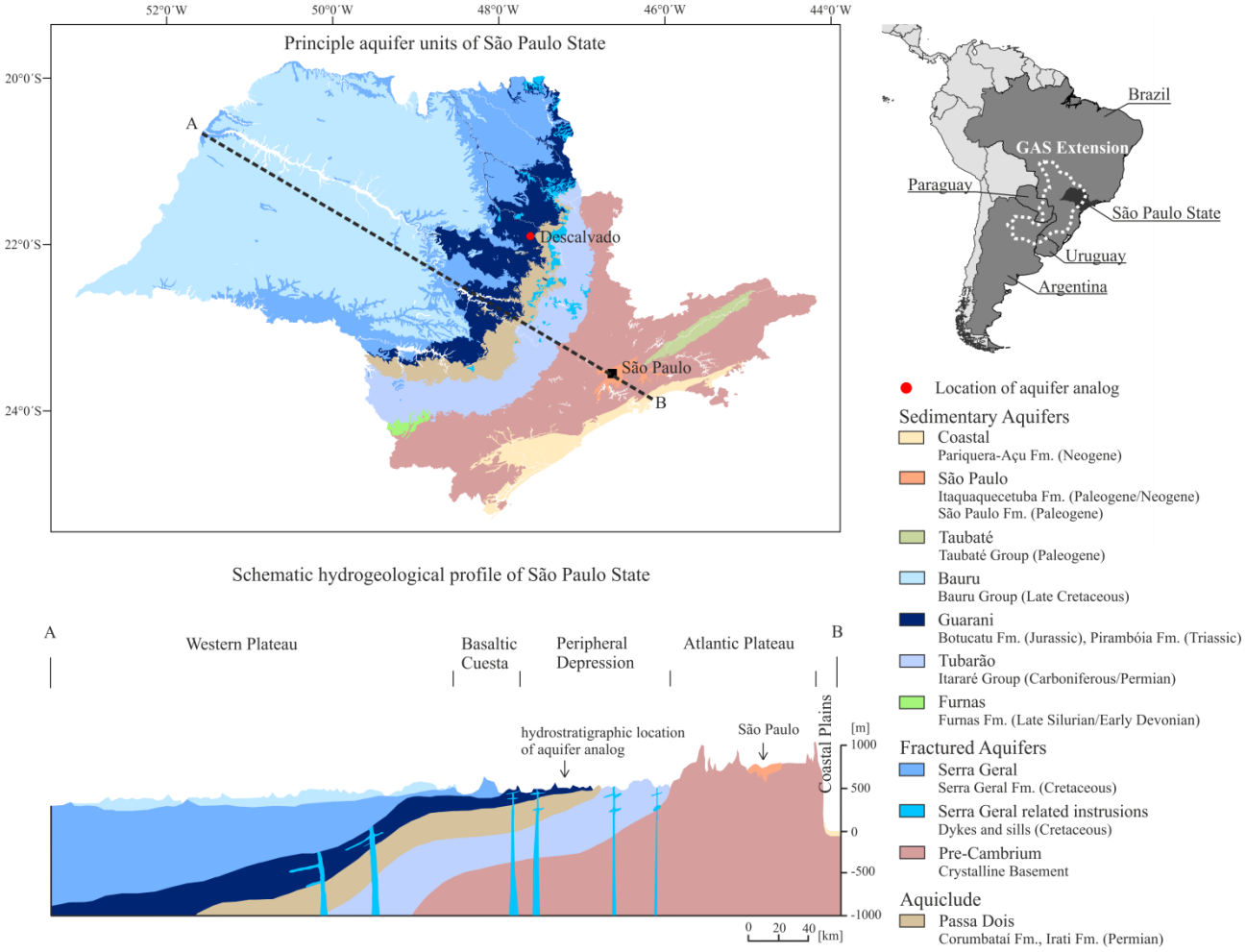

Figure 2.1. GAS extension (after Araújo et al. (1999)) and schematic hydrostratigraphic map and profile of São Paulo State (modified after: DAEE; IG, IPT; CPRM. *Mapa de Águas Subterrâneas do Estado de São Paulo*. São Paulo, 2005) and the location of the aquifer analog.

[1] Chapter 2 contains partly content which is published in:Höyng, D., D´Affonseca F.M., Bayer, P., de Oliveira, E.G., Perinotto, J.A.J., Reis, F., Weiß, H., Grathwohl, P. (2014), High-resolution aquifer analog of fluvial-aeolian sediments of the Guarani aquifer system. *Environmental Earth Sciences*, 71: 3081-3094.

The GAS is mostly confined and direct recharge occurs only in its outcropping areas, which add up to 10% of the total GAS area (Rabelo and Wendland, 2009). Brazil alone accounts for more than 90% of the withdrawal from a total volume of 1, 039 M m^3 per year, where 80% of this volume is abstracted in São Paulo State (Schmidt and Vassolo, 2011). The release of agro-chemicals caused by intense agro-industrial activities (e.g., sugar cane production in São Paulo State) in the GAS recharge areas, mean a high pollution threat. Moreover, accidental or uncontrolled discharge of domestic wastes or manufactured persistent chemicals in the GAS recharge areas (e.g., Lago et al., 2009) pose a high risk for long-term groundwater contaminations, adding further strain on this relevant groundwater reservoir (Dantas et al., 2011; Goldemberg et al., 2008; Marimon et al., 2013).

Although a deep understanding of surface/subsurface and surface/atmosphere interactions is crucial for a sustainable water quality management on a catchment and basin scale (Grathwohl et al., 2013), a comprehensive and detailed knowledge of the spatial distribution of hydraulic parameters on a local scale is necessary for proper planning of any groundwater protection and remediation action (Comunian et al., 2011). Realistic representation of these parameters in mathematical models is challenging and needed for reliable prediction of groundwater flow and contaminant transport (Whittaker and Teutsch, 1999). However, as economic and practical constraints often restrict proper aquifer characterization, crucial hydrogeological features may remain unnoticed (e.g., Parker et al., 2008), resulting in high degrees of uncertainty and, consequently, in model impreciseness. The use of reservoir analog models is an established alternative approach to support and improve the characterization and conceptualization of groundwater (e.g., Bayer et al., 2011; Bersezio, 2007; Heinz et al., 2003; Huggenberger and Aigner, 1999; Klingbeil et al., 1999; Whittaker and Teutsch, 1999) and hydrocarbon reservoirs (e.g., Flint and Bryant, 1993; Pringle et al., 2006). Information on the spatial variability of groundwater reservoir parameters for the construction of aquifer analogs

can either be generated by structure-imitating, process-imitating or by descriptive approaches (Koltermann and Gorelick, 1996). Numerous aquifer analog studies reproduce the sedimentary structures and the corresponding hydraulic properties of different depositional environments (Anderson et al., 1999; Bersezio et al., 2007; Bersezio et al., 2004; Cardenas and Zlotnik, 2003; Felletti et al., 2006; Heinz and Aigner, 2003; Heinz et al., 2003; Hornung and Aigner, 1999; Kessler et al., 2013; Kostic et al., 2005; Sweet et al., 1996; Weissmann et al., 1999; Zappa et al., 2006). For instance, Bayer et al. (2011) successfully constructed a high-resolution aquifer analog of high-energy environment deposits (e.g., braided river channels), where hydraulic properties significantly vary on a cm to dm-scale vertically and horizontally.

The enormous capacity and economic significance of the GAS have made this groundwater reservoir subject to multi-national and multi-disciplinary research efforts to use this resource in a sustainable manner for current and future demand (e.g., Puri et al., 2001). Although comprehensive studies have been conducted to characterize and understand the hydrogeology and hydrogeochemistry of this system (e.g., Bonotto, 2012; Bonotto, 2013; Foster et al., 2009; Gastmans et al., 2012; Hirata et al., 2011; Soares et al., 2008; Wendland et al., 2007; Zuquette et al., 2009), no high-resolution description of its hydrogeological and sedimentological facies exist. According to Donatti et al. (2001), in São Paulo State the GAS consists of a Triassic succession of siltstones, sandy siltstones, sandstones and coarse to pebbly sandstones of a wet-aeolian system (Pirambóia Formation), followed by Jurassic dune deposits of a dry-aeolian system (Botucatu Formation,). The wet-aeolian system is characterized by a higher phreatic level due to the vicinity to the coast (Donatti et al., 2001). Coarser sediment was supplied by discharging streams and rivers, cutting into the aeolian deposits and resulted in a fluvial-aeolian facies association. In contrast to the homogeneous aeolian deposits of the Botucatu Formation, the heterogeneous fluvial-aeolian sediments, where channel deposits intermingle with well-sorted aeolian sands are of particular relevance in the upper part of the Pirambóia

Formation. Groundwater flow patterns are potentially non-uniform and complex in those aquifer portions and therefore, a general understanding of the heterogeneous architecture is required to assist the prediction of plume geometry and evolution in case of a possible contamination on a local scale. Extensive sedimentological investigations of this sedimentary unit has already been carried out (Caetano-Chang and Wu, 2006; Dias and Scherer, 2008), nevertheless no previous study investigated the heterogeneity and hydrogeological role of these fluvial-aeolian deposits within the Pirambóia Formation, as well as in the overall context of the GAS in São Paulo State.

This work is the first application of the aquifer analog approach at the GAS for fluvial-aeolian sediments deposited in a transitional environment of a wet-aeolian system. In order to understand the specific hydraulic characteristics of the fluvial-aeolian sediments occurring at the upper part of the Pirambóia Formation, an aquifer analog is constructed from sedimentary outcrops in a sandy open-pit mine. For that purpose, three parallel and equally spaced vertical outcrops were investigated according to the common aquifer analog construction procedure (e.g., Anderson et al., 1999; Bayer et al., 2011; Bersezio et al., 1999; Heinz and Aigner, 2003). Additionally, two perpendicular outcrops were recorded during pit excavation. It facilitates the reconstruction of the sediment body geometries between two parallel main sections and enables the assemblage of a quasi-three-dimensional (3D) model (Felletti et al., 2006; Kessler et al., 2013). It also minimizes, for instance, the uncertainties inherent to geostatistical models of aquifer analogs without perpendicular sections, such as the one developed by Comunian et al. (2011). In order to capture the fine-scale heterogeneity of the fluvial-aeolian facies association, sedimentary facies were mapped on a cm-scale. Hydrogeological investigations were conducted in the field and laboratory. The combined geological analysis of sedimentary structures and determination of hydraulic properties (K, n) enables, for the first time, the identification of the most important elements of heterogeneity in terms of preferen-

tial flow paths, connectivity, and high permeable facies of the fluvial-aeolian deposits of the Pirambóia Formation on a local scale. Hydrofacies types are derived and the 2D spatial *K* distribution of the examined sediments is related to the lithofacies and represented a quasi-three-dimensional aquifer analog model consisting of 2D cross-sectional profiles.

2.2 Sedimentology

The GAS belongs to the most important groundwater reservoirs in the world and is the biggest groundwater system in South America. With a storage volume of some 40 000 km³, it underlies a total area of about 1, 200 000 km² in Brazil, Paraguay (both Paraná Basin), Argentina (Chaco-Paraná Basin), and Uruguay (North Basin) (Puri et al., 2001). The accumulated thickness of the sedimentary and igneous rocks filling up the Paraná and Chaco-Paraná basins is about 8,000 m. The Paraná basin comprises six super-sequences bounded by unconformities from the Lower Ordovician (450 M years) to the Upper Cretaceous (65 M years), which represent major transgressive-regressive cycles and continental sedimentation and erosion processes (Milani et al., 1998).

The groundwater-hosting formations comprising the GAS are built up of weakly-cemented, mainly continental siliciclastic sedimentary rocks of Triassic and Jurassic age (~ 250 - 145 M years) (Figure 2.1), deposited on a Permo-Triassic erosional surface (250 M years) (Assine et al., 2004) during progressive continentalization of Western Gondwana at a late stage of the complex geologic evolution of the Paraná basin (Hirata et al., 2011). The end of the basin evolution is marked by Early Cretaceous thick basalt layers (~ 1 500 m) of the Serra Geral Formation, which extensively cover and confine the GAS. The average thickness of the GAS sediments is about 250 m, but it greatly varies from more than 600 m to less than 50 m (Foster et al., 2009). Almost two thirds of the transboundary aquifer system in the Paraná basin is located on Brazilian territory.

In São Paulo State (Brazil), the GAS is formed by siltstones, sandy siltstones, sandstones and coarse to pebbly sandstones of the Pirambóia Formation and aeolian sandstones of the Botucatu Formation (Figure 2.1). For São Paulo State an overall thickness for the Pirambóia Formation of 75 - 270 m and of 20 - 238 m for the Botucatu Formation is reported (Hirata et al., 2011). The lower and upper boundaries of the GAS are defined by the occurrence of coastal siltstones (e.g., Corumbataí Formation) and basalt layers (Serra Geral Formation), respectively (Donatti et al., 2001). Although the Pirambóia and the Botucatu Formation are often regarded as a single unit from a groundwater reservoir perspective, they differ in terms of age, deposition and diagenetic evolution (Hirata et al., 2011). Several studies address facies characteristics, rock properties, and distinct depositional environment for the Pirambóia (wet-aeolian system) and Botucatu Formation (dry-aeolian system), and correlate them to present environments for an in-depth understanding of the depositional system (e.g., Assine et al., 2004; Donatti et al., 2001). According to Donatti et al. (2001), the sandstone succession comprising the GAS in São Paulo State can be subdivided into five main facies associations: (1) tidal plain with aeolian sand sheets; (2) coastal dunes with frequently flooded interdune flats; (3) coastal dunes with rarely flooded interdune flats; (4) braided alluvial plain with aeolian dunes; (5) giant dunes with interdune depressions. Facies associations 1 to 4 correspond to the Pirambóia Formation, while facies association 5 is related to the Botucatu Formation.

The fluvial-aeolian sandstones of the upper part of the Pirambóia Formation (facies association 4), the focus of this study, crop out in the central-eastern part of São Paulo State in the vicinity of the cities of Descalvado, Itirapina and São Pedro with a varying thickness from a few meters up to approximately 45 m (Caetano-Chang and Wu, 2006). This facies association shows fluvial deposits of braided rivers reworked by the prevailing winds and mixed with aeolian dune deposits (Caetano-Chang and Wu, 2006).

The coarse grained sandstones and conglomerates of the top of the Pirambóia Formation are mainly quartzarenites (mineralogically supermature) and rarely subarcosean (considered to be mature to submature). The cement occurring at the upper Pirambóia Formation consists of iron oxide and autogenic clay, adhering to the surface of the grains or partially filling the pores. Calcite and, to a lesser extent, locally pyrite might occur as patches that cement grains (Caetano-Chang and Wu op. cit.). In the contact zone with the mafic dykes and sills of the Serra Geral Formation (Figure 2.1), the deposits of the Pirambóia Formation can be locally "cooked" due to contact metamorphism.

2.3 Area of investigation

The study area is located in the recharge area of the GAS at the central-eastern part of São Paulo State (Brazil), in the vicinity of Descalvado city (Figure 2.1). Here, the basalts of the Serra Geral Formation and the sandstones of the Botucatu Formation are eroded and the sandstones of the Pirambóia Formation crop out and appear as bedrock, partially superimposed by Tertiary sandy deposits of the Santa Rita do Passa Quatro Formation. Here, the Pirambóia Formation is slightly weathered and the deposits partially cemented with iron oxide and autogenic clay. There are no digenetic overprints in the area of investigation from Serra Geral related intrusions. The field site is situated in a sandy open-pit mine with multiple levels of operation in the Pirambóia Formation, where sand is excavated from contiguous banks.

Several locations in the sand pit were inspected and compared in terms of the appearance of typical and common sedimentary features of the fluvial-aeolian deposits of the upper part of the Pirambóia Formation. Based on characteristic structures of the fluvial-aeolian sediments and on operational feasibility issues, a suitable outcrop was selected in the central part of the sand pit for the aquifer analog construction (Figure 2.2). The geographical coordinates of the outcrop are: 21° 56' 46.5" S, 47° 36' 45.8" W. The selected sand bank pro-

vided ideal insights into the physical heterogeneities and allowed a cm-scale depiction of the existing lithofacies and hydrofacies.

Figure 2.2. Aerial view of the open-pit mine near Descalvado city (© 2014 Google, Image © 2014 Digital Globe), and fieldwork at the outcrop in the upper Pirambóia Formation.

2.4 Hydrogeological aquifer analog model

2.4.1 Fieldwork

The overall dimension of the selected rectangular shaped sand body is 28 m in length (*Lx*), 7 m in width (*Ly*) and 5.8 m in height (*Lz*). A set of poles and markers were equidistantly placed along each outcrop face as reference points for the mapping procedure and photographic documentation. In order to characterize the spatial variations of sedimentary structures in three dimensions, three parallel cross-sections (spacing 3.5 m along the y-axis) and two perpendicular lateral sections at x = 0 m and x = 28 m were constructed by stepwise horizontal excavation of the selected sand bank, as schematically illustrated in Figure 2.3. First, the original outcrop wall (section A-A´) was mapped (Figure 2.3a) and afterwards, the sand body carefully excavated by 3.5 m. Subsequently, the exposed new frontal outcrop wall (sec-

tion B-B´) and the first part of the lateral outcrop walls (A-C, A´-C´) were recorded (Figure 2.3b). Again, the sand body was excavated by 3.5 m to map the section C-C´ and the second part of the lateral outcrop walls (A-C, A´-C´) (Figure 2.3c).

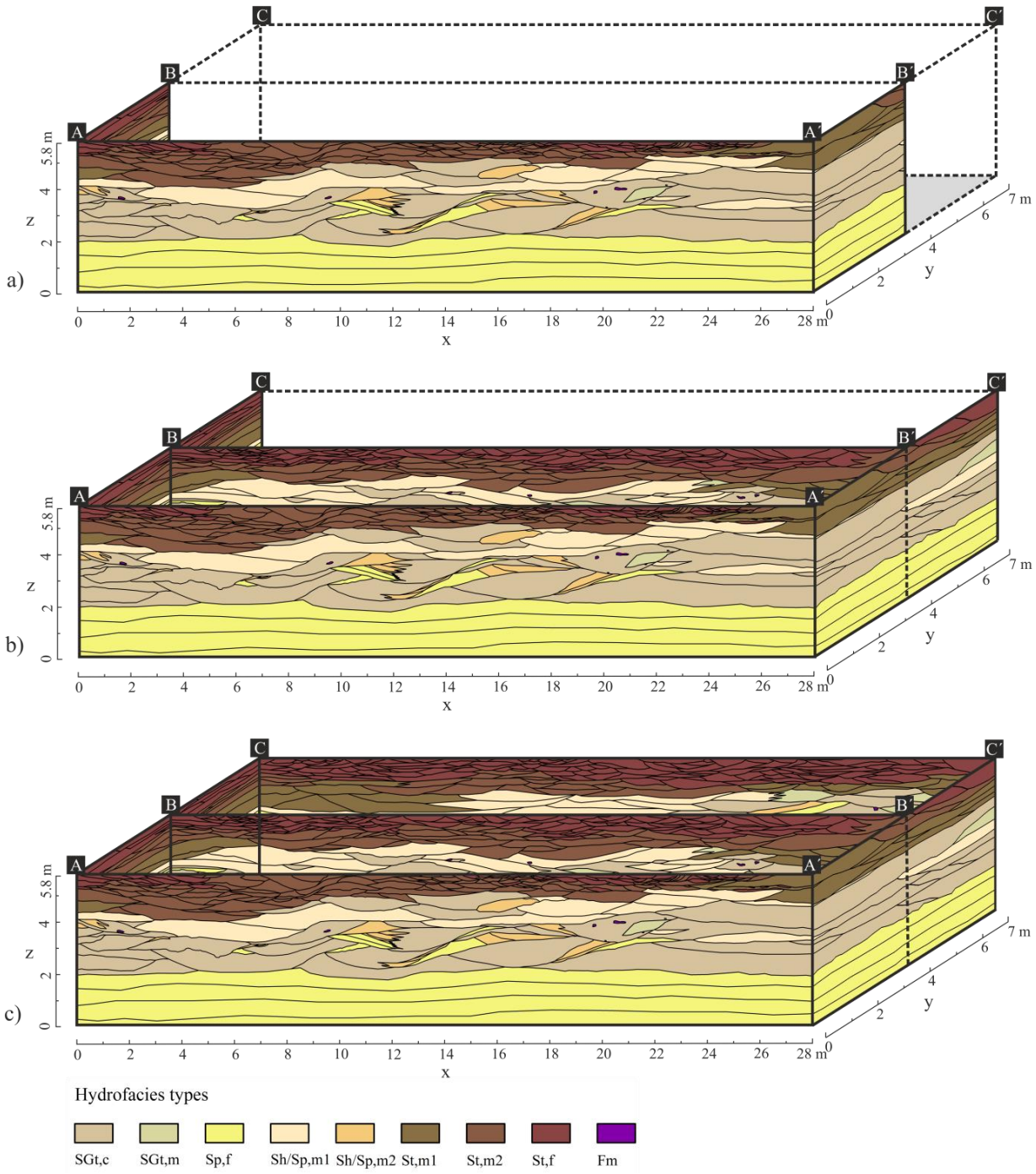

Figure 2.3. Schematic representation of the stepwise quasi-three-dimensional aquifer analog model construction process and the geometry and distribution of the identified hydrofacies at a) section A-A´ and first half of the lateral sections A-C and A´-C´, b) section B-B´ and second half of the lateral sections A-C and A´-C´, c) and section C-C´. For illustrative purposes the longitudinal extension of the lateral sections is exaggerated by a factor of 1.2.

The mapping process was assisted by systematic description and sedimentological interpretation of the complex structured sediments. The sedimentary structures were recorded in the field with a 5 cm × 5 cm resolution, producing outcrop maps at a 1:50 scale for posterior data processing. Close-up photographs of the entire outcrop were taken to provide basic digital images.

Lithofacies types were depicted following the approach proposed by Miall (1978). This method is based on a two-letter scheme, allowing the categorization of sedimentary units on the basis of their sedimentary structures and genetic processes. The dominant grain size is indicated by a capital letter (G = gravel, S = sand, F = fine grained facies, including silt and mud), whereas the lowercase letters describe the characteristic texture and structure of the lithofacies (t = trough bedded, h = horizontal, p = planar, m = massive). In case of equal shares of two dominant grain sizes, a combination of both is employed.

A comprehensive sediment sampling campaign from multiple locations over each outcrop was carried out in order to allow the determination of the hydraulic properties of each lithofacies types in the laboratory by means of grain size analysis. In order to validate the laboratory derived hydraulic conductivity estimates by infiltration test, wells were temporarily installed on top of the outcrop bench and in front of the outcrop prior to excavation. Due to restrictions during the ongoing mining operations, only five wells (depth: 0.5 m) could be installed. The infiltration tests were performed for three hydraulic conductivity zones using a constant-head (Guelph permeameter) and a falling-head well permeameter. The wells with a depth of 0.5 m were located at x = 7 m, y = 1.5 m and from z = 5.3 m to 5.8 m, at x = 27 m, y = 1.5 m and from z = 5.3 m to 5.8 m, and right in front of the first outcrop at x = 23 m, y = 0, and from z = 0 m to - 0.5 m.

2.4.2 Laboratory work

Empirical grain-size methods for the estimation of hydraulic conductivity, *K*, in porous media are standard in hydrogeological practice (Carrier, 2003; Kasenow, 2002; Vukovic and Soro, 1992). For the collected samples, grain size analysis was carried out by sieving (Tyler sieves with a mesh size from 0.053 mm to 31.7 mm for the gravel and sand fraction). A laser diffraction method served for characterization of the fines distribution (< 0.053 mm, Malvern Mastersizer 2000, Malvern Instruments). The total porosity, *n*, was determined by direct methods in the laboratory from undisturbed field samples for all hydrofacies types (total number of samples = 62) (Table 2.1). Since the Kozeny-Carman and the U.S. Bureau of Reclamation (USBR) formula are not applicable for the estimation of hydraulic conductivity in silt and clay materials, a falling-head permeameter test was alternatively conducted in the lab on irregular shaped undisturbed clay samples of only a few decimeters in size. However, because the classical falling head method requires a regular geometric shape of the sample (ABGE, 1981), an approach for irregular shaped undisturbed bulk samples developed by Oliveira (2000) was employed instead.

2.4.3 Determination of hydraulic properties and hydrofacies types

The lithological classification only considers the main grain size classes as previously described (e.g., G = gravel, S = sand, F = fines) and does not embrace the varying proportions of the subclasses of the grain size spectrum (e.g., fine sand, medium sand, coarse sand), which may significantly influence the hydraulic properties within a single lithofacies. Different lithofacies may have variable hydraulic properties and therefore, from a hydrogeological perspective, a translation into hydrofacies types is required to describe the permeability distribution and hydraulic connectivity within the aquifer. The term hydrofacies is defined as a relatively homogeneous but anisotropic and hydrogeologically meaningful unit (Anderson, 1989; Poeter and Gaylord, 1990), which has a horizontal correlation length that is finite, but

that in most cases is significantly greater than the vertical correlation length (Anderson, 1989). The determination of hydrofacies types, therefore, allows for recognizing preferential flow paths, low permeable flow units and flow barriers, and helps to quantitatively describe the flow parameter distribution of the reservoir (Heinz et al., 2003; Klingbeil et al., 1999), which is the ultimate objective of the aquifer analog construction.

For that reason the different hydraulic conductivities of each lithofacies are determined by the widely accepted Kozeny-Carman formula and the USBR formula (Kasenow, 2002; Vukovic and Soro, 1992). For the latter, the value for kinematic viscosity of water is related to a temperature of 20° C. To reflect the grain size spectra for different hydrofacies types and corresponding *K* values, a classification scheme according to DIN EN ISO 14688-1 (2002) is applied. This scheme uses capital letters for the dominant grain size class of the hydrofacies type (e.g., CSa = coarse sand, MSa = medium sand, FSa = fine sand). Minor grain size mass fractions are indicated by small letters in ascending order in front of the main classes, which can be further denoted with an apostrophe in case they are minor or with an asterisk if they are prominent (e.g., csa´fsa*MSa = medium sand with a very minor portion of coarse sand and a prominent portion of fine sand).

Although this scheme is a precise way to reflect grain size shares in a letter based code, it is rather elusive for fast comprehension. Therefore, a convenient and more intuitive hydrofacies code based on the lithofacies code is applied in this study. The employed code uses similar letters as the lithofacies code, indicating sedimentary structures, a small letter to denote the dominant grain size (f = fine, m = medium, c = coarse) and a number for further differentiation if necessary. The lithofacies and hydrofacies recorded and classified in this study, as well as the hydraulic properties, are summarized in Table 2.1.

Table 2.1. Lithofacies and hydrofacies types with hydraulic properties.

Lithofacies (after Miall, 1978)	Hydrofacies code used	Hydraulic conductivity K (m/s)	Porosity n (-)	Number of samples	Hydrofacies classified after DIN EN ISO 14688-1, 2002
SGt	SGt,c	$2.96 \times 10^{-4} \pm 9.90 \times 10^{-5}$ [(a)]	0.32 ± 0.04	7	Sa/Gr
	SGt,m	$9.44 \times 10^{-5} \pm 6.60 \times 10^{-5}$ [(a)]	0.32 ± 0.04	7	fgr´fsamsaCSa
Sp	Sp,f	$1.63 \times 10^{-4} \pm 1.74 \times 10^{-5}$ [(b)]	0.25 ± 0.05	9	msaFSa
Sh/Sp	Sh/Sp,m1	$1.38 \times 10^{-3} \pm 6.88 \times 10^{-5}$ [(b)]	0.33 ± 0.05	8	fsa´csaMSa
	Sh/Sp,m2	$7.77 \times 10^{-5} \pm 3.05 \times 10^{-5}$ [(b)]	0.33 ± 0.05	6	csa´fsa*MSa
St	St,m1	$5.97 \times 10^{-5} \pm 2.91 \times 10^{-5}$ [(a)]	0.29 ± 0.04	7	csa´fsaMSa
	St,m2	$2.49 \times 10^{-5} \pm 1.34 \times 10^{-5}$ [(a)]	0.29 ± 0.04	6	si´csa´fsa*MSa
	St,f	$6.23 \times 10^{-6} \pm 5.25 \times 10^{-6}$ [(a)]	0.24 ± 0.05	7	si´msa*FSa
Fm	Fm	$7.84 \times 10^{-8} \pm 4.22 \times 10^{-8}$ [(c)]	0.29 ± 0.03	5	Cl

Hydrofacies code: SGt,c = trough cross-bedded coarse sand and gravel; SGt,m = trough cross-bedded medium sand and gravel; Sp,f = planar cross-bedded fine sand; Sh/Sp,m1 = horizontally laminated to planar cross-stratified medium sand; Sh/Sp,m2 = horizontally laminated to planar cross-stratified medium sand with fine sand; St,m1 = trough cross-bedded medium sand; St,m2 = trough cross-bedded medium sand with find sand; St,f = trough cross-bedded fine sand; Fm = massive clay intraclasts.

[(a)] derived by empirical equation according to Kozeny-Carman, [(b)] derived by empirical equation according to USBR, [(c)] from laboratory permeameter tests.

2.4.4 Model development

The outcrop based sedimentological and the hydrogeological information was stored in a database and subsequently linked to digital high-resolution images. One individual panorama image was created for each outcrop. The panorama images were produced by assembling multiple high-resolution and overlapping close-up terrestrial outcrop orthophotos. To avoid optical distortion effects from the left and right side of the photograph, a share of 25% was cut following the approach of Morales et al. (1997). Subsequently the remaining center parts of the photographs were stitched together using Corel DRAW X5. The obtained 2D photo-panels were then used for onscreen digitization with a GIS software (ArcGIS 9, ESRI®), encompassing the following steps: (1) sedimentary structures and forms were delineated as polygons based on the outcrop images and generated field maps; (2) each constructed polygon constituting a single hydrofacies was attributed to the respective hydrofacies code and hydraulic parameters from the sedimentological and hydrogeological database; (3) the digitized hydrofacies assemblages from outcrop data were saved as shapefiles and converted into grid format

with specified cell size and number in order to use the aquifer analog for future numerical modeling experiments.

2.4.5 Litho- and hydrofacies distribution

In the examined upper part of the Pirambóia Formation, conglomeratic pebbly and coarse sands interspersed with very poorly sorted fine to coarse pebbles were found adjacent to clean and very well-sorted and well-rounded medium to fine sand with minor amounts of fines. The sands often gradually intermingle with pebbly and coarse deposits, locally containing large pieces of clay (up to 50 cm in diameter). Based on the outcrop analysis, five distinctive litho-facies are recognized on the basis of their primary sedimentary features. The five lithofacies and their corresponding hydraulic properties are described in detail hereafter and summarized in Table 2.1. The order of the description is based on the main occurrence of the facies from the bottom to the top of the outcrops.

2.4.5.1 Planar cross-bedded aeolian sand lithofacies (*Sp*)

Geological description

This lithofacies appears in the outcrops mainly at $z \leq 2$ m, with some localized occurrence at 3 m $\leq z \leq$ 4 m, composing approximately 35% of the outcrop area based on the three main cross-sections. The most prominent feature of the *Sp* lithofacies is the clean and very well-sorted and well-rounded medium to fine sands with minor amounts of silt deposited under aeolian conditions (Figure 2.4d). The primary sedimentary structure is characterized by low dipping foresets (~ 15°) of planar cross-beds and horizontal to sub-horizontal lamina. The sets of cross-strata have an average thickness of ~ 50 cm. Drill cores executed in front of the out-crop confirmed a minimum thickness of ~ 2.5 m of this sand package. The upper part of the cross-stratified foresets has been eroded and covered by coarse fluvial deposits (*SGt* lithofa-cies), indicating an erosional surface (Figure 2.4d).

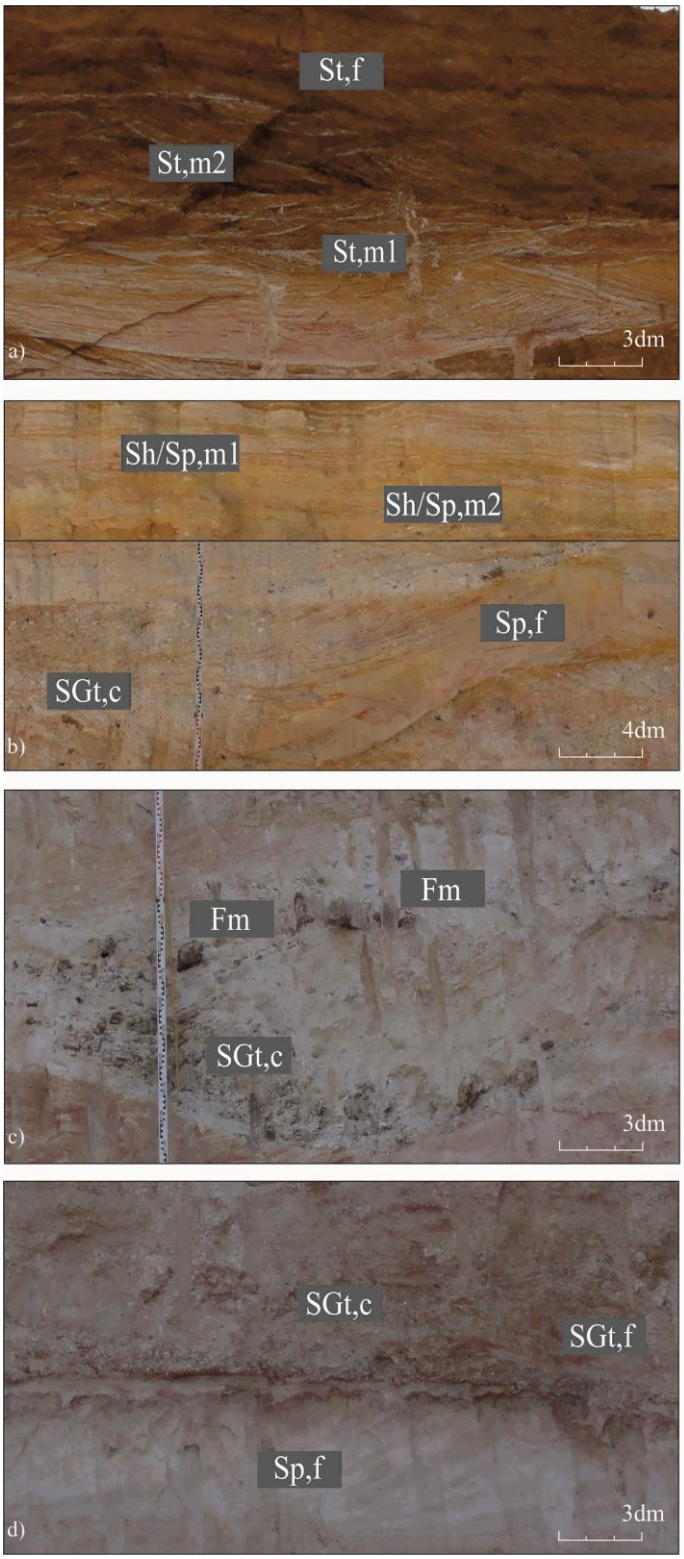

Figure 2.4. Photographs of identified lithofacies and corresponding hydrofacies types in the outcrop: a) trough cross-bedded sand lithofacies (St), b) horizontally laminated to planar cross-stratified sand lithofacies (Sh/Sp), c) trough cross-bedded sand and gravel lithofacies (SGt) with massive clay intraclasts (Fm), d) planar cross-bedded aeolian sand lithofacies (Sp) and overlying lithofacies (SGt).

Hydraulic characterization

For the homogeneous aeolian sands of the *Sp* lithofacies a hydraulic conductivity value of $1.63 \times 10^{-4} \pm 1.74 \times 10^{-5}$ m/s ($n = 0.25 \pm 0.05$) is obtained, defining the hydrofacies type *Sp,f* (hydrofaciestype *Sp,f* = planar cross-bedded fine sand) (Figure 2.5a-d). The hydraulic conductivity of the field test performed at the location $x = 23$ m, $y = 0$, and from $z = 0$ m to -0.5 m, which refers to this hydrofacies, is $K = 6.6 \times 10^{-4}$ m/s. Although the field derived value is in agreement with the laboratory determined values, it has to be treated with caution. The field test was carried out with great care but possible effects of the mining operations, such as soil compaction or occurrence of small fissures, might adversely influence data reliability. Thus, the field values only serve well for a rough cross-check of laboratory derived values.

2.4.5.2 Trough cross-bedded sand and gravel lithofacies (*SGt*)

Geological description

This is the main lithofacies occurring from 2 m ≤ *z* ≤ 5 m in the outcrops, representing a total area fraction of ~ 30% of the three main cross-sections, with restricted occurrence around *z* = 5.5 m. The *SGt* lithofacies is built up of a mixture of chaotically structured conglomeratic pebbly and coarse sands, with varying amounts interspersed with very poorly sorted fine to coarse pebbles. The deposits are presented as bodies of channel-shape geometry (Figure 2.4c), varying vertically and horizontally in size between ~ 0.5 m and 3 m and ~ 0.3 and 1.5 m, respectively. The pebbles are angular to rounded and mixed with coarse sand and clay fragments in a silt matrix. Large irregularly shaped intraclasts of dark reddish clay (lithofacies *Fm*) of a few decimeters in size can be found in these deposits (Figure 2.4c). The sediment bodies often internally cut into each other, both laterally and vertically. Along the margin of the channel bodies the deposits frequently interfinger and interbed with medium and fine-grained well-sorted sands of the *Sh/Sp* lithofacies (Figure 2.4b), which are described later in detail. The strata of the *SGt* lithofacies display an irregular lower bounding surface sitting on top of the aeolian well-sorted fine sands (*Sp* lithofacies) (Figure 2.4d). The medium-scale channel fills observed in the outcrop reveal a typical trough cross-bedded structure. They can be interpreted on the basis of their multiple erosional surfaces and coarse grained and pebbly nature as the depositional response to high-energy fluvial processes of a braided river channel system bearing a heavy suspended bed load.

Hydraulic characterization

Varying amounts of pebbles and coarse sand of the *SGt* lithofacies result in two different hydrofacies (hydrofaciestype *SGt,c* = trough cross-bedded coarse sand and gravel; and *SGt,m* = trough cross-bedded medium sand and gravel). The *SGt,c* hydrofacies vary by equal amounts of sand and gravel over all grain size classes (very fine to coarse) with an estimated

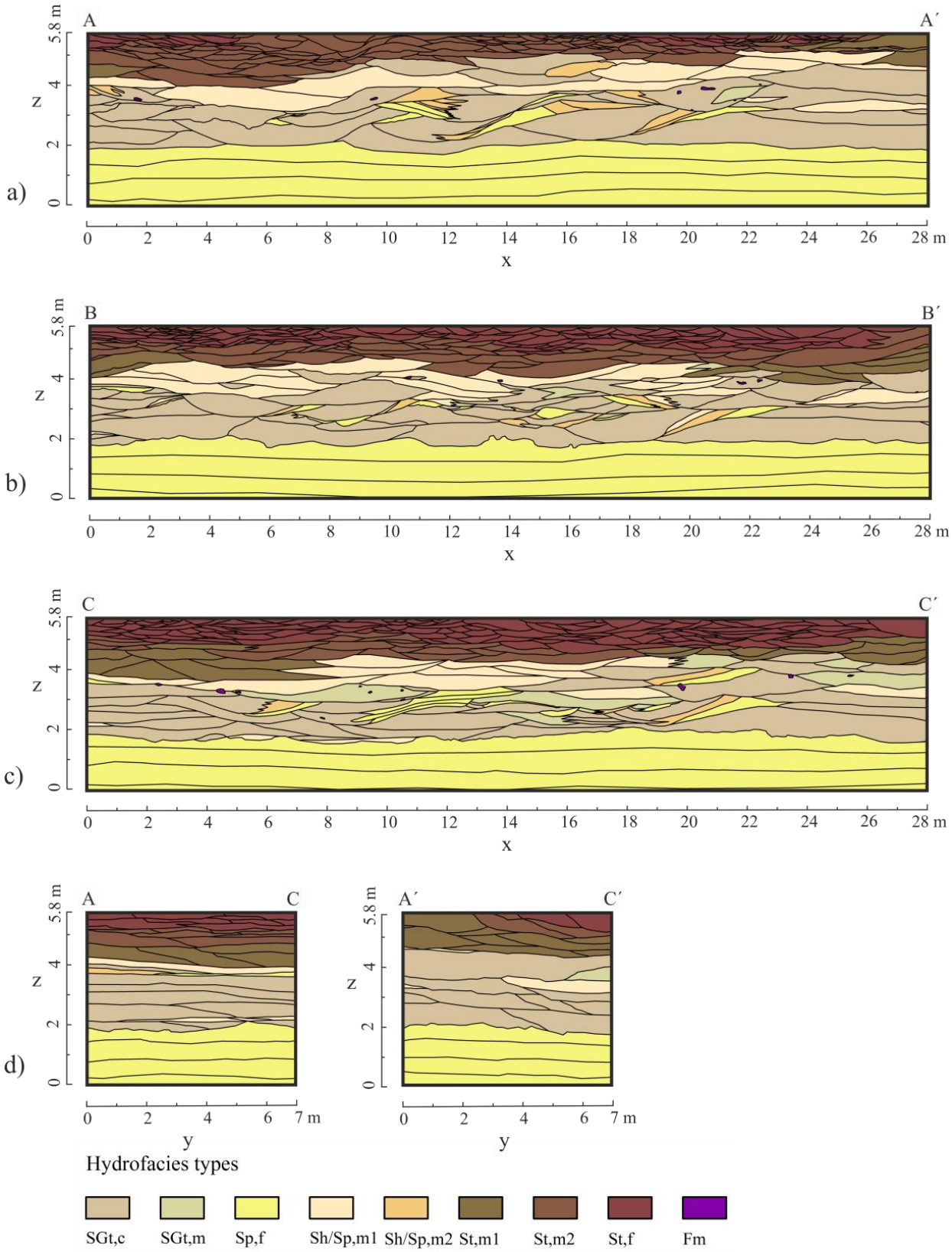

Figure 2.5. Geometry and distribution of the identified hydrofacies at the aquifer analog frontal sections a) A-A´, b) B-B´, c) C-C´, and lateral sections d) A-C e) and A´-C´.

mean hydraulic conductivity of $K = 2.96 \times 10^{-4} \pm 9.90 \times 10^{-5}$ m/s and $n = 0.32 \pm 0.04$. The *SGt,c* hydrofacies dominate the *SGt* lithofacies. In the areas where the *SGt* lithofacies predominantly consists of coarse sand with portions of medium and fine sand, the hydrofacies type *SGt,m* is defined, with a $K = 9.44 \times 10^{-5} \pm 6.60 \times 10^{-5}$ m/s and $n = 0.32 \pm 0.04$. Overall, this lithofacies contains a significant amount of fines. The higher surface area of small size grains increases the frictional resistance of flow and reduces the intrinsic permeability of sediments (Fetter, 2001), which is reflected by a rather low *K* value for this coarse, pebbly sand.

2.4.5.3 Massive clay intraclasts (*Fm*)

Geological description

At some positions in the outcrop (e.g., Figure 2.3a, at location: $x = 20.8$ m, $z = 4$ m), randomly oriented dark-brownish irregularly shaped intraclasts of clay can be found embedded in the coarse fluvial deposits of the *SGt* lithofacies (Figure 2.4d). The size of the muddy intraclasts ranges from a few centimeters up to several decimeters. The intraclasts can be attributed to reworked, thin muddy layers of floodplains from marginal channels in a braided river environment or from small and ephemeral lakes.

Hydraulic characterization

The obtained hydraulic conductivity for the hydrofacies type *Fm* (hydrofacies type *Fm* = massive clay intraclasts) is very low ($K = 7.84 \times 10^{-8} \pm 4.22 \times 10^{-8}$ m/s, $n = 0.29 \pm 0.03$). However, as this hydrofacies is discontinuous and of minor presence in the outcrops (total area fraction of < 1% within the three main cross-sections). Therefore, from a hydrogeological point of view it is not considered relevant in the examined aquifer analog.

2.4.5.4 Horizontally laminated to planar cross-stratified sand lithofacies (*Sh/Sp*)

Geological description

This lithofacies locally appears from 2 m ≤ *z* ≤ 5 m (total area fraction of ~ 11% within the three main cross-sections) within the *SGt* lithofacies. It is characterized by laminated sheets, small bodies and lenticular units of very well-sorted medium to very fine sands (Figure 2.4b). The small bodies and lenticular units of sand either occur as wedges along the margins of coarse grained channel fills exhibiting internal cross-stratification (*Sp*), or as relatively laterally continuous laminated sheets (*Sh*). The medium to very fine sands along the sides of the channel display a prominent complex interfingering pattern and gradual changes with the pebbly sands of the *SGt* lithofacies (Figure 2.4b).

This junction of coarse fluvial deposits with fine aeolian sands is a common sedimentological feature for wet-aeolian systems, where during the wet period fluvial processes prevail, and in the dry season wind reworks fluvial deposits and supplies fine sand into the system (Assine et al., 2004; Caetano-Chang and Wu, 2006). The eroded wedges and lenticular units of fine sand present vestiges of the aeolian influence on the depositional system. Plane sandy bed forms are associated with fluvial processes and can be rather attributed to upper flow regime conditions, as lower flow regime conditions are characterized by cross-stratified sands under a waning current velocity (Miall, 2010).

Although the deposits of the study site are carefully mapped, how the sedimentary bed forms evolve between two parallel outcrops could not always be clearly derived how the sedimentary bed forms evolve between two parallel outcrops. Gradual changes of the internal stratification from horizontal to cross-stratified are frequently observed. Therefore, for practical reasons, the lithofacies classes *Sh* and *Sp* are merged (*Sh/Sp*) and treated as one facies class for the outcrop.

Hydraulic characterization

The grain size ranges mainly from fine to medium sand, but also includes varying amounts of fine and coarse sand. This allows a classification of the *Sh/Sp* lithofacies into three different hydraulically relevant units (hydrofaciestype *Sh/Sp,m1* = horizontally laminated to planar cross-stratified medium sand; *Sh/Sp,m2* = horizontally laminated to planar cross-stratified medium sand with fine sand; *Sp,f* = planar cross-bedded fine sand). The *Sh/Sp,m1* hydrofacies type shows the highest hydraulic conductivity observed in the outcrops, with $K = 1.38 \times 10^{-3} \pm 6.88 \times 10^{-5}$ m/s ($n = 0.33 \pm 0.05$). The fine parts of the lithofacies class *Sh/Sp* have the same hydraulic properties as the previously described aeolian lithofacies (*Sp*). Thus, the fine parts of the lithofacies *Sh/Sp* can also be denoted as hydrofacies type *Sp,f* with $K = 1.63 \times 10^{-4} \pm 1.74 \times 10^{-5}$ m/s and $n = 0.25 \pm 0.05$.

2.4.5.5 Trough cross-bedded sand lithofacies (*St*)

Geological description

The *St* lithofacies is observed in the outcrops at 4.5 m $\leq z \leq$ 5.8 m (total area fraction of 24% within the three main cross-sections) and primarily consists of sets of trough cross-bedded very fine to medium sand (Figure 2.4a). The trough beds are commonly at the decimeter to meter scale and are formed by well to poorly sorted, rounded grains. This lithofacies can be separated into three different sets based on the grain size and the degree of coating with detrital ferric hydroxides of syndepositional origin. The trough beds of moderately sorted white medium sand with portions of fine and coarse sands are followed by trough beds of light brownish color including higher portions of fines. On top, sets of very well sorted, very fine to fine sand of dark brown color are identified. The trough bed forms can be interpreted as subaqueous sinuous-crested 3D dunes. The term *dunes* can be synonymously used for sand bars in river channels to interpret trough cross-bed stratification.

Hydraulic characterization

Following the grain size distribution of the trough beds, three different hydrofacies can be distinguished for the *St* lithofacies (Table 2.1). The dark brown sets of fine sand (hydrofacies type *St,f* = trough cross-bedded fine sand) show a low hydraulic conductivity of $K = 6.23 \times 10^{-6} \pm 5.25 \times 10^{-6}$ m/s ($n = 0.24 \pm 0.05$). The coarser sets have hydraulic conductivities of $K = 5.97 \times 10^{-5} \pm 2.91 \times 10^{-5}$ m/s (hydrofacies type *St,m1* = trough cross-bedded medium sand) and $K = 2.49 \times 10^{-5} \pm 1.34 \times 10^{-5}$ m/s (hydrofacies type *St,m2* = trough cross-bedded medium sand with find sand) ($n = 0.29 \pm 0.04$ for both types). Field tests were performed on top of the outcrop at the locations $x = 7$ m, $y = 1.5$ m and $z = 5.8$ m to 5.3 m for the hydrofacies type *St,m2* and at $x = 27$ m, $y = 1.5$ m and $z = 5.8$ m to 5.3 m for the hydrofacies type *St,m1*. The received data from the Guelph permeameter test (*St,m1*: $K = 6.85 \times 10^{-5}$; *St,m2:* $K = 6.80 \times 10^{-5}$ m/s) and falling head permeameter test (*St,m1*: $K = 1.78 \times 10^{-5}$; *St,m2* $K = 2.17 \times 10^{-5}$ m/s) are in the same range as the laboratory values. Although field derived values approximate the laboratory data well, the data are only suitable for a rough cross-check due to low data quantity and afore mentioned situation in the outcrop.

2.4.6 Hydrogeology of the entire aquifer analog

The spatial distribution of the previously described lithofacies and hydrofacies reveals a distinctive succession throughout all outcrop sections. As shown in Figure 2.5, three genetic units can be determined from the bottom to the top of the outcrop: (1) a continuous layer of aeolian sands (*Sp,f* hydrofacies) at $z < 2$ m, (2) braided river channel deposits of pebbly to fine sands of the hydrofacies types *SGt,c*; *SGt,m* with clay intraclasts (*Fm*), plane sandy bed forms and cross-bedded medium sands of the hydrofacies types *Sp,f*; *Sh/Sp,m1*and *Sh/Sp,m2* at 2 m $\leq z \leq$ 4 m; (3) fluvial sets of cross-bedded medium to fine sands of the hydrofacies types *St,m1*; *St,m2*; *St,f* at 4 m $\leq z \leq$ 5.8 m.

The additional information delivered from the lateral sections A-C and A´-C´ (Figure 2.5d) proved to reduce the uncertainties related to the spatial distribution of the litho- and hydrofacies. For instance, a thin layer of the hydrofacies types *Sh/Sp,m1* occurs in each cross-section at x = 26 m and z = 3 m (Figure 2.5a-c). Intuitively, it could be assumed that this layer is laterally continuous through all sections based on the information from the three main cross-sections. Only with the lateral section could it be observed that this layer is discontinuous, pinches out and reappears in section B-B´ as demonstrated in the lateral cross-section E-E´ in Figure 2.3c.

The average hydraulic conductivity and porosity of the aquifer analog, using a geometric mean, result in $K = 1.36 \times 10^{-4}$ m/s ± 3.83×10^{-4} and $n = 0.29 \pm 0.03$. The average values are calculated based on the areal percentage of the hydrofacies types for all cross-sections. The range of hydraulic conductivity varies over five orders of magnitude from $K = 1.38 \times 10^{-3}$ to 7.84×10^{-8} m/s within the examined deposits (Table 2.1, Figure 2.6). Considering the layered heterogeneity of the system and the high degree of connectivity of the hydrofacies, it can be assumed that the integral hydraulic conductivity for a horizontal flow regime is best approximated by the arithmetic mean with $K = 2.74 \times 10^{-4}$ m/s. An important fact has to be regarded for the highly conductive portions (hydrofacies *Sh/Sp,m1*: $K = 1.38 \times 10^{-3}$ m/s) of the aquifer analog in terms contaminant transport. Conductivity contrasts with high permeable zones in heterogeneous porous media cause groundwater streamlines to converge and diverge, resulting in flow focusing and enhanced transverse mixing and reaction (Werth et al., 2006). For vertical flow directions the low permeable units of the trough cross bedded fine sands (*St,f*: $K = 6.23 \times 10^{-6}$ m/s) on top are more relevant for the system. The minor presence of the clay fragments (*Fm*: $K = 7.84 \times 10^{-8}$ m/s) of < 1% in the entire outcrop does not play a hydraulically relevant role in the aquifer analog.

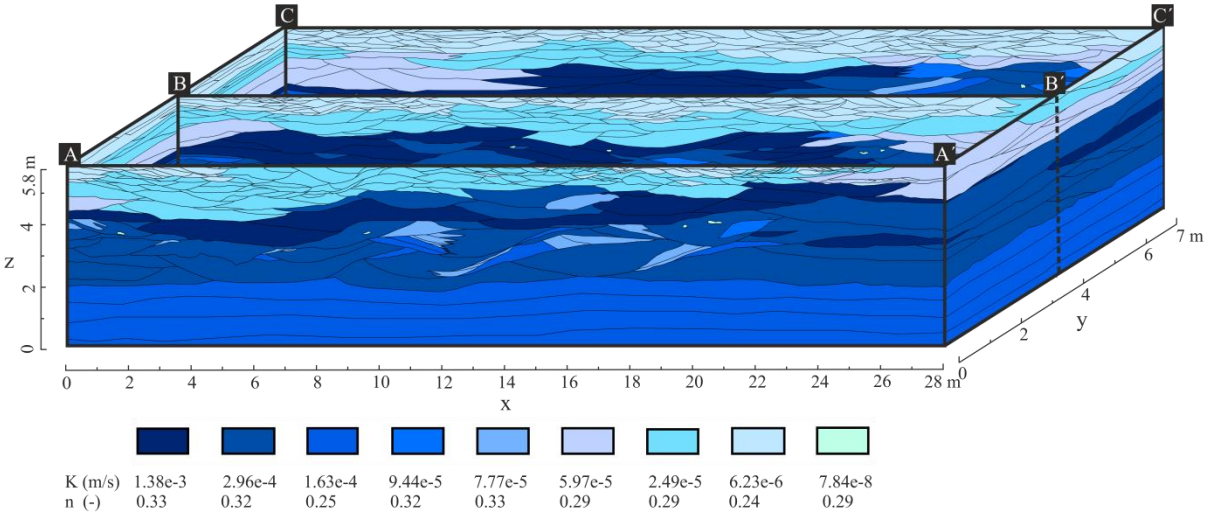

Figure 2.6. Hydraulic conductivity (*K*) and porosity (*n*) distribution of the quasi-three-dimensional aquifer analog model.

2.5 Discussion and hydraulic implications for the GAS

Detailed sedimentological and hydrogeological investigations were conducted in an open pit mine near the city of Descalvado (SP), Brazil, to identify hydraulic properties and spatial hydraulic variations of the heterogeneous fluvial-aeolian deposits in the upper part of the Pirambóia Formation of the Guarani Aquifer System. A sand body of the size Lx = 28 m, Ly = 7 m and Lz = 5.8 m was carefully examined and gradually excavated to construct three equally spaced 2D cross-sections following the common aquifer analog construction practice. The existing aquifer analog construction procedure (Bayer et al., 2011) was amended in this study by additionally constructing cross-sections of the corresponding lateral sections of the sandy body as described in (Kessler et al., 2013). The assemblage of the three 2D cross-section maps with the corresponding lateral cross-sections considerably reduced the uncertainties related to the three-dimensional shape of identified sedimentary structures. Although the aquifer analog construction process and the chosen discretization scale yield satisfying results, additional lateral sections throughout the outcrop are recommended in future aquifer

analog studies, in order to better represent discontinuities and small-scale variations of sedimentary features in the middle of the sedimentary block.

Five lithofacies types were identified and further categorized into nine hydrofacies types providing a detailed insight into the heterogeneity of the fluvial-aeolian facies association in the upper Pirambóia Formation. A quantitative description of spatial hydraulic parameter distribution, based on lithofacies and hydrofacies categories with their spatial distribution and volumetric shares is provided. In combination with modeling tools, the generated dataset allows for the simulation of groundwater pollution scenarios representing realistic field conditions of similar sedimentary settings. Therefore, it serves as a platform to test and evaluate the potential effects of anisotropic flow and contaminant migration patterns as well as the feasibility of the necessary remediation measures on a local scale.

Further, the dataset provides the basis to develop a volumetric 3D model conditioned by the outcrop cross-sections using stochastic methods, as well as numerical up-scaling procedures. For these above mentioned purposes and applications primary geostatistical quantities such as facies specific volumetric fractions, correlation lengths, and anisotropies can be derived. Alternatively, transition probabilities between different facies may be determined or the facies mosaics may serve as training patterns to apply multi-point geostatistics (Comunian et al., 2011) (see appendix A for a 3D multiple-point simulation of the aquifer analog).

The following hydrogeological outcomes of the aquifer analog study are considered especially relevant: 1) the horizontally laminated to planar cross-stratified sands could be identified as the most the permeable unit within the examined facies association (hydrofacies *Sh/Sp,m1* = 1.38×10^{-3} m/s); 2) the high permeable hydrofacies *Sh/Sp,m1* is relatively well connected throughout the entire outcrop and therefore, can serve as preferential groundwater flow path. If an aquifer with this type of sediments is contaminated a pronounced fingering of a contaminant plume can occur.

Commonly, practitioners see the GAS as a relatively homogeneous system. Existing studies report *K* estimates for the entire Priambóia Formation in São Paulo State, which range from 3.47×10^{-5} m/s to 5.78×10^{-6} m/s with an average value of 2.89×10^{-5} m/s. (Hirata et al., 2011). This data is in concordance with the work of Araújo et al. (1999), which reports an average *K* of 2.19×10^{-5} m/s for the entire Pirambóia Formation. The Botucatu Formation in São Paulo State has an average hydraulic conductivity of $K = 4.05 \times 10^{-5}$ m/s (range from 2.31×10^{-5} to 4.63×10^{-5}m/s), which is in the same range as reported for the entire Pirambóia Formation (Hirata et al., 2011). The average *K* value derived in this study for the fluvial-aeolian facies association of the Pirambóia Formation is higher than the reported range of *K* values of the entire GAS at São Paulo State. A higher hydraulic conductivity implies higher aquifer vulnerability for areas in São Paulo State, where the fluvial-aeolian deposits of the upper part of the Pirambóia Formation crop out or are close to the ground surface. Additionally, the more pronounced hydraulic conductivity contrasts compared to reported values by Hirata et al. (2011) and Araújo et al. (1999) indicate that in case of contamination, this portion of the Pirambóia Formation is more complex to characterize and remediate.

Although the GAS is very extensive in its dimension, the scale of the presented aquifer analog might be considered as pre-ergodic and at an operative scale is only suited for local applications, the provided approach proved to be helpful for the identification of possible relevant hydrostratigraphic units. It gives valuable insight into local scale aquifer heterogeneities of the GAS in the upper Pirambóia Formation, which should also be considered in a regional scale context. The overall thickness of the fluval-aeolian deposits of the upper Pirambóia Formation ranges from only a few meters to ~ 45 m (Caetano-Chang and Wu, 2006). In contrast to the overall thickness of the GAS units in São Paulo State (Pirambóia Formation: 75 - 270 m, Botucatu Formation: 20 - 238 m (Hirata et al., 2011), the examined deposits might seem of subordinated importance. However, considering the pollution threats

of the GAS in the São Paulo State, it must be pointed out that only detailed hydraulic information of all hydrostratigraphic units, even if they are thin, allows the recognition of potential contaminant flow pathways, which is necessary for reliable mass flux calculations to assess down gradient risks (ITRC, 2010). This is particularly true for highly permeable aquifer units, e.g., the fluvial-aeolian sediments examined in this study.

The detailed characterization of parts of the reservoir helps to improve the understanding of the entire GAS. In particular, the findings aid conceptual model development of aquifer segments where little or no site-specific data is available or for confined areas. Eventually, the work should initialize and foster the construction of additional aquifer analogs of other stratigraphic units of the GAS, to contribute to an advanced reservoir understanding and to support local and regional groundwater management policies.

2.6 Hydrogeochemical investigations

2.6.1 Fieldwork

Hydrogeological characterization of the aquifer analog was complemented by a description of solid-phase sediment Fe(III) concentrations at the same resolution. For this, sediment samples for iron analysis were collected at the site during the fieldwork described in chapter 2.4.1. These sediment samples were taken at the same locations where hydraulic properties of each lithofacies type were determined. For each of the nine hydrofacies types, three sediment samples were taken to determine Fe(III) concentrations in solid phase. The sediment samples were stored in plastic bags and shipped to the University of Tübingen, Germany, for analysis of sediment iron concentration by sequential extraction.

Additionally, each hydrofacies type was examined for its organic carbon content. However, the measured organic carbon contents were below the detection limit (< 0.04 %). Therefore sorption-induced effects on contaminant transport are not considered relevant for the

investigated sediments. In front of the outcrop (completion depth = 2.5m), a 5-cm groundwater monitoring well was temporarily installed to obtain the chemical composition (major ions) of the ambient pristine groundwater for later reactive transport modelling purposes described in chapter 3. The groundwater sample was analyzed at the Análises Ambiental laborator in Rio Claro (Brazil).

2.6.2 Sediment extraction

Fe(II) and Fe(III) contents were measured by sequential extraction of Fe from the 27 sediment samples. For this, 0.5 g sediment was filled in 58 mL serum bottles (triplicate of each sample). After adding 25 mL 0.5 M HCl, the samples were put on a shaker table for 1 hour to dissolve amorphous and poorly crystalline Fe phases. Crystalline Fe was extracted by adding 6 M HCl to the sample and incubation for 24 hours in a 70° C water bath. The dissolved Fe(II) was determined in the liquid phase by ferrozine assay (Stookey, 1970). The purple-colored ferrozine complex was quantified spectrophometrically at 562 nm using a microtiter plate reader (FlashScan 550; Analytik Jena, Jena, Germany). The concentrations of Fe(III) were determined by the difference between Fe(II) and Fe(total).

2.6.3 Sedimentary Fe(III) distribution

In the first sediment extraction step with 0.5 M HCl, the amount of amorphous and poorly crystalline Fe phases could not be quantified, because concentrations did not reach the measureable level (< 10µM). Analysis of crystalline phases by the second sediment extraction step with 6 M HCl showed mainly low concentrations of Fe(III) for most parts of the outcrop (< 5 mg Fe(III)/g sediment) (Figure 2.7).

For instance, the sand and gravel facies with $K = 2.96 \times 10^{-4}$ m/s contains very little Fe(III) (0.19 mg/g sediment) (Figure 2.8). Higher Fe(III) concentrations (> 5 mg Fe(III)/g sediment) were found in the upper part of the outcrop (Figure 2.9), where low permeable facies with

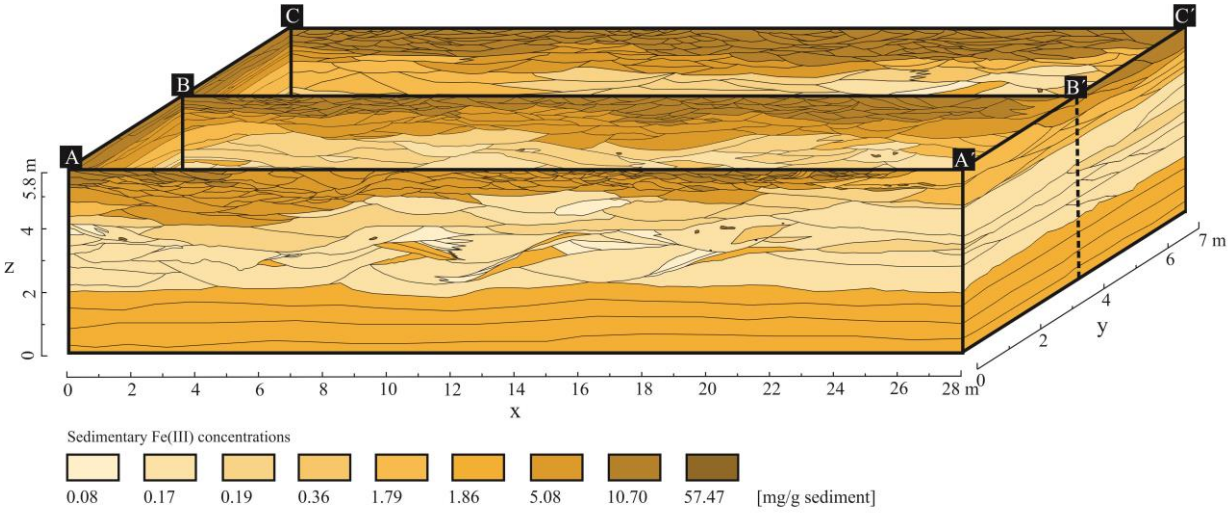

Figure 2.7. Sedimentary Fe(III) distribution of the quasi-three-dimensional aquifer analog model.

$K = 6.23 \times 10^{-6}$ and 2.49×10^{-5} m/s predominate (Figure 2.6).

The highest Fe(III) concentrations (57.47 mg Fe(III)/g sediment) were found in low permeable clay lenses, which cover less than 1% of the cross section and thus play a negligible role for the bulk sedimentary oxidation capacity of the outcrop.

Figure 2.8. Sand and gravel lithofacies with minor iron-oxide grain coatings (refers in Figure 2.6 to zones with $K = 2.96 \times 10^{-4}$ (m/s) and in Figure 2.7 to zones with Fe(III) = 0.17 (mg/g sediment)).

Overall, the Fe(III) concentrations in the outcrop vary over nearly four orders of magnitude (0.08 – 57.47 mg Fe(III)/g sediment) and correlate inversely on log scale (R = -0.3) with hydraulic conductivity values (Figure 2.10). Although the laboratory analyses revealed no

amorphous or poorly crystalline Fe(III) oxide minerals, such as ferrihydrite, a relevant amount of crystalline Fe(III) species (goethite, hematite) is available at the site.

Figure 2.9. Trough cross-bedded sand lithofacies with iron-oxide grain coatings (refers in Figure 2.6 to zones with K = 6.2 × 10^{-6} (m/s) and in Figure 2.7 to zones with Fe(III) = 10.7 (mg/g sediment)).

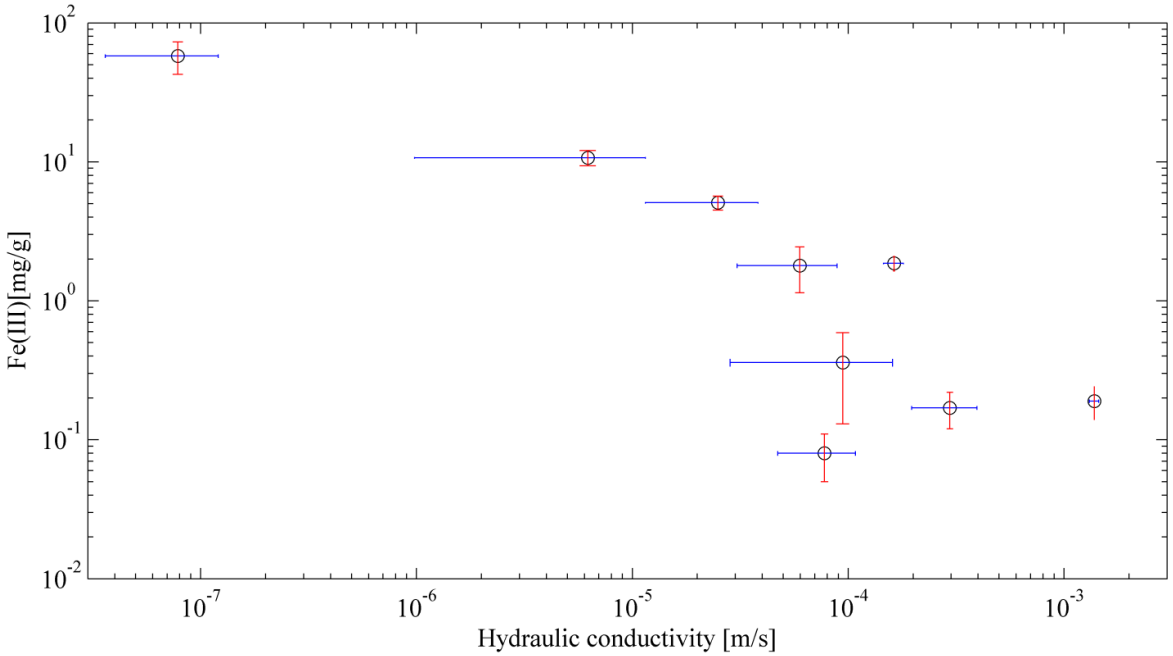

Figure 2.10. Inverse correlation between the hydraulic conductivity and Fe(III) concentrations at the site.

While microorganism prefer amorphous and poorly crystalline Fe(III) as readily accessible species during dissimilatory Fe(III) reduction, the less thermodynamically favorable crystalline solid-phase Fe(III) oxides (goethite, hematite and magnetite) can also be utilized by Fe(III) reducing microorganisms (Weber et al., 2006) as suggested in previous studies (e.g.,

Bonneville et al., 2009; Childers et al., 2002; Lovley et al., 1996; Nevin and Lovley, 2002). Based on the laboratory findings goethite as crystalline Fe(III) species are assumed for the reactive transport simulations in the following chapter 3.

3 Modelling (I): Investigations of solid-phase Fe(III) distribution for NA potential

3.1 Problem description

Sedimentary aquifers often exhibit a high spatial variability of hydraulic properties, which profoundly affects the transport, mixing and distribution of groundwater pollutants. Classical remediation efforts, such as pump-and-treat, to restore aquifers to pre-contaminant-release conditions turned out to be inefficient and expensive in many cases. Therefore, natural attenuation (NA) has become a preferred strategy to remediate polluted groundwater at many contaminated sites (MacDonald, 2000; Wiedemeier et al., 1999). NA includes physical, chemical and biological processes and reactions, that may reduce the mass, toxicity, mobility, volume and concentrations of groundwater and soil contaminants under favorable conditions (USEPA, 2004). For instance, BTEX (benzene, toluene, ethyl-benzenes, xylenes) can be readily degraded or transformed via microbially mediated oxidation with dissolved oxygen, nitrate, sulfate and with sedimentary iron-oxyhydroxides, if the appropriate electron acceptors are available (Wiedemeier et al., 1999). Important for *in situ* biodegradation of contaminants is the mixing of dissolved electron acceptors (mobile, such as O_2, nitrate, sulphate) from the ambient groundwater with electron donors (e.g., groundwater pollutant) by transverse and longitudinal dispersion. It has been shown that in heterogeneous aquifers exhibiting high permeability zones within low-permeability fields flow focusing occurs, which leads to a significant enhancement of transverse mixing and enhanced biodegradation in reactive plumes (Bauer et al., 2009; Rolle et al., 2009; Werth et al., 2006). Microbially mediated degradation, however, can also occur when electron donors from the dissolved plume get into contact with solid or adsorbed (immobile) oxidants in the aquifer matrix causing e.g., reduction of solid phase Fe(III). Fe(III) oxides in amorphous (ferrihydrite) or crystalline phases (goethite, hematite, magnetite) are abundant in most sedimentary aquifers and play a crucial role as

solid state electron acceptors for intrinsic bioremediation and as a consequence, they may constrain the propagation of organic contaminants (e.g., Christensen et al., 2000; Cornell and Schwertmann, 2003; Dethlefsen et al., 2004; Jakobsen and Postma, 1999; Lyngkilde and Christensen, 1992; Tuccillo et al., 1999).

In natural systems commonly not only the physical but also the chemical properties vary spatially. This applies to the mineral components of sediments, as well as to the distribution of organic matter and ferric iron. Both the physical and chemical heterogeneity are crucial factors for the effectiveness of *in situ* bioremediation processes (e.g., Cunningham and Fadel, 2007; Scheibe et al., 2006). For instance, if immobile electron acceptors (e.g., mineral-bound ferric iron) are associated with rather fine grained/low permeable aquifer units, while dissolved electron donors (contaminant) preferentially migrate along highly permeable and well-connected zones, this may adversely affect and limit the extent of *in situ* bioremediation processes (Scheibe et al., 2006). Cunningham and Fadel (2007) underlined the relevance of the spatial correlation between physical properties and abiotic degradation rates for plume behavior. In particular, they demonstrated that if physical and chemical aquifer parameters inversely correlate the fingering of a plume can be more pronounced and the overall contaminant degradation is slower. These findings point out the importance to accurately localize and quantify geochemical aquifer parameters and to account for both physical and chemical heterogeneities in conceptual and numerical models for realistic assessment of natural attenuation success. Consideration of dual and highly resolved aquifer heterogeneities in models is rare due to large efforts and high costs. For only a few cases physical and chemical heterogeneities have been resolved in detail (e.g., Allen-King, 1998; Allen-King et al., 2006; Allen-King et al., 2002; Anneser et al., 2010; Cozzarelli et al., 2001; Ritzi et al., 2013; Scheibe et al., 2006). Commonly hydrogeological site description is limited to information obtained from point data. An adequate reproduction of relevant small-scale (cm-

dm) sedimentary and geochemical heterogeneities requires comprehensive high-resolution depth resolved sediment and groundwater samples, which have to be further analyzed in the laboratory.

The ultimate approach to highly resolve dual subsurface heterogeneity is investigating geological formations exposed in outcrops, which are images of those that host aquifers at other locations. Insight can be gained for example in young open-pit gravel mines, were the water table is temporarily lowered. Outcrops found here allow a high-resolution mapping, sampling and description (cm-scale) of physical and chemical aquifer parameters. This minimizes uncertainty of sedimentary structures and properties in comparison to models based on point data only. The detailed information from an outcrop can be incorporated into a numerical flow and transport model, which serves as an analog model of an aquifer portion. A variety of aquifer analog studies exist so far that describe sedimentary structures and related hydraulic properties (Bayer et al., 2011; Bersezio et al., 1999; Bersezio et al., 2004; Heinz et al., 2003; Höyng et al., 2014; Kessler et al., 2013; Weissmann and Fogg, 1999), but none of these studies considers small-scale (cm-dm) geochemical heterogeneities, such as facies specific Fe(III) content. Since the aquifer analog concept is best applicable on a local scale (Bersezio, 2007), it provides the ideal platform in combination with reactive transport modelling to examine and forecast NA processes and potentials, for instance, for a hypothetical contamination from a petroleum hydrocarbon spill. A self-evident and tempting step towards even more realistic characterization of NA processes is modelling not only the observed physical but also chemical heterogeneity.

This chapter describes a numerical reactive transport experiment that employs a 2D high-resolution outcrop cross-section from the previously constructed analog model with physical and chemical properties (Figure 2.6, Figure 2.7). This experiment investigates the influence of small-scale physical and chemical heterogeneities on the transport and fate of a hypothetical

petroleum hydrocarbon contamination. The focus of the study is on the heterogeneous distribution of sediment bound Fe(III) as a solid-phase electron acceptor. Its role for the effectiveness of *in situ* bioremediation of organic compounds in the upper Pirambóia Formation of the Guarani aquifer is modelled and discussed.

Additionally to the previously described fieldwork for the aquifer analog construction, a groundwater monitoring well was installed in front of the outcrop to determine the chemical composition of the ambient groundwater. By combining the information on geology and groundwater, a 2D numerical reactive transport model was developed that incorporates the physical and chemical properties at the site as much realistic as possible.

The presented aquifer analog model of a segment of the Guarani aquifer is unique in the aspect that it honors cm-scale variation in hydraulic properties, solid-phase Fe(III) concentrations based exclusively on hard data and dissolved electron acceptors of the background groundwater representing true and realistic field conditions. It is the first time that the Pirambóia Formation of the Guarani aquifer was investigated in such hydrogeological and hydrogeochemical detail for a numerical experiment to assess the transport dynamics and potential for *in situ* biodegradation.

3.2 Reactive transport modelling

3.2.1 Model setup

A numerical groundwater flow and transport model was setup to simulate reactive processes of an oxidizable organic compound. The model represents a detailed reconstruction of the 2D outcrop cross-sections as shown in Figure 3.1. The cross-section in Figure 3.1a corresponds to the profile A-A´ in Figure 2.6. The cross-section in Figure 3.1b corresponds to profile A-A´ in Figure 2.7. Due to a maximum number of 500 columns in the used

groundwater modelling software, Visual MODFLOW, the cross-section length was set to 25 m instead of 28 m, while maintaining the resolution of the original dataset (cell size 0.05 m).

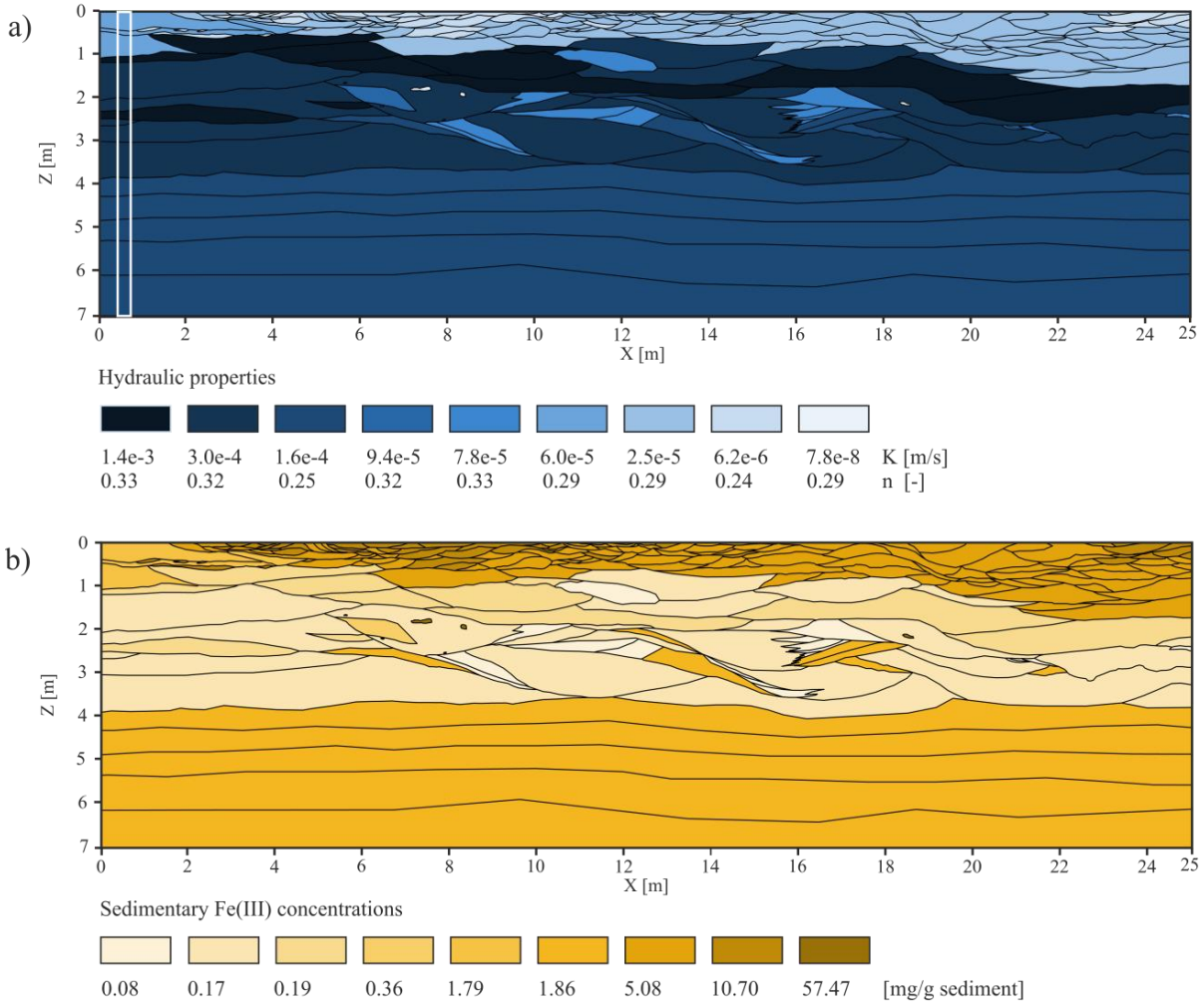

Figure 3.1. a) Hydraulic conductivity and porosity distribution of the 2D aquifer analog section. The dimension of the hypothetical source zone is delineated with a solid white line. b) Corresponding sedimentary Fe(III) concentrations of the analog section.

Further, additional samples from drill cores in front of the outcrop allowed to extent the thickness of the continuous and homogeneous bottom layer by 1.2 m. Thus, the dimensions of the cross-section used in the model are 25 m in length and 7 m in depth. In the groundwater model, a general flow direction from the left to the right is assumed. For modelling and illustration purposes, here the original cross-sectional profile was reversed in x-direction to ensure sufficient release of dissolved contaminant into the aquifer through highly permeable zones.

The model domain was discretized into 70 000 cells by a regular grid ($\Delta x = \Delta y = 0.05$ m). Hydraulic conductivity (K) and porosity (n) values as well as iron concentrations were assigned to the grid cells according to the distribution presented in Figure 3.1. A constant head boundary was used for both the inflow (left) and outflow (right) boundary of the model domain imposing a regional hydraulic gradient of 0.001. The steady-state groundwater flow was simulated using USGS finite differences code MODFLOW 2000 (Harbaugh et al., 2000). A homogeneous toluene source over the full depth of the model domain was emplaced at the upgradient model boundary between x = 0.6 m and 0.9 m. This is illustrated schematically in Figure 3.1a. Toluene (C_7H_8) was selected as a single reactive compound. This represents a simplification to keep the study focused, although commonly petroleum contaminations at many sites contain a mixture of multiple components (e.g., BTEX´s) (Vencelides et al., 2007). Toluene is an important component of gasoline and, for example, considered by the U.S. Environmental Protection Agency as a priority pollutant (ATSDR, 2000). The initial concentration of the source zone contains 0.1 mol toluene/L_{bulk}, below its solubility chosen to induce transient source conditions within the short simulation period of 100 days. It has to be mentioned that the model set up in terms of initial concentration, source geometry and simulation period impacts the general transferability of the simulated plume dynamics. Often contamination occurs in larger volumes over several decades (e.g., Vencelides et al., 2007). However, these assumptions are favored to limit the computational burden, while obtaining precious insight into transient contaminant plume behavior.

To account for local scale microdispersivity, the longitudinal (α_L) and transverse (α_T) dispersivity was set to local low values of 2.5×10^{-2} m and 2.5×10^{-4} m, respectively. The high-resolution physical heterogeneity deduced from detailed outcrop investigation directly accounts for larger-scale mixing and dilution processes such as flow-focusing (e.g., Rolle et al., 2009; Werth et al., 2006). The reactive transport simulations were performed using the

multicomponent reactive transport code PHT3D (Prommer et al., 2003a), which couples MT3DMS (Zheng and Wang, 1999) with the geochemical model PHREEQC-2 (Parkhurst and Appelo, 1999).The reaction module by D'Affonseca et al. (2011) was applied. The reaction network defined in the model accounts for dissolution, degradation under aerobic, denitrifying, iron-reduction and sulfate-reduction conditions and mineralization of the NAPL, as well as dissolution/precipitation reactions of goethite and siderite. The hydrochemical composition of the simulated groundwater was defined according to the sampled groundwater from the site (Table 3.1).

Table 3.1. Initial chemical composition of pristine groundwater from the site in Descalvado used in the model.

Parameter	Unit	Value
temperature	C	21
pH	-	5.48
Ca^{2+}	mol/L	3.20×10^{-5}
Fe^{2+}	mol/L	7.82×10^{-6}
Fe^{3+}	mol/L	7.83×10^{-10}
K^{+}	mol/L	1.40×10^{-5}
Mg^{2+}	mol/L	8.47×10^{-6}
NO_3^{-}	mol/L	4.83×10^{-5}
O_2	mol/L	5.00×10^{-4}
Alkalinity	mol/L	6.55×10^{-5}

Two different scenarios of different solid-phase electron acceptor distribution were set up for the analog cross-section, and for each the toluene plume evolution was investigated for a simulation time of 100 days. Both scenarios rely on the same hydraulic parameters, source geometry, contaminant concentration, and initial chemical composition of pristine groundwater. Scenario 1 (HOM FeOOH) represents a homogeneous distribution of goethite (FeOOH) as electron acceptor. This imitates standard hydrogeological practice, which commonly has to rely on sparse point data or hydraulic measurements only. The goethite concentration was calculated as weighted average from the distribution in the outcrop (8×10^{-5} mol/L_{bulk}). Scenario 2 (HET FeOOH) accounts for the measured hydrofacies specific iron concentrations.

3.2.2 Plume development and tempo-spatial evolution of redox zonation

Scenario 1, HOM Fe(OOH)

The dissolution of the emplaced toluene source at the left model boundary leads to the formation of dissolved phase of toluene evolving into the downgradient model domain. The physical heterogeneity represented in the outcrop analog (Figure 3.1a) strongly influences the development and migration of the plume (Figure 3.2a). The moderately layered structure of the outcrop analog with predominantly lower conductivities (K = 6.23 × 10^{-6} - 7.77 × 10^{-5} m/s) in the upper part (z = 0-1 m), highest ones in the middle (z = 1-4 m) and medium ones in the bottom part (z = 4-7 m) causes a distinct stretching and fingering of the plume. For instance, after simulation period of 20 days, it can be seen from the toluene concentration profiles (Figure 3.2a) that the plume has propagated by < 1.5 m in the top layer and by < 3m in the bottom part, whereas in the center it advanced over almost 9 m through well connected higher conductive pathways.

Small scale (cm-dm) highly conductive units (at z ~ 1.1 m and 1.7 m) in the source zone cause the most rapid depletion of the source and lead to locally lower concentrations in internal parts of the plume. After a simulation period of 100 days a small fraction of the plume in the top low permeable layer has not traveled further than 3 m in horizontal direction. This fraction is still connected to the central part of the plume, which has already partially left the model domain (Figure 3.2a). Highly permeable zones adjacent to the low permeable top layer provide thin “feeder channels”, which constantly release low concentrations of toluene into the central part of the model domain. Here, transverse mixing with pristine groundwater happens which enters the model domain through the depleted source zone.

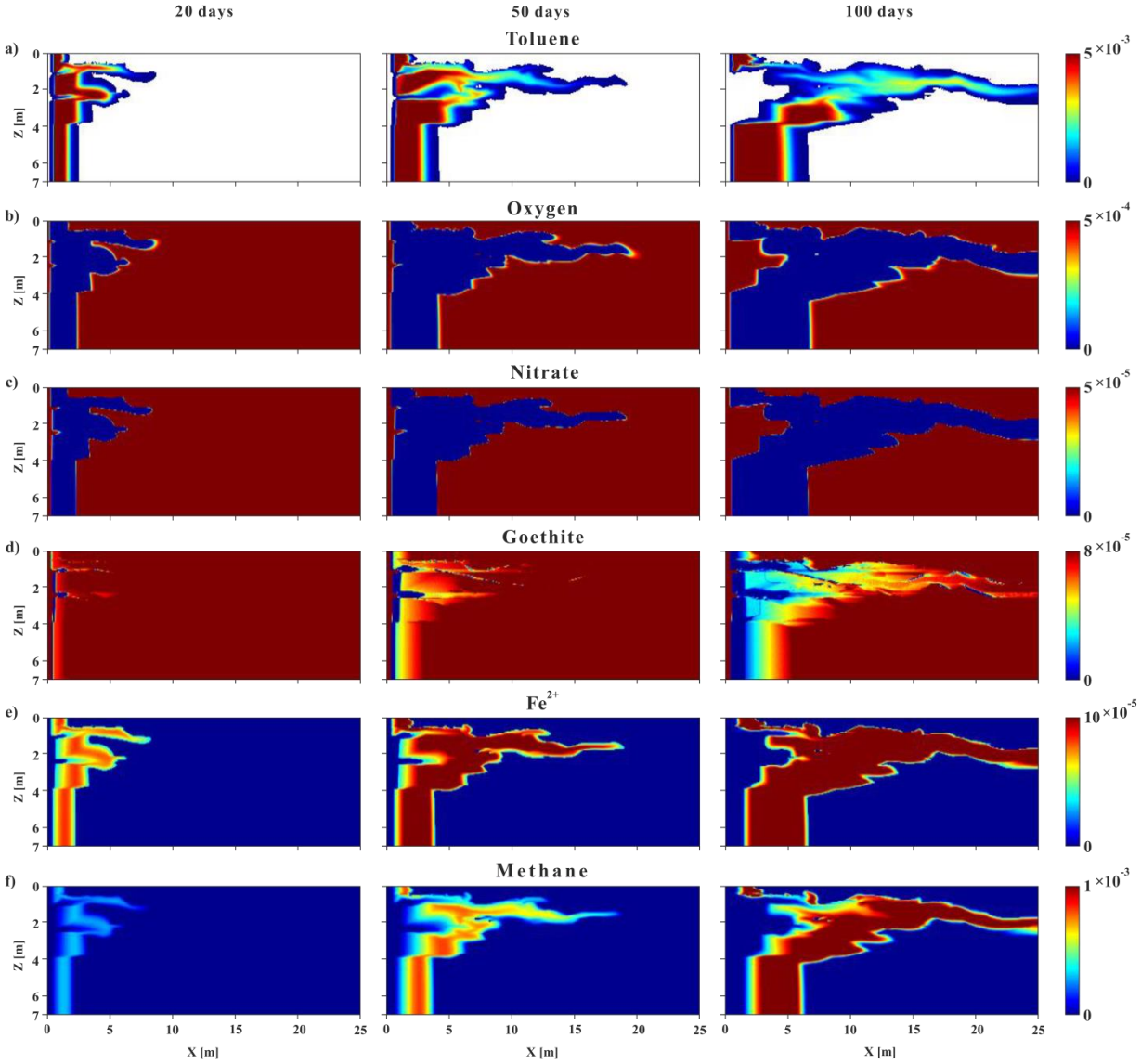

Figure 3.2. Simulated geochemical evolution in the outcrop analog for a initially homogeneous distribution of solid-phase Fe(III); a) toluene concentrations, b-d) consumption of dissolved mobile electron acceptors oxygen and nitrate, and consumption of goethite, e-f) generation of dissolved ferrous iron and methane for the time snap shots at 20, 50, 100 days simulation period. Note, all concentrations refer to mol/L and mol/L_{bulk} for goethite.

During the development and degradation of the contaminant plume the evolution of the redox zonation is a dynamic process. Redox conditions vary spatially involving aerobic and anaerobic processes and the dissolution of goethite and methanogenesis. Electron accepting processes change when formerly abundant and more favorable electron acceptors become depleted. After the start of simulation and the source zone release, reducing conditions start to emerge downgradient where the plume develops. The *in situ* biodegradation of toluene induces a rapid depletion of dissolved oxygen and these aquifer areas becomes anoxic. Like-

wise, a fast shift from nitrate reducing conditions to Fe(III) reduction occurs (Figure 3.2b,c). It can be seen from the concentration profiles for oxygen and nitrate that the depleted areas coincide with the shape of the horizontally expanding plume (Figure 3.2a). After the consumption of dissolved oxygen and nitrate, redox processes rapidly progress and consequently iron reduction becomes the terminal electron accepting process (TEAP). The reductive dissolution of Fe(OOH) leads to decreased concentrations along the plume fringe and full depletion in the interior part of the plume and around the source area (Figure 3.2d).

Along with the reductive dissolution of Fe(OOH) ferrous iron is released and dissolved Fe^{2+} concentrations start to increase at the plume fringe (Figure 3.2e, time = 20 days). Although the model allows for the formation of siderite ($FeCO_3$), precipitation is prevented, due to pH values below 6, and cannot be observed within the simulation period of 100 days. Siderite formation is favorable under slightly acid to neutral pH values (Appelo and Postma, 2005; Stumm and Morgan, 1996). If the conditions for siderite formations are met at later stages during plume development, the released ferrous iron would be consumed and incorporated into the formation of secondary minerals (siderite). Since sulfate does not exist in the background groundwater composition no sulfate reduction occurs and consequently no precipitation of pyrite (FeS) is possible. The formation of secondary minerals such as siderite or pyrite potentially may provide a temporary sink for the oxidation capacity as described in Vencelides et al. (2007). Due to the relatively low goethite concentrations the reduction of iron oxides diminishes and the conditions in the aquifer quickly shift to the final stage in the reductive sequence. The model suggests the start of methane production already after 20 days of simulation (Figure 3.2e).

Scenario 2, HET Fe(OOH)

Scenario 2 accounts for a heterogeneous distribution of goethite as electron acceptor. The geochemical response induced by the degradation of toluene is partly similar as described for

scenario 1. Electron donors are preferentially delivered to the highly permeable portions, which contain overall very low goethite concentrations. Thus, the concentration profiles for toluene for the time shots at 20 days and 50 days of the simulation period (Figure 3.3a) are almost identical to scenario 1 (Figure 3.2a). Slightly elevated toluene concentrations can only be observed at 100 days in the most advanced part of the plume (Figure 3.3a) but the overall effect due to chemical heterogeneities on the shape and length of the toluene plume is negligible. In contrast to scenario 1, the simulated distribution of dissolved ferrous iron concentrations (Figure 3.3e), generated by microbial iron reductions, now differs significantly. Since it is related to the distribution and concentration of solid-phase iron (goethite), lower concentrations occur in the middle layer of the aquifer.

Important to note is that after a simulation period of 100 days the upper part of the model domain with the highest goethite concentrations still remains free of electron donors due to the low permeability of the sediments, which significantly reduces the effective oxidation capacity.

3.3 Implictions of solid-phase Fe(III) heterogeneity for NA potential in the GAS

The laboratory results identified that the ferric iron in the investigated sediments of the upper Pirambóia Formation do not contain measurable amounts of amorphous or low crystalline phases. Only crystalline phases are present but these are heterogeneously distributed with the highest concentrations in the low permeable hydrofacies. The numerical simulations reveal a minor impact of a homogeneous (scenario 1) versus a heterogeneous (scenario 2) ferric iron distribution on plume concentrations for the chosen set-up. This might be related to the fact that the homogeneous scenario assumes a solid-phase iron concentration based on the weighted mean (8×10^{-5} mol/L_{bulk}), which is close to the low values present in most parts of the outcrop.

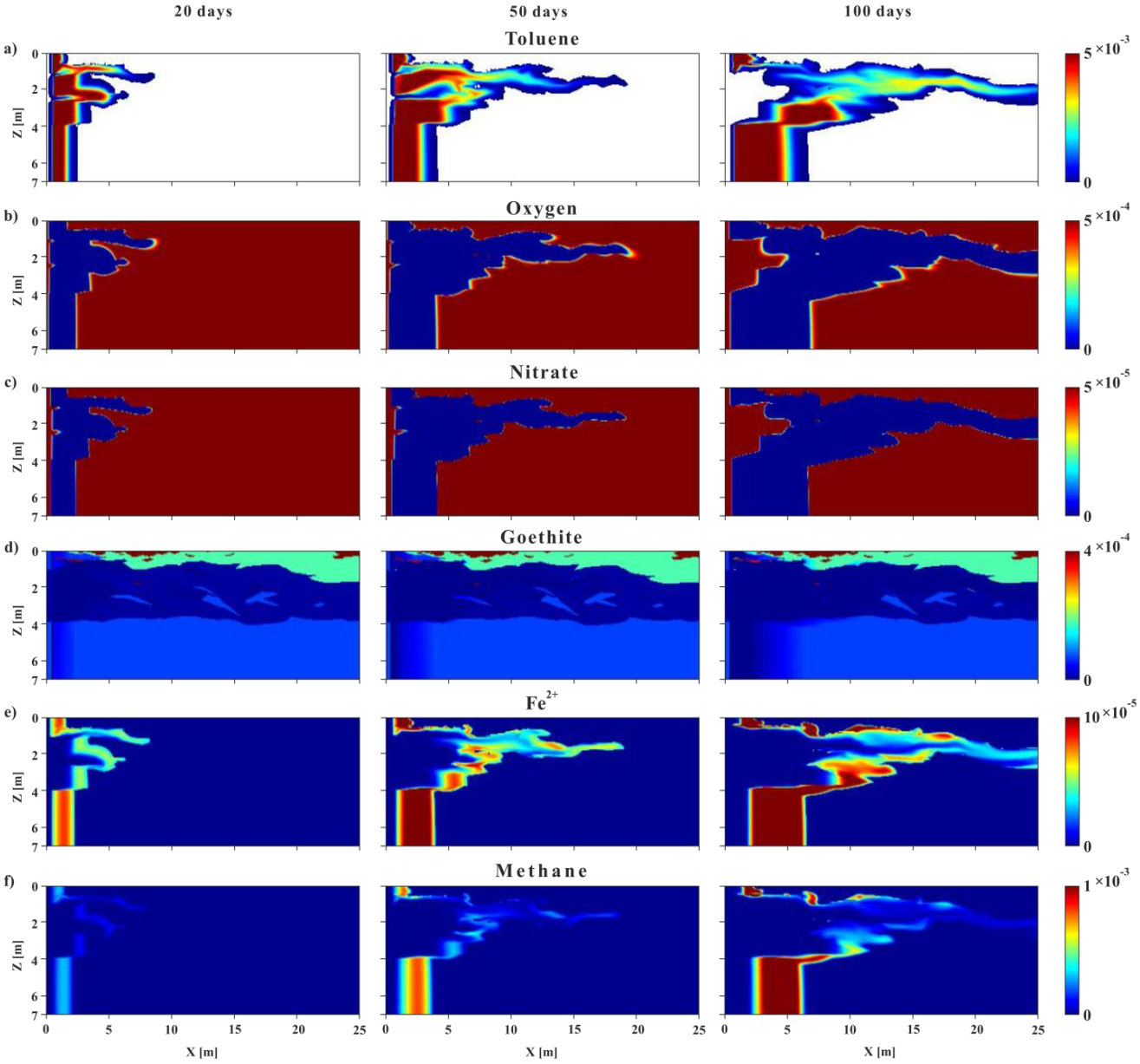

Figure 3.3. Simulated geochemical evolution in the outcrop analog for a initially heterogeneous distribution of solid-phase Fe(III); a) toluene concentrations, b-d) consumption of dissolved mobile electron acceptors oxygen and nitrate, consumption of goethite, e-f) generation of dissolved ferrous iron and methane for the time snap shots at 20, 50, 100 days simulation period. Note, all concentrations refer to mol/L and mol/L_{bulk} for goethite.

If only the highest or the lowest iron concentrations found in the outcrop would be assumed for the entire model domain differences to the heterogeneous distribution (hydrofacies specific iron content) are expected to have a stronger impact on toluene concentrations. However, the results demonstrate the importance of hydrofacies related assessment of immobile electron acceptors for reliable assessment of microbial natural attenuation potential in

aquifers. This is stressed by the fact that the hydraulic conductivity and solid-phase ferric iron concentrations inversely correlate, and thus electron donor and solid-phase electron acceptor do not co-occur, which strongly limits the natural attenuation potential.

The study underlines the importance of a realistic representation of small-scale physical and chemical heterogeneities when assessing the natural attenuation of organics in groundwater. The concept of the joint application of outcrop analog models and reactive transport simulations provide a unique way to elucidate and understand subsurface processes. The simulated complex reaction network incorporates field condition dual heterogeneities and envisions for the first time the degradation and geochemical evolution during a hypothetical petroleum hydrocarbon contamination in the Guarani aquifer on the field scale. The simulations clearly illustrate that the transport and fate of petroleum hydrocarbons in this moderately heterogeneous portion of the Guarani aquifer is governed by the spatial distribution of physical and chemical parameters. The integration of analog models and numerical simulations helps to evaluate *in situ* biodegradation potential, reduces subsurface uncertainties and aids risk assessment in the vulnerable recharge zones of the Guarani aquifer, where the Pirambóia Formation crops out. The findings intend to motivate the construction of additional outcrop analogs in order to develop realistic models that incorporate dual heterogeneities based on hard data and further ask for a three dimensional (3D) simulation of the system.

4 Modelling (II): Effects and implications of aquifer heterogeneity for CSIA based biodegradation estimates

4.1 Problem statement

Over the last two decades monitored natural attenuation (MNA) has become the preferred option to manage aquifers polluted with organic contaminants, mostly due the lack of alternative, truly cost-efficient active remediation technologies (Wiedemeier et al., 1999). As biodegradation is the only natural process that irreversibly reduces contaminant mass, its accurate quantification is essential for the evaluation of MNA effectiveness (e.g., Blum et al., 2009; Meckenstock et al., 2004). Biodegradation is typically accompanied by a measurable enrichment of heavier isotopes (e.g., ^{13}C, ^{2}H) in the non-degraded residual fraction of the contaminant. Therefore, compound-specific isotope analysis (CSIA) has become a regularly used tool to quantify biodegradation and to distinguish the extent of biodegradation from other concentration-attenuating processes in the field (D'Affonseca et al., 2011; Elsner, 2010; Elsner et al., 2005; Griebler et al., 2004; Meckenstock et al., 2004; USEPA, 2008; Van Breukelen and Prommer, 2008). CSIA relies on identifiable changes of stable isotope ratios (e.g., $\delta^{13}C$, $\delta^{2}H$) and the extent of biodegradation is commonly quantified using the Rayleigh equation (Abe and Hunkeler, 2006; Blum et al., 2009; Elsner et al., 2005; Meckenstock et al., 2004). The key advantage of this approach is that it is easy-to-use. Strictly, the application of the Rayleigh equation requires a fully mixed and closed system where degradation is the only isotope fractionation process and can be expressed as:

$$\frac{R_t}{R_0} = \left(\frac{C_t}{C_0}\right)^{\alpha-1} \tag{1}$$

where C_0 and C_t denote the concentrations of a compound with the corresponding stable isotope ratios R_0 and R_t. The subscript indicates the time when the transformation reactions begins ($t=0$) and any later time ($t>0$). The extent of isotope fractionation is quantified by the

isotope fractionation factor α. The isotope fractionation factor α can also be expressed as the enrichment factor ε, which is defined as $\varepsilon = \alpha$-1. However, the criteria for the Rayleigh equation are not always met under field conditions, where besides biodegradation other processes (e.g., dilution/dispersion/sorption) cause concentration changes (Mak et al., 2006).

Physical aquifer heterogeneity affects the fate of biodegrading compounds in various ways. For example, heterogeneity plays an important role on the shape and the time-scales of depletion of contaminant source zones (D'Affonseca et al., 2008; Fure et al., 2006). It is equally relevant for the geometry and longevity of the plumes that develop in the dissolved phase since non-uniform permeability distribution enhances mixing and thus accelerates biodegradation reactions (e.g., Bauer et al., 2009; Dentz et al., 2011; Werth et al., 2006). Consequently the biodegradation rates of dissolved contaminants can be highly variable during aquifer passage between the contaminant source zone and downgradient sampling locations (Abe and Hunkeler, 2006). Thus, a reliable quantification of the accumulated extent of *in situ* contaminant degradation becomes challenging (e.g., Braeckevelt et al., 2012; Fischer et al., 2007; Thullner et al., 2012; Van Breukelen and Prommer, 2008). For instance, in complex field situations CSIA-based *in situ* biodegradation estimates for BTEX compounds can be accompanied by relatively high uncertainties for a variety of reasons and accordingly restricts its applicability to being only a qualitative indicator (e.g., Van Keer et al., 2012).

Numerous non-destructive isotope-fractionating processes (e.g., dissolution, sorption, volatilization, diffusion) potentially impact biodegradation-induced shifts in isotope signals to a different degree (Braeckevelt et al., 2012). Processes previously believed to be non-isotope-fractionating were recently found to also cause fractionation such as dispersion and mixing (Eckert et al., 2012; Rolle et al., 2010; Van Breukelen and Rolle, 2012). Although dilution and mixing count as the most important non-destructive processes affecting Rayleigh equation based degradation estimates other non-destructive physical processes affecting reaction-in-

duced isotope shifts have been reported (Thullner et al., 2012). They are considerably smaller than for biodegradation itself and potentially negligible for most sites (Thullner et al., 2012). Possible effects of small-scale mass transfer (Thullner et al., 2013), mass transfer from non-aqueous phase liquids to aqueous phase (Aeppli et al., 2009), sorption (Höhener and Atteia, 2010; Höhener and Yu, 2012; Kopinke et al., 2005; Van Breukelen and Prommer, 2008), volatilization (Kuder et al., 2009), diffusion (Bouchard et al., 2008; LaBolle et al., 2008). Furthermore, Qiu et al. (2013) and Eckert et al. (2013) systematically investigated and discriminated the effects of biodegradation-induced, sorption-induced, and transverse-dispersion-induced effects on the overall isotope shift in a meso-scale tank experiment and reactive modeling study. Their results show that for process identification highly resolved data for concentrations and isotope ratios are required as well as reactive transport models that account for nonlinear degradation kinetics and isotope fractionation by reactive and physical processes.

Alternatively, CSIA-based quantification of biodegradation may also be carried out using numerical models, which allow for the consideration of more complex physical and chemical conditions, such as simultaneous occurrence of multiple degradation pathways and spatio-temporal variations of the aquifer's redox conditions (Atteia et al., 2008; D'Affonseca et al., 2011; Pooley et al., 2009; Prommer et al., 2009; Van Breukelen et al., 2005; Van Breukelen and Prommer, 2008). A range of recent studies have addressed the effects of aquifer heterogeneity on the reliability of biodegradation quantification by CSIA (Abe and Hunkeler, 2006; Fischer et al., 2006; Green et al., 2010; Kopinke et al., 2005; USEPA, 2008; Van Breukelen, 2007; Van Breukelen and Prommer, 2008), whereby both theoretical modeling studies of Abe and Hunkeler (2006) and Van Breukelen and Prommer (2008) concluded that physical heterogeneity may cause an underestimation of the extent of biodegradation if the Rayleigh equation is employed for data interpretation. However, these previous studies, which

investigated the impact of physical heterogeneity on CSIA data interpretation were either limited to investigations of simple, homogeneous and layered aquifers (e.g., Kopinke et al., 2005), employed macro-scale approaches in which Fickian dispersion was employed to represent heterogeneity (Van Breukelen and Prommer, 2008) or assumed streamline assemblages without lateral exchange of mass (e.g., Abe and Hunkeler, 2006; Fischer et al., 2007). Only few studies exist that investigated the effect of physical heterogeneities and mixing during transport for hydrogeologically more complex scenarios (e.g., Green et al., 2010). Green et al. (2010) examined in a combined field and numerical modeling study in a complex geological setting the effects of mixing due to aquifer heterogeneities on reaction parameter estimates. They demonstrated that apparent and true rate constants and fractionation parameters associated with denitrification can differ by an order of magnitude or even more.

Given the potential failure of macro-scale dispersion approaches to accurately represent the local-scale dispersion processes that control mixing of biodegrading organic compounds with dissolved electron acceptors (Cirpka et al., 1999; Rolle et al., 2009) this study illustrates and investigates for the impact of non-isotope fractionating processes (dilution/mixing) on CSIA based biodegradation estimates. Numerical experiments are used in which realistic, cm-scale heterogeneities are considered to explore the evolution of carbon isotope signatures at the field scale and assess the reliability of CSIA under such conditions.

Since natural physical cm-scale heterogeneity is ideally depicted by direct examination of outcrops from natural aquifer analogs (Whittaker and Teutsch, 1999), five extremely well characterized aquifer analogs were selected for inclusion in our analysis, ranging from moderately to highly heterogeneous aquifer sections. A successively depleting non-aqueous phase liquid (NAPL) source was emplaced to induce transient source conditions throughout the simulation. Time-lapse concentration and isotope signature snapshots were extracted as primary model outputs. The effects of sorption-induced isotope fractionation processes were not

considered in this study since the measured organic carbon content was below the detection limit (< 0.04 %, at the site in Descalvado) and not explicitly measured at the other sites. Simulated results from both synthetic fully-screened and from multi-level monitoring wells were evaluated and the comparison from different field-estimated and laboratory-derived enrichment factors were used to identify which factors and processes pose the most significant challenges for an accurate CSIA-based field data interpretation in highly heterogeneous geological systems.

4.2 Modelling approach

4.2.1 Aquifer analogs

To warrant a high degree of realism in the numerical experiments, i.e., to consider representative sedimentary heterogeneities on a cm-scale the use of high resolution data is vitally important. In this study this was facilitated by using aquifer analogs that provided highly resolved images of subsurface heterogeneity. Such aquifer analogs are typically constructed from detailed investigations of geological formations at outcrops. Accordingly, they provide a realistic image of the subsurface with respect to similarities in the geological processes and the depositional environment. Hence, instead of employing stochastically generated random permeability fields, five exceptionally well characterized aquifer analogs from outcrops in SW-Germany and SE-Brazil were selected for the present study to represent a range of characteristic 2D spatial facies architectures, geometries, and distribution of unconsolidated gravel and sand deposits as well as their associated hydraulic properties (Figure 4.1).

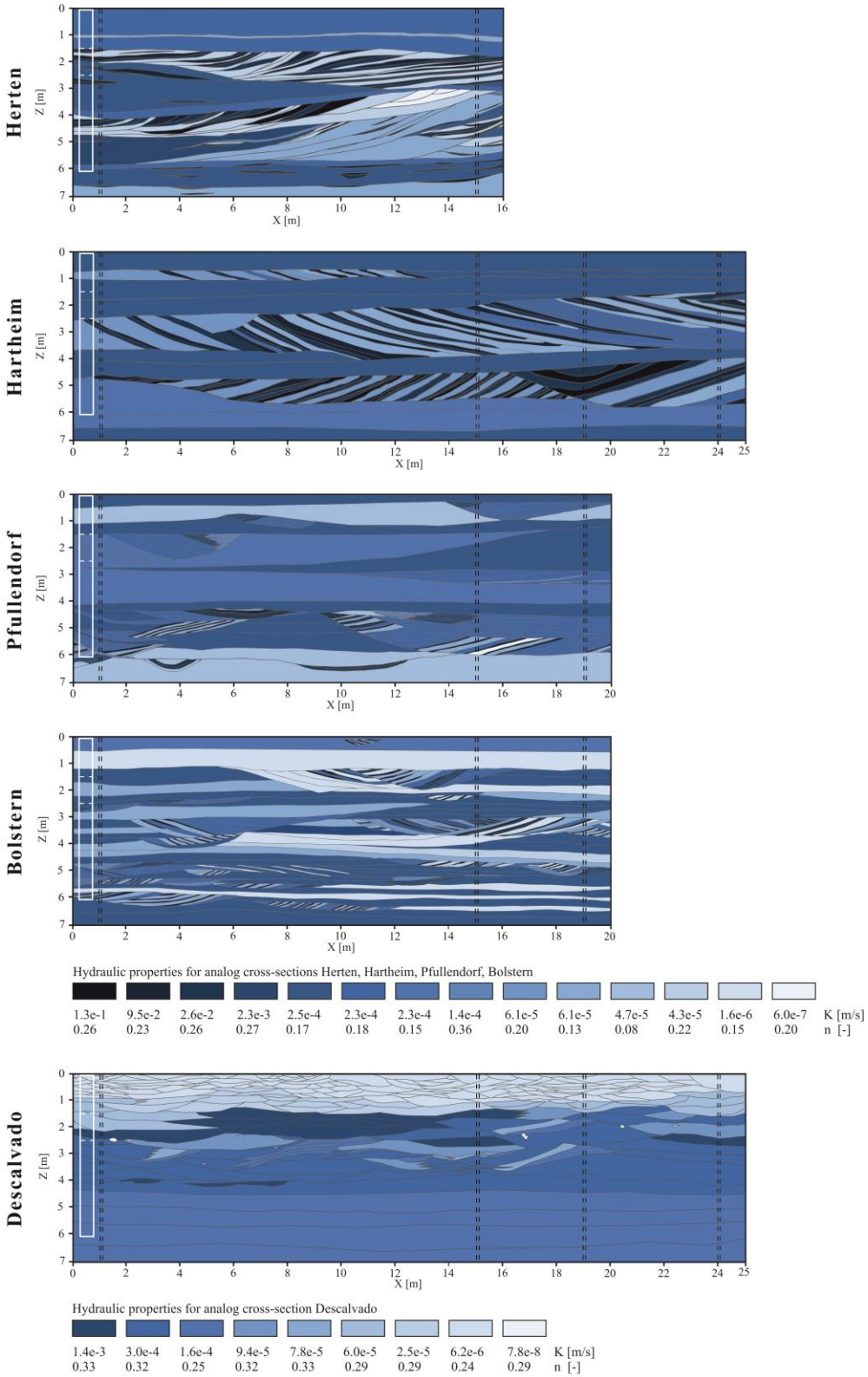

Figure 4.1. Hydraulic conductivity and porosity distribution of high-resolution 2D aquifer analog sections derived from sedimentary architecture of fluvio-glacial gravel beds and fluvial braided river deposits in Herten, Hartheim, Pfullendorf, Bolstern (SW-Germany), and from fluvio-aeolian deposits in Descalvado (SE-Brazil). The maximum dimension of the source zone and virtual well locations are delineated with solid white and black dashed lines, respectively. The white dashed line indicates the lower limit of 1.5m and 2.5m source length and upper and lower limit of 1m source length.

The data were derived from high-resolution outcrop analog studies of fluvio-glacial gravel beds and fluvial braided river deposits from sites near Herten (SW-Germany (Bayer et al., 2011)), Hartheim, Pfullendorf, Bolstern (SW-Germany (Heinz et al., 2003)), and of fluvio-aeolian sediments cropping out near Descalvado (SE-Brazil, São Paulo State (Höyng et al., 2014)). The datasets from SW-Germany (Herten, Hartheim, Pfullendorf, Bolstern) exhibit the common characteristics of sedimentary unconsolidated gravel aquifers (Quarternary), which host some of the most important drinking water resources in Central Europe. The outcrops are located within the paleo-discharge zone of the Rhine glacier in SW-Germany. The variations in depositional environments are reflected in the different characteristic patterns of sedimentary architecture, which allowed a distinction between three basic facies assemblages: (1) The outcrops in Herten and Hartheim represent 'main' discharge areas, which are dominated by thick and extensive 'cut and fill' elements that create a highly complex interfingering of high and low permeable zones; (2) in the Pfullendorf outcrop, which displays a matrix of homogeneous 'accretionary' elements with interbedded small heterogeneous 'cut-and-fill' elements that is typical for the 'intermediate' discharge area; and (3) the Bolstern outcrop which represents 'minor' discharge areas that mainly reveal very small-scale interfingering sedimentary units that result in complex heterogeneity patterns (Heinz et al., 2003). Finally, the Descalvado outcrop in SE-Brazil, located in the upper Pirambóia Formation (Triassic), shows a typical fluvial-aeolian facies association (Höyng et al., 2014) , a relevant portion of the Guarani aquifer, which is one of the most important groundwater reservoirs in the world and the largest aquifer system in Brazil (Puri et al., 2001). The fluvial-aeolian facies association exhibits a rather moderate heterogeneity, which is characterized by continuous layers of aeolian sands, braided river channel deposits interspersed with aeolian sand and sets of fluvial cross-bedded sands (Höyng et al., 2014).

All aquifer analogs were constructed from vertical outcrop walls in sand pits by means of systematic mapping, sedimentological analysis and interpretation of the gravel and sand bodies (Bayer et al., 2011; Heinz et al., 2003; Höyng et al., 2014). The dimensions of the rectangular 2D aquifer analog cross-sections used in this study are 16 m width and 7 m height for the site in Herten, 25 m × 7 m for Hartheim and Descalvado, and 20 m × 7 m for Pfullendorf and Bolstern (Figure 4.1). In related studies at numerous field sites in SW-Germany, comprehensive sedimentary analyses as well as hydrogeological field and laboratory experiments were carried out (Heinz, 2001; Whittaker and Teutsch, 1999). They demonstrated that the typical facies types that can be distinguished in this area represent the building blocks of braided river deposits. As each sedimentary facies is characterized by specific hydraulic properties, outcrop walls can also be depicted by a mosaic of hydrofacies types. Höyng et al. (2014) followed a similar approach for hydraulic parameterization and derivation of hydrofacies types for the fluvial-aeolian facies association at the field site near Descalvado (SE-Brazil). The term 'hydrofacies' was first introduced by Anderson (1989) for units that are relatively homogeneous and hydrogeologically meaningful for purposes of field experiments and modeling. The aquifer analogs from SW-Germany (fluvio-glacial deposits) were classified into 14 different hydrofacies types of distinct sizes and forms. The corresponding hydraulic conductivities of these hydrofacies range from 6.0×10^{-7} m/s to 1.3×10^{-1} m/s and porosities vary from 0.13 to 0.36 (Figure 4.1). Hydraulic conductivity was determined by empirical equations based on the grain size distribution from sieve analysis. The aquifer analog from SE-Brazil (fluvial-aeolian deposits) was classified into 9 hydrofacies types with associated hydraulic conductivity from 7.8×10^{-8} m/s to 1.4×10^{-3} m/s and porosities from 0.24 to 0.33 (Figure 4.1). The hydraulic conductivity statistics for all sites were calculated and are summarized in Table 4.1.

Table 4.1. Hydraulic conductivity statistics for the five aquifer analogs (*K* in m/s); all sites have fluvio-glacial sediments but Descalvado (fluvio-aeolian).

Site	mean ln *K*	$\delta^2 K$
Herten	-7.98	5.13
Hartheim	-7.64	5.03
Pfullendorf	-8.53	1.66
Bolstern	-9.57	5.77
Descalvado	-9.01	1.91

4.2.2 Model setup

For all considered sites the numerical models representing the outcrop analogs were defined by a detailed reconstruction of the fully characterized vertical transect. In each of the sites a hypothetical NAPL source (Figure 4.1) was emplaced near the upstream end of the model domain such that a dissolved toluene plume could evolve during the simulation period. Toluene was selected as a representative model compound and as a suitable proxy for many other similarly behaving compounds due to its abundance at many contaminated sites and its well documented redox-specific enrichment factors reported from laboratory studies (Meckenstock et al., 2004; USEPA, 2008; Vogt et al., 2008). The model domains for the five analogs were discretized by regular grids ($\Delta x = \Delta y = 0.05$ m). The discretization yielded 140 layers for the height of all five analogs and 320 (Herten), 400 (Pfullendorf, Bolstern), and 500 (Hartheim, Descalvado) columns in length-direction, respectively. Steady-state two-dimensional groundwater flow was simulated for all analogs with the USGS finite differences code MODFLOW 2000 (Harbaugh et al., 2000). Fully saturated and confined conditions were assumed for all simulations. Constant heads were assumed for the inflow boundaries, imposing a regional hydraulic gradient of 0.001 between the inflow and outflow model boundaries. Hydraulic conductivity (*K*) and porosity (*n*) values were assigned to the grid cells according to the values mapped for the aquifer analog sites (Figure 4.1). To avoid potential

undesired boundary effects a short, homogenous zone of 0.05 m length was implemented at the upstream and downstream boundaries. The longitudinal (α_L) and vertical transverse (α_T) dispersivities were set to 2.5×10^{-2} m and 2.5×10^{-4} m, respectively. These small values represent local-scale dispersivities, while the explicit definition of the physical heterogeneity via the analog-specific high resolution *K*-fields directly accounts for larger-scale mixing and dilution processes such as flow focusing (e.g., Rolle et al., 2009; Werth et al., 2006). The hydrochemical and mineral composition of the aquifer was defined such that it reflects typical conditions for the respective sedimentary unconsolidated gravel and sand aquifers (see Table 4.2 for details).

Table 4.2. Model initial and inflow conditions.

Parameter	Unit	Value
temperature	C	10
pH	-	7.01
pe	-	14.87
Ca^{2+}	mol/L	1.061×10^{-3}
Cl^-	mol/L	2.18×10^{-3}
Fe^{2+}	mol/L	3.28×10^{-18}
Fe^{3+}	mol/L	6.11×10^{-9}
K^+	mol/L	3.02×10^{-4}
Mg^{2+}	mol/L	1.32×10^{-4}
N	mol/L	1.85×10^{-23}
NO_2^-	mol/L	6.80×10^{-19}
NO_3^-	mol/L	2.10×10^{-5}
Na^+	mol/L	5.96×10^{-4}
O_2	mol/L	3.19×10^{-4}
S^{2-}	mol/L	0
SO_4^{2-}	mol/L	4.06×10^{-4}
$Fe(OH)_3$	mol/L_{bulk}	8.00×10^{-3}

The selected setup was defined such that biodegradation of toluene could occur under aerobic, denitrifying, iron-reduction and sulfate-reduction conditions. The homogeneous source zone containing 1 mol toluene/L_{bulk} was placed between x = 0.4 m and x = 0.9 m (Figure 4.1). This configuration allowed for the generation of a dynamically changing (i.e., expanding, stable and shrinking) dissolved contaminant plume within the selected simulation period, which was limited to 300 days. In order to account for various sizes of the source zone causing partial and full contamination of the model domain four different scenarios were simulated with varying source geometries and locations at depths ranging from (1) z = 0 m to z = 1.5 m, (2) z = 0 m to z = 2.5 m, (3) z = 1.5 m to z = 2.5 m, (iv) z = 0 m to z = 6.0 m (Figure 4.1). The carbon isotope ratio of the toluene source was assumed to be -23.1 ‰. The aquifer was assumed to be initially (i.e., at time t = 0) free of dissolved toluene.

PHT3D (Prommer et al., 2003a) was employed to simulate reactive transport using an earlier developed and applied reaction module, as described in detail by D'Affonseca et al. (2011). The adopted degradation rate constants and laboratory-derived enrichment factors are listed in Table 4.3 and 4.4, respectively.

The reaction network defined for this study considered source zone depletion, the degradation of the released compounds, the associated geochemical response, and the redox-dependent carbon isotope shift of toluene. All calculations and figures refer to toluene concentrations

Table 4.3. Degradation rate constants [s-1] under aerobic (K_{aerob}), denitrifying (K_{denit}), iron-reduction ($K_{iron,red}$) and sulfate-reduction ($K_{sulf,red}$) conditions.

Parameter	Value
K_{aerob}	5.0×10^{-10}
K_{denit}	1.0×10^{-10}
$K_{iron,red}$	5.0×10^{-11}
$K_{sulf,red}$	1.0×10^{-11}

Table 4.4. Laboratory-derived enrichment factors under aerobic (ε_{aerob}), denitrifying (ε_{denit}) and iron/sulfate reducing ($\varepsilon_{iron/sulf}$) conditions, adopted in the model.

Parameter	Value
ε_{aerob}	-1.1[a]
ε_{denit}	-1.7[b]
$\varepsilon_{iron/sulf}$	-1.8[b]

a)Morasch et al. (2002),
b)Meckenstock et al. (1999)

equal or greater than 10^5 times of the aqueous concentrations near the source (5.8×10^{-3} mol/L), the approximate range between common source concentrations and the analytical limits of CSIA (Van Breukelen and Prommer, 2008).

4.3 Quantification approaches

4.3.1 Reactive transport based calculations

In order to distinguish the individual effects of dilution/dispersion and biodegradation on concentration changes, auxiliary 'conservative' model runs were carried out, in which degradation rates were set to zero assuming no biodegradation. Then, for each model cell *n*, the extent of biodegradation (B_{true}) was calculated based on the concentrations in the reactive (C_n) and conservative (C_n^c) simulations:

$$B_{true}[\%] = \left(1 - \frac{C_n}{C_n^c}\right) \times 100 \tag{2}$$

The extent of dilution for each *n* (D_n) was defined as:

$$D_n[\%] = \left(1 - \frac{C_n^c}{C^s}\right) \times 100 \tag{3}$$

where C^s is the model source concentration. The isotopic signature $\delta^{13}C_n$ is reported as per mil [‰] and computed from the fraction of lighter and heavier isotopes of toluene for each cell *n*:

$$\delta^{13}C_n = \left(\frac{R_n}{R_{std}} - 1\right) \times 1000 \tag{4}$$

where R_n is the carbon isotope ratio ($^{13}C/^{12}C$) at *n* and R_{std} the carbon isotope ratio of the international Vienna-PDB (Pee Dee Belemnite) standard.

4.3.2 Rayleigh equation based calculations

Field-derived enrichment factors (ε_f) were determined by two different types of estimates, i.e., either based on pairs of (i) fully-screened (7 m length) or (ii) shorter-screened (1 m length) hypothetical monitoring wells. The upgradient monitoring well was placed 0.1 m downgradient of the toluene source at a distance of *x* = 1 m (Figure 4.1). Downgradient monitoring wells were placed at *x* = 15 m (Figure 4.1) in all five aquifer analogs. For the aquifer analogs Pfullendorf, Bolstern (length 20 m) and Hartheim and Descalvado (length 25 m) additional monitoring wells were placed at *x* = 19 m and *x* = 24 (Figure 4.1). The concentrations in each well ($\overline{C}$) were calculated based on flow-rate-weighted mean concentrations of grid cells located along the entire filter screen length (Halford and Hanson, 2002):

$$\overline{C} = \frac{\sum_{n=1}^{N} C_n Q_n}{\sum_{n=1}^{N} Q_n} \tag{5}$$

C_n and Q_n represent the concentration and the inflow rate of each cell *n*, respectively. The toluene isotopic signature in the well ($\overline{\delta^{13}\mathrm{C}}$ [‰]) was quantified similarly to Eq. 4:

$$\overline{\delta^{13}\mathrm{C}} = \left(\frac{\overline{R}}{R_{std}} - 1 \right) \times 1000 \tag{6}$$

where $\overline{R}$ is the carbon isotope ratio in the well. The field-derived enrichment factor (ε_f) was estimated by substituting the original biodegradation time dependency of the Rayleigh equation into a field-scale spatial dependency (e.g., Blum et al., 2009; Griebler et al., 2004):

$$\varepsilon_f = \frac{\Delta\overline{\delta^{13}\mathrm{C}}}{\ln\left(\frac{\overline{C_{dg}}}{\overline{C_{ug}}}\right)} \tag{7}$$

where $\Delta\overline{\delta^{13}\mathrm{C}}$ is the difference in the isotope signatures between two wells along the flow direction. The ratio of simulated concentrations in the upgradient ($\overline{C_{ug}}$) and the downgradient ($\overline{C_{dg}}$) wells were used to define the fraction of remaining dissolved toluene. The field-derived enrichment factor was corrected for dilution (ε_{fcd}), as proposed by Mak et al. (2006). This was achieved by substituting $\overline{C_{ug}}$ in Eq. 7, i.e., the concentration in the downgradient well with the concentrations computed by corresponding conservative transport simulations ($\overline{C_{dg}^c}$) in which the biodegradation reactions were switched off:

$$\varepsilon_{fcd} = \frac{\Delta\overline{\delta^{13}C}}{\ln\left(\frac{\overline{C_{dg}}}{\overline{C_{dg}^c}}\right)} \tag{8}$$

$\overline{C_{dg}^c}$ is calculated by substituting C_n with C_n^c in Eq. 5. The estimation of the extent of biodegradation by the Rayleigh equation (B_{Ray}) is then based on the $\overline{R}$ calculated for the upgradient ($\overline{R_{ug}}$) and downgradient ($\overline{R_{dg}}$) wells, and on the isotope enrichment factor ε (e.g., Blum et al., 2009; Meckenstock et al., 2004):

$$B_{Ray}[\%] = \left(1 - \left(\frac{\overline{R_{dg}}}{\overline{R_{ug}}}\right)^{\frac{1000}{\varepsilon}}\right) \times 100 \tag{9}$$

Note that the selection of a suitable enrichment factor ε is one of the critical issues for an accurate quantification of B_{Ray} (Meckenstock et al., 2004).

Fischer et al. (2007) and Thullner et al. (2012) both presented an extension of the Rayleigh equation approach to improve CSIA-based biodegradation estimates in complex field environments. This approach, which they termed "*Rayleigh equation streamline approach*", was developed to account for the effects of dilution/dispersion caused by aquifer heterogeneity. Under the assumption that dilution/dispersion and degradation occur simultaneously at a constant ratio along a flow path then the extent of biodegradation can be expressed as:

$$B_{Ray\_streamline}[\%] = \frac{\ln\left(\left[\frac{\overline{R_{dg}}}{\overline{R_{ug}}}\right]^{\frac{1000}{\varepsilon}}\right)}{\ln\left(\frac{\overline{C_{dg}}}{\overline{C_{ug}}}\right)} \times \left(1 - \frac{\overline{C_{dg}}}{\overline{C_{ug}}}\right) \times 100 \qquad (10)$$

In order to assess the applicability of the Rayleigh equation streamline approach under the complex and realistic hydrogeological conditions represented by the selected aquifer analogs the extent of biodegradation $B_{Ray\_streamline}$ was calculated and compared against the true intrinsic biodegradation (B_{true}) and the conventional Rayleigh approach B_{Ray} (Eq. 9). A bulk enrichment factor was employed in Eq. 10 to represent the average laboratory-derived values for toluene.

4.4 Reactive transport simulations

4.4.1 Plume development and isotope fractionation

The model simulations illustrate how the physical heterogeneity depicted in the aquifer analogs strongly influences the transport behavior of the toluene plumes that are created through the dissolution from the emplaced toluene source. The cm-scale heterogeneity in-

duces transverse excursions of the plumes from the general flow direction. Dipping high permeable units of cross-bedded poorly sorted gravel and massive well sorted gravel bodies at the Herten site (Bayer et al., 2011) and well sorted sand grains at the Hartheim site (Heinz et al., 2003) form preferential flow paths where the toluene mass flux concentrates, as for example, illustrated in Figure 4.2 (results only shown for scenarios with source length from x = 0 to 6 m).

The prevailing high conductivity inclusions considerably influence the temporal and spatial contaminant concentration patterns through flow focusing and enhanced mixing, with effects similar to those discussed by Werth et al. (2006) for laboratory-scale experimental studies. This is for instance demonstrated in the simulations of the Pfullendorf analog, where a high permeable lense (near x = 5 m and z = 4.5 m) leads to flow focusing. Downstream of this convergence de-focusing causes a distinct spread of the contaminant distribution, as illustrated by the concentration contours shown in Figure 4.2 for 50 days simulation time. Within the toluene-contaminated source zone itself, variations in the groundwater flux trigger a successive, heterogeneously progressing depletion of the toluene source, with the most rapid depletion occurring in the zones of the highest hydraulic conductivities. This process creates areas where more oxidized, i.e., electron acceptor-bearing groundwater can pass through the source zone without being affected by degradation reactions. The high conductivity zones are gradually converted into preferential transport pathways for electron acceptors (e.g., via dissolved oxygen, nitrate and sulfate) across the source zone. The redox zonation throughout these zones is transient and highly irregular patterns form, as illustrated exemplarily for the Herten site (Figure 4.3). Similarly, complex spatiotemporal patterns of isotope signatures develop (Figure 4.4).

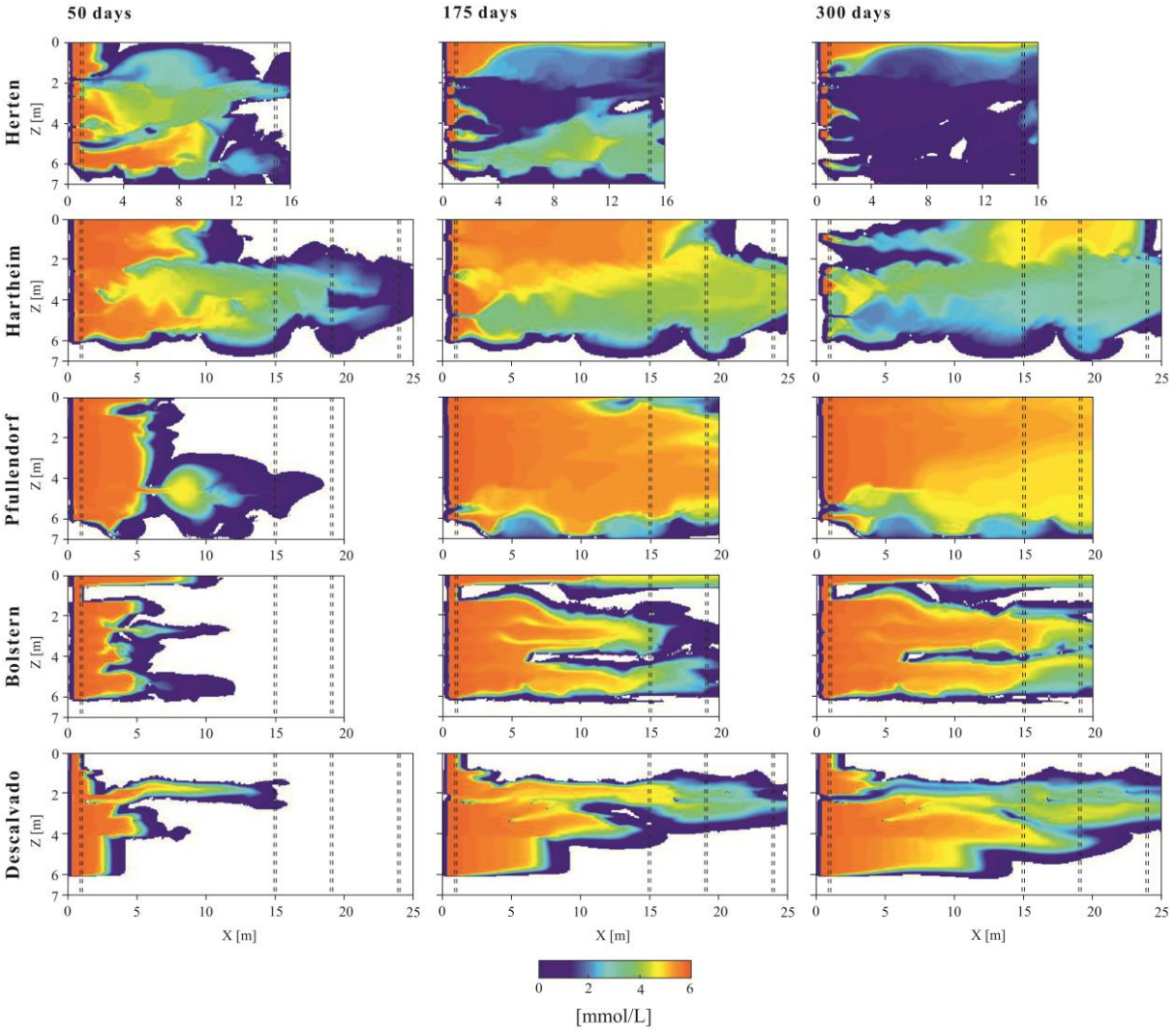

Figure 4.2. Evolution of toluene concentrations over 300 days at the sites in Herten, Hartheim, Pfullendorf, Bolstern and Descalvado. Source zone from z = 0-6m. Vertical dotted lines denote the well locations.

During the first 50 days, the toluene plumes are expanding and the simulated isotope fractionation is most pronounced at the fringes of the plumes, where biodegradation is facilitated by the simultaneous presence of toluene and soluble electron acceptors (Figure 4.5). After some 175 days the plumes at the Herten and Hartheim site approach a pseudo-stationary phase, while for Pfullendorf, Bolstern and Descalvado the plumes are still growing further (Figure 4.2). As a consequence of the gradual depletion of the source zone, biodegradation is no longer limited to the advancing plume fringes alone. Triggered by the intrusion of electron acceptor bearing groundwater along preferential flow paths significant biodegradation occurs within the plume, accompanied by a more expressive isotope fractionation (Figure 4.4).

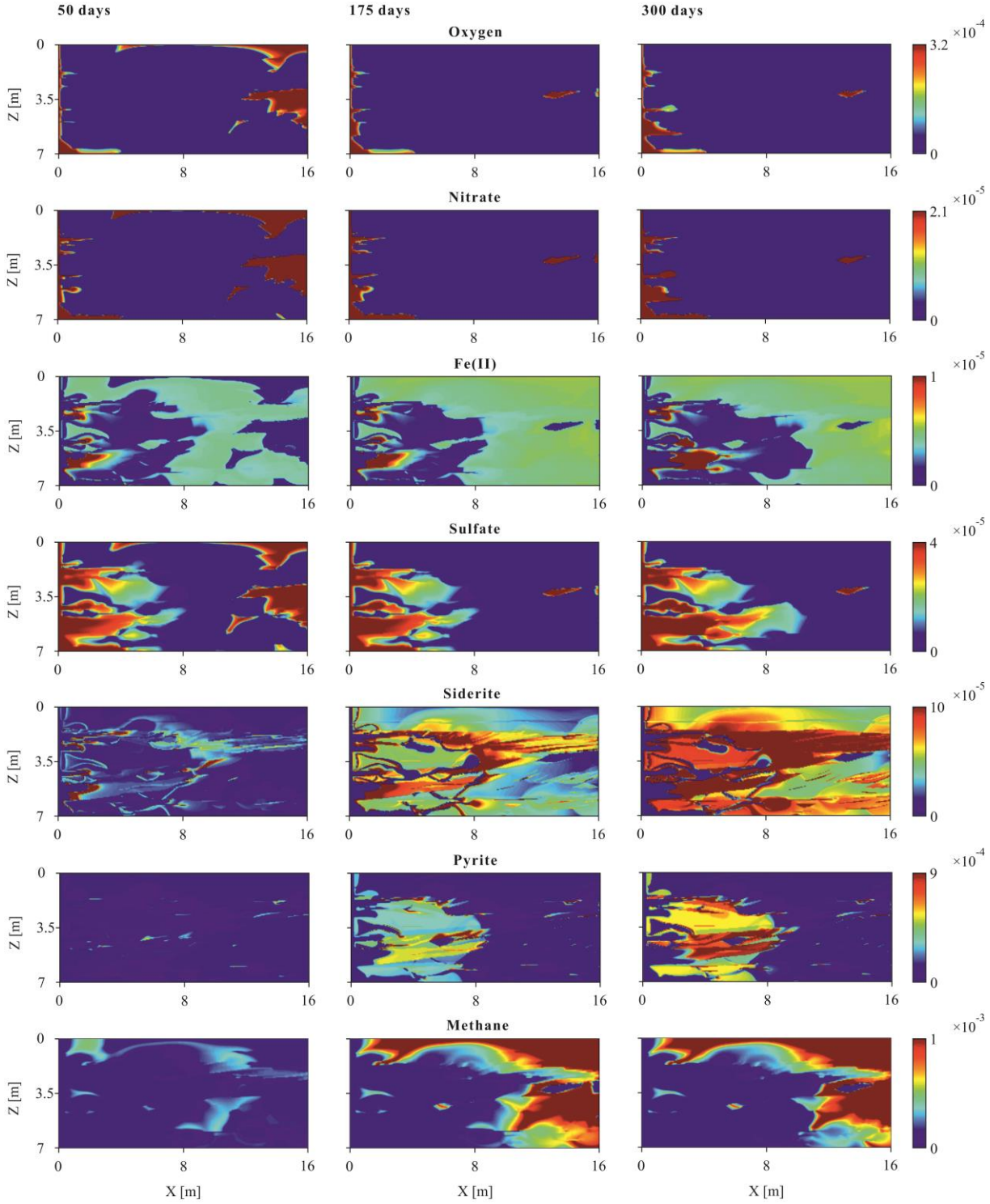

Figure 4.3. Evolution of hydrogeochemical features in the heterogeneous aquifer analog from the Herten site over 300 days. Note, all concentrations refer to mol/L and mol/L_{bulk} for siderite and pyrite, respectively. After the available oxygen and nitrate are consumed by the toluene degradation, amorphous iron hydroxide, Fe(OH)3, starts to be consumed, resulting in the release of ferrous iron. Sulfate reduction takes place where Fe(OH)3 becomes exhausted and finally methanogenesis occurs. The changes in the aquifer chemistry leads to precipitation of secondary minerals (i.e. siderite and pyrite), which consume the ferrous iron, sulfide and bicarbonate produced by the toluene degradation reactions.

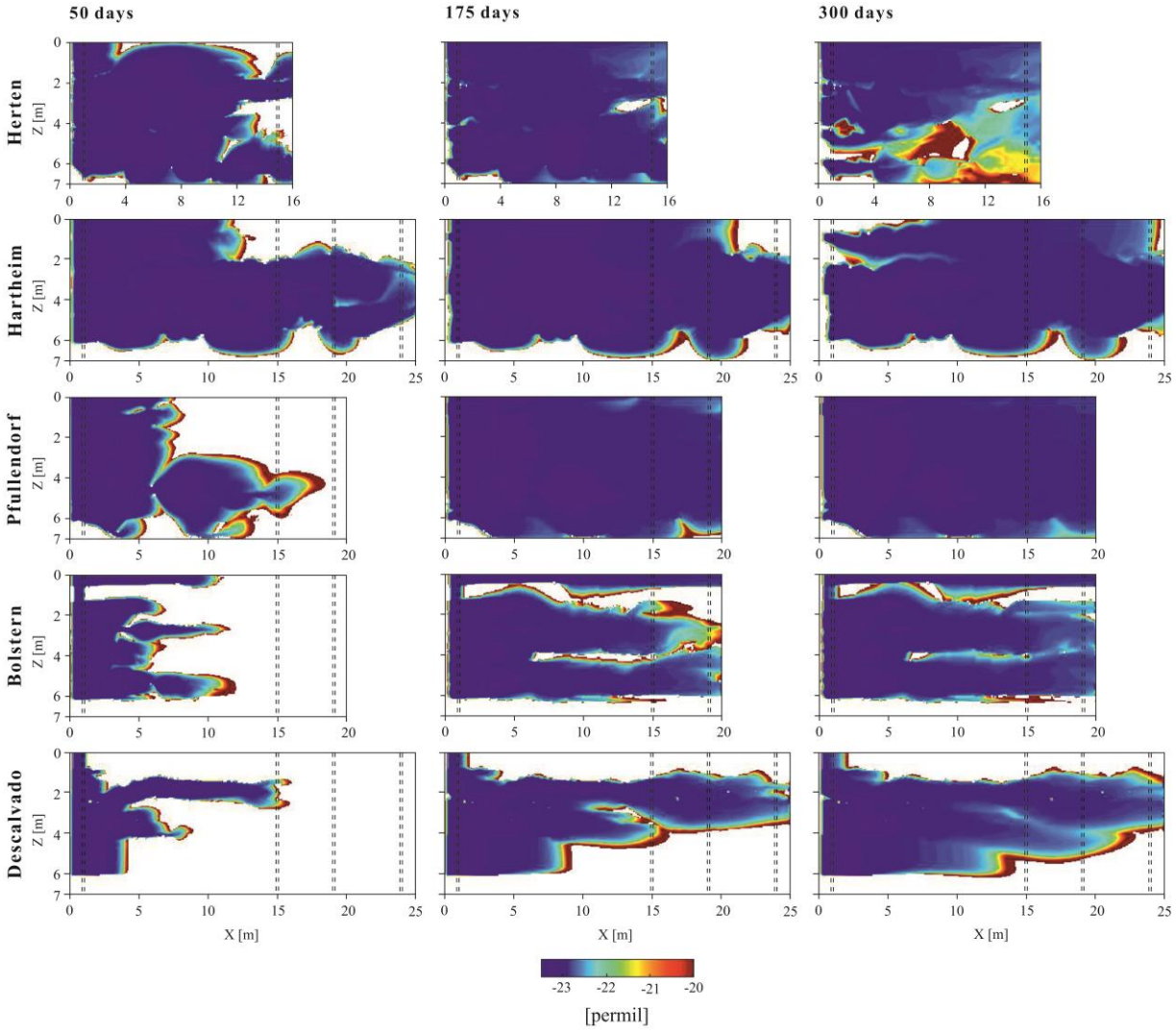

Figure 4.4. Evolution of isotope fractionation ($\delta^{13}C$) over 300 days at the sites in Herten, Hartheim, Pfullendorf, Bolstern and Descalvado. Source zone from *z* = 0-6m. Vertical dotted lines denote the well locations.

4.4.2 Implication for CSIA-based assessment

Assuming that the simulated scenarios can closely mimic true field-scale transport and reaction behavior, field-derived enrichment factors (ε_f and ε_{fcd}) were determined from a series of hypothetical monitoring events, thereby employing Eqs. 7 and 8 to interpret multiple hypothetical field data sampling events. To evaluate the accuracy of the so-derived values, they were compared against the laboratory-derived enrichment factors that were originally specified as model input parameters (Table 4.4). The comparison in Figure 4.6 shows that the computed (e.g., field-derived) enrichment factors (ε_f) from fully-screened wells are mostly

underestimated at all sites, e.g., less negative than the laboratory-derived enrichment factors (ε_{aerob} , ε_{denit} , $\varepsilon_{iron/sulf}$). This can be linked to the fact that the estimation of ε_f does not account for the effects induced by dilution/dispersion. Consequently, measurable concentration reductions are exclusively attributed to intrinsic biodegradation, as discussed earlier by Van Breukelen (2007).

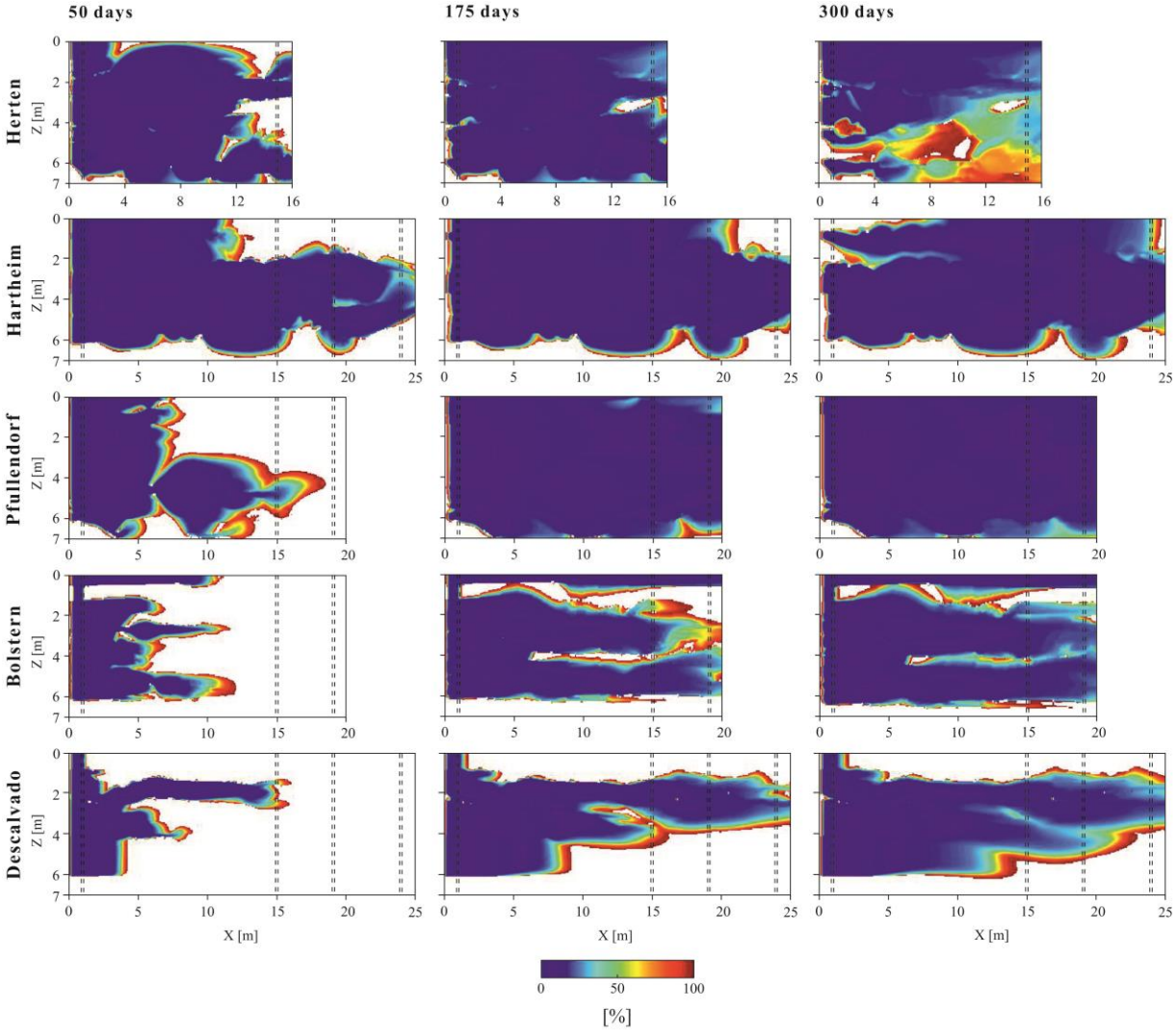

Figure 4.5. Evolution of extents of biodegradation (0% to 100% degraded) over 300 days at the sites in Herten, Hartheim, Pfullendorf, Bolstern and Descalvado. Source zone from *z* = 0-6m. Vertical dotted lines denote the well locations.

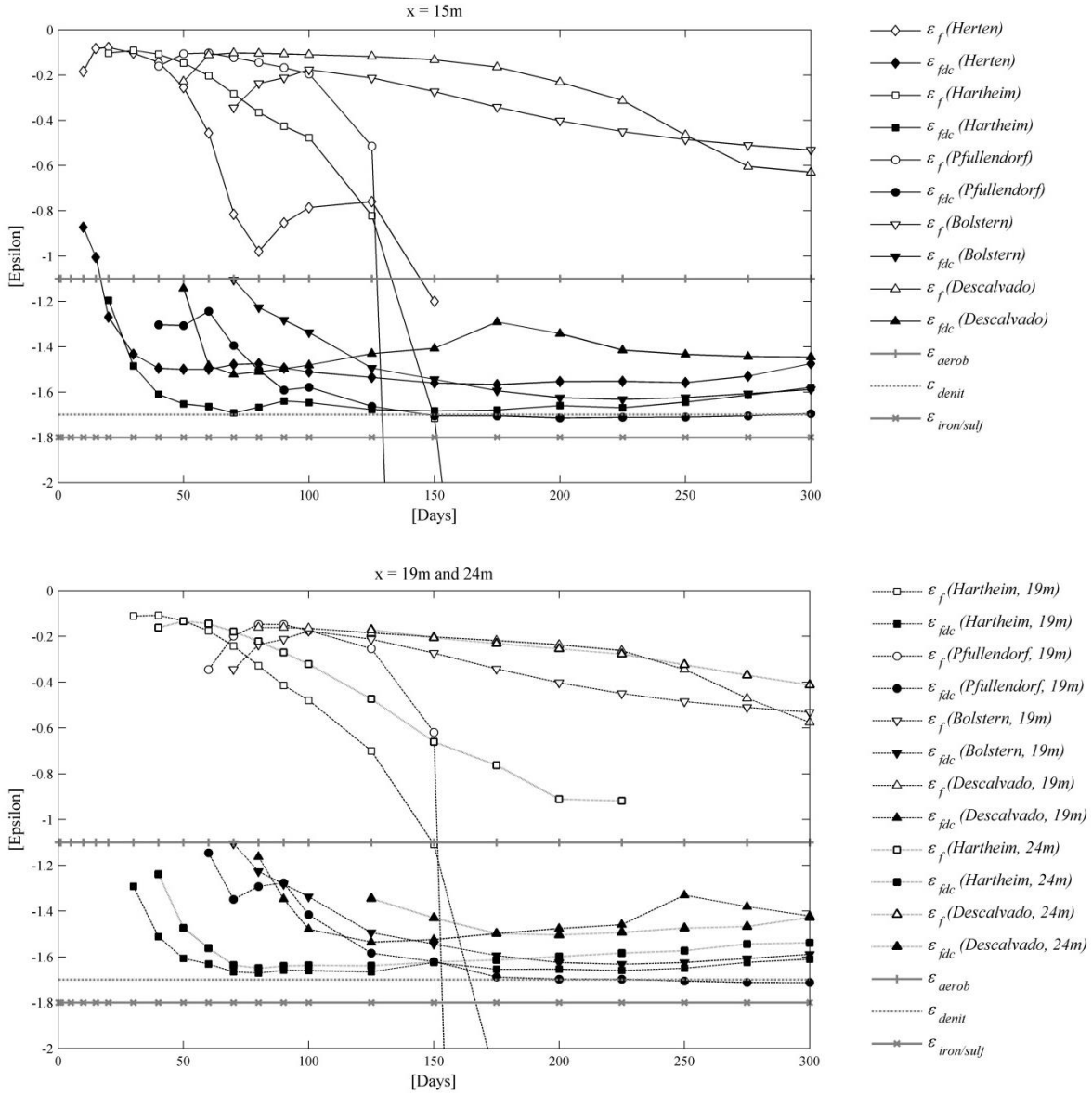

Figure 4.6. Sequential comparison between field-derived enrichment factors (ε_f) and field-derived enrichment factors corrected for dilution (ε_{fdc}) against the laboratory-derived enrichment factors (ε_{aerob}, ε_{denit}, $\varepsilon_{iron/sulf}$) adopted in the models for fully screened wells at all analogs at the location *x* = 15, 19, 24m.

Such dilution effects were already previously suggested to explain the differences between laboratory- and field-derived enrichment factors (Vieth et al., 2005). Blum et al. (2009) for instance, estimated an ε_f of -0.05 for naphthalene, while previously reported laboratory-derived values for this compound ranged between -0.1 for oxic conditions and -1.1 for sulfate-reducing conditions, respectively (Meckenstock et al., 2004).

In cases where the source partially depletes (Figure 4.2 for simulation results for the Hartheim and Pfullendorf site), the concentration gradient between upgradient and downgradient wells can gradually decrease, whilst the isotope fractionation between these wells further increases, as biodegradation reactions are enhanced in parts of the plume. For such specific conditions, the magnitude of ε_f can be overestimated, i.e., be more negative than the laboratory-derived enrichment factors (Figure 4.6). Furthermore, partial source depletion can also lead to an inversion of the concentration gradients. This means, concentrations measured at downgradient wells are higher than concentrations at their upgradient counterparts. In this particular case no reasonable ε_f value can be estimated (e.g., Herten site, Figure 4.6).

In contrast, this problem does not occur if the calculations of the field-derived enrichment factors consider a correction for dilution (ε_{fcd}), as the respective calculation procedure does not use concentration differences (Eq. 8). The estimated values of ε_{fcd} are for all analogs mostly within the range of the laboratory-derived enrichment factors (Figure 4.6). Hence, the concept that underlies ε_{fcd} appropriately accounts for the miscellaneous biodegradation reactions, which occur between the upgradient and downgradient monitoring wells. When the plume initially reaches the downgradient wells (e.g., the results for the Herten site in Figure 4.2) ε_{fcd} values might be underestimated. As the plumes expand, overall more reducing conditions prevail (see e.g., Figure 4.3) and accordingly the estimated ε_{fcd} values become more negative (Figure 4.6). The general trends are occasionally interrupted and ε_{fcd} values determined from long-screen wells become temporarily slightly less negative. This occurs where plumes exhibit a pronounced fingering, as for example shown for the Descalvado site at around 175 days (Figure 4.2, Figure 4.6). In this case the fully-screened downgradient well records at elevations around z = 2-4 m the plume under denitrifying conditions, whereas at z =

4-5 m parts of the plume fringe arrive and oxidizing conditions prevail, which results in a mixed signal.

The use of multi-level sampling wells provides high resolution data that more closely capture the spatial and temporal irregularities in the redox zonation and the variability of the enrichment factors within the aquifer analogs (e.g., Anneser et al., 2008). For instance, enrichment factors corrected for dilution from multi-level wells (screen length 1m) for the Herten analog (Figure 4.7) can vary significantly over short vertical distances.

While in the upper part at ~75 days aerobic redox conditions still prevail (Figure 4.7, z = 0-2 m) the enrichment factors derived from the depth of z = 2-3 m clearly indicate denitrifying conditions. This underlines the potential of multi-level wells and redox specific enrichment factors from high resolution data to derive local-scale biodegradation estimates within heterogeneous aquifers, where different redox conditions simultaneously occur over short vertical distances.

For each considered hypothetical sampling event, five distinct values describing the extent of biodegradation B_{Ray} were calculated for the downgradient wells. Calculations at x = 15 m (x = 19 m and 24 m, results not shown) using field-derived (ε_f, ε_{fcd}) and laboratory-derived enrichment factors (Figure 4.8 as example from the Herten site, other sites are not shown). The results are compared against the highest ($B_{true(\max)}$), the lowest ($B_{true(\min)}$) and the average ($B_{true(mean)}$) simulated intrinsic biodegradation values, as separately derived from Eq. 2 for each filter screen location. The comparison of the results for all analogs shows a general agreement. Thus, the focus is more on a detailed discussion of results on the Herten analog, while similar findings can also be derived from the other investigated sites.

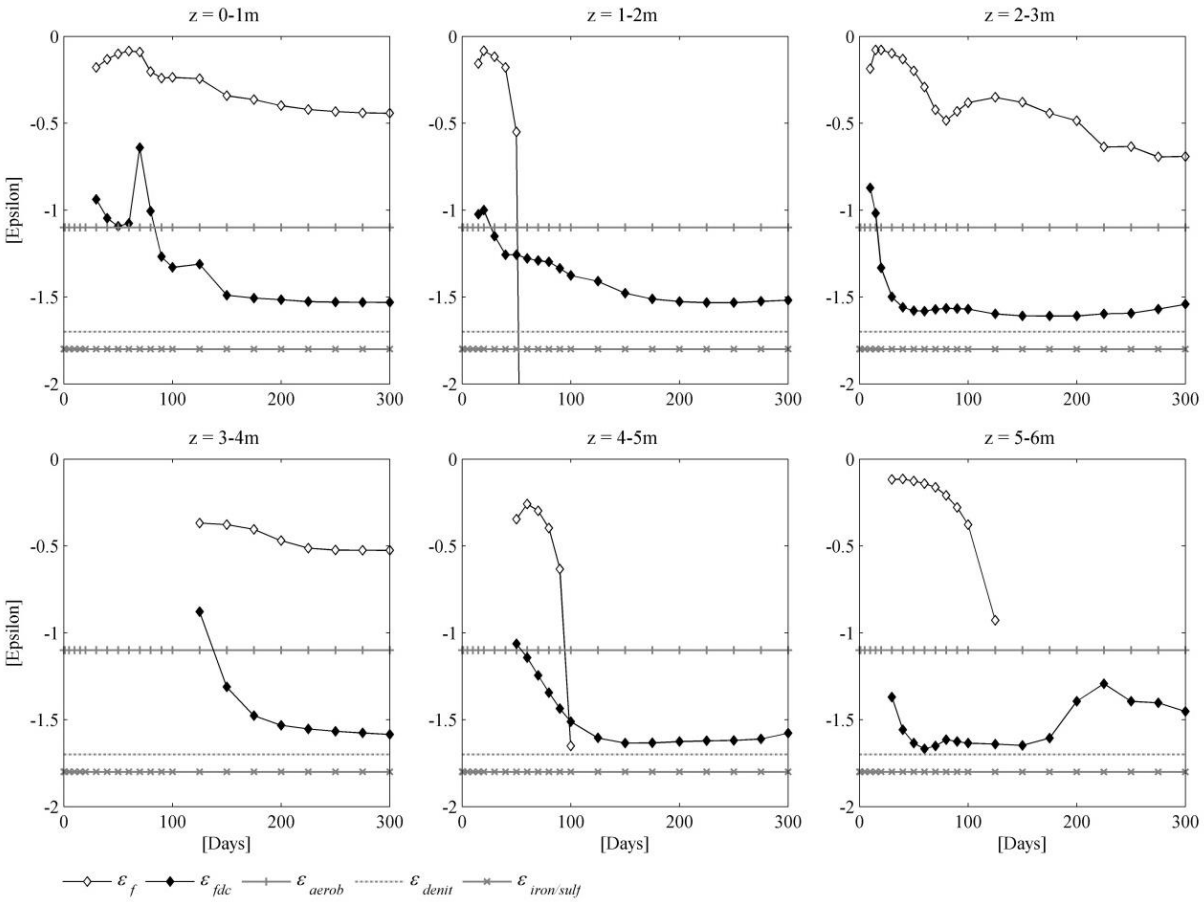

Figure 4.7. Sequential comparison between field-derived enrichment factors (ε_f) and field-derived enrichment factors corrected for dilution (ε_{fdc}) against the laboratory-derived enrichment factors (ε_{aerob}, ε_{denit}, $\varepsilon_{iron/sulf}$) adopted in the models for multi-level wells for the Herten analog at x = 15m.

For the Herten site Figure 4.8 illustrates that the simulated B_{true} values vary considerably along the filter screens. For instance, after 300 days simulation time, B_{true} values range between 22% and 31% at the short-screened downgradient well (from 1 to 2 m), while for the fully-screened downgradient well B_{true} values vary considerably more, i.e., between $B_{true(\min)}$ = 12% and $B_{true(\max)}$ = 91%. However, the calculated average biodegradation based on a dilution corrected enrichment factor $B_{Ray(\varepsilon_{fdc})}$ with 32% agrees well with $B_{true(mean)}$ (38%). Thus, the average value can be used for a quantitative assessment of the biodegradation extent. As demonstrated and discussed earlier, the extent of biodegradation is heterogeneously

distributed within the aquifer. Accordingly, accurate biodegradation estimates for a certain aquifer compartment requires the use of short-screen wells.

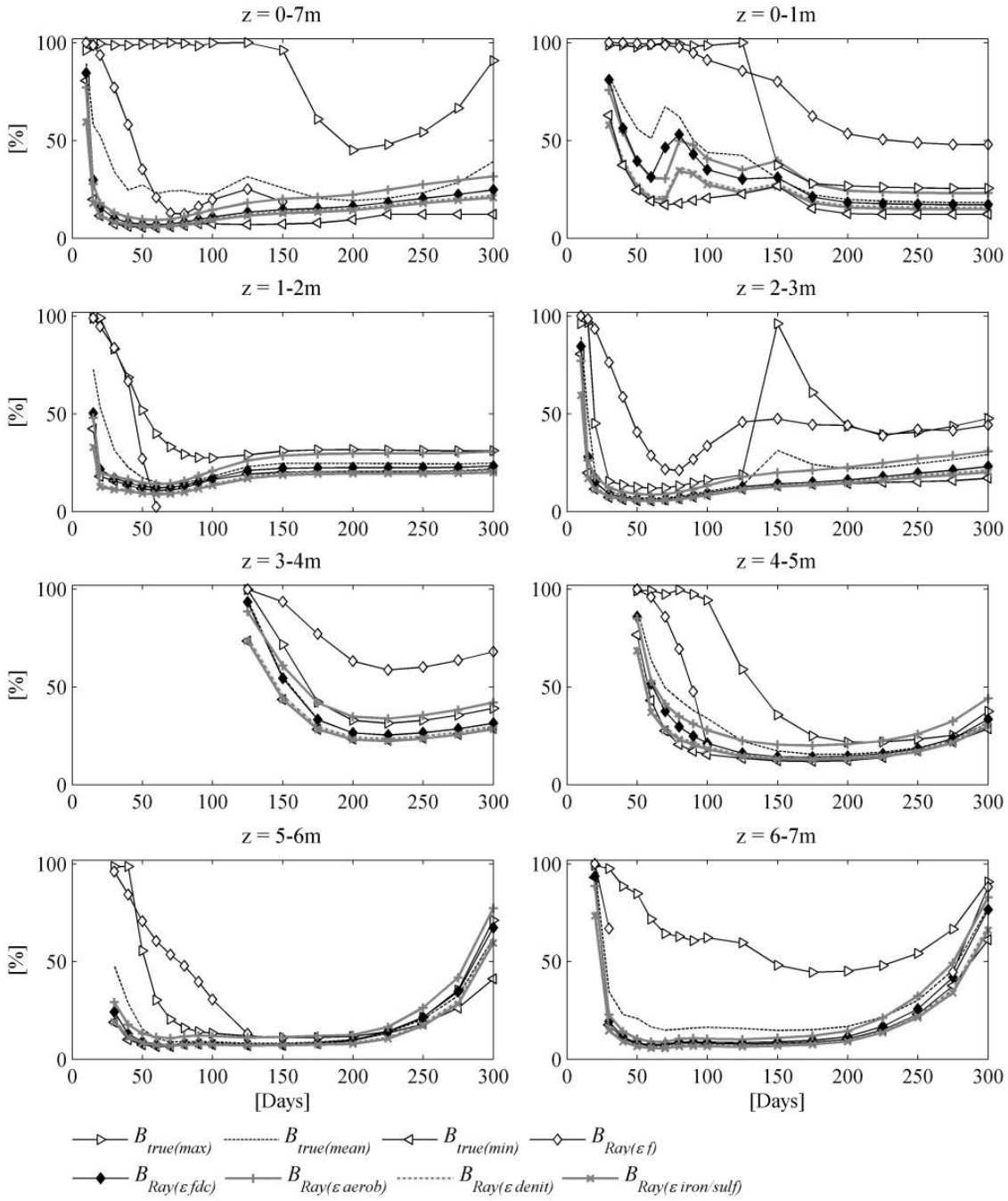

Figure 4.8. Time series of true intrinsic biodegradation (B_{true}) versus calculated Rayleigh-derived values (B_{Ray}), for fully and multi-levels wells for the Herten analog at x = 15m.

It is important to point out, that if short screens are applied for a point to point comparison of $\delta^{13}C$ for a quantification of the relative amount of biodegradation, the most negative

$\delta^{13}C_{source}$ values has to be captured (USEPA, 2008). This might be challenging in case of small or discontinuous source zones in heterogeneous aquifers, where significant biodegradation potentially occur at the fringe of the source or in highly permeable areas close to the source zone (Figure 4.4, Herten at 300 days, location x ~ 1 m , z ~ 4-6 m). Hence, more enriched $\delta^{13}C$ values can be erroneously considered as $\delta^{13}C_{source.}$

Furthermore, the simulation results also show (Figure 4.8) that for short-screened wells (≤ 1 m) the degraded fraction of the contaminant is mostly overestimated ($B_{Ray(\varepsilon_f)} > B_{true}$), if field-derived enrichment factors (ε_f) are used. Accurate estimates, i.e., within the B_{true} range, are only accidentally obtained while the source zone progressively depletes, for instance, after 70 days in the downgradient well screened from 1 to 2 m (Figure 4.8). For the subsequent phase of the simulation period $B_{Ray(\varepsilon_f)} < B_{true}$ and ε_f cannot be determined since Eq. 7 provides positive values. For the fully-screened downgradient well, the estimated $B_{Ray(\varepsilon_f)}$ values are within the range of B_{true} values. However, this occurs in particular due to the large variety of calculated intrinsic biodegradation values.

The simulation results indicate that improved biodegradation estimates can be obtained when laboratory-derived enrichment factors are employed in the calculations. However, this requires that the selected enrichment factors truly reflect the prevailing redox- and other conditions. For instance, if laboratory-derived enrichment factors that either represent denitrifying (ε_{denit}) or iron/sulfate reducing ($\varepsilon_{iron/sulf}$) conditions are used, the respective estimated extent of biodegradation, i.e., $B_{Ray(\varepsilon_{denit})}$ and $B_{Ray(\varepsilon_{iron/sulf})}$ are mostly below the true intrinsic biodegradation values (Figure 4.8). This indicates that the extent of aerobic biodegradation is not properly accounted for if biodegradation estimates are only based on ε_{denit} or $\varepsilon_{iron/sulf}$. However, if ε_{aerob} is used instead, the estimated B_{Ray} values tend to be close to the upper

bound of the B_{true} range. More robust and reliable results are obtained if dilution is accounted for when estimating field-derived enrichment factors (ε_{fcd}). For all occasions, the respective estimated extent of biodegradation, i.e, $B_{Ray(\varepsilon_{fdc})}$, falls within the respective range of the (true) intrinsic biodegradation, i.e., between the mean and the minimum simulated values of B_{true} (Figure 4.8).

Previously Abe and Hunkeler (2006) and Van Breukelen and Prommer (2008) suggested that a systematic underestimation (< 5%) of the degree of biodegradation is obtained if the Rayleigh equation is applied in heterogeneous aquifers. Green et al. (2010) reported significant differences between estimated apparent denitrification rates and ε that were lower than true values by a factor of up to 10 or even higher for faster reactions and higher dispersivities. The results of the current study suggest that this bias can be overcome if dilution/dispersion is appropriately considered during the estimation of field-derived enrichment factors. With such a correction in our study the respective $B_{Ray(\varepsilon_{fdc})}$ represents the lower range of the intrinsic biodegradation, i.e., no underestimation.

Further, simulated time-lapse concentrations and isotope shifts were also employed to assess the accuracy of the "*Rayleigh equation streamline approach*" after Fischer et al. (2007) (Eq. 10). For this comparison the calculated extent of biodegradation was compared against the highest ($B_{true(\max)}$), the lowest ($B_{true(\min)}$) and the average ($B_{true(mean)}$) simulated intrinsic biodegradation values, as determined for each filter screen location using Eq. 2. $B_{Ray\_streamline}$[%] estimates derived from fully-screened wells for the scenario simulating a NAPL source extending over the full depth of the model domain (source length z = 0 m to z = 6.0 m) are significantly below $B_{true(mean)}$ at the plume fringe (Figure 4.9).

For later stages of the simulation period when plumes have further evolved the $B_{Ray\_streamline}$ estimates range mostly between $B_{true(mean)}$ and $B_{true(\min)}$, thus providing a good

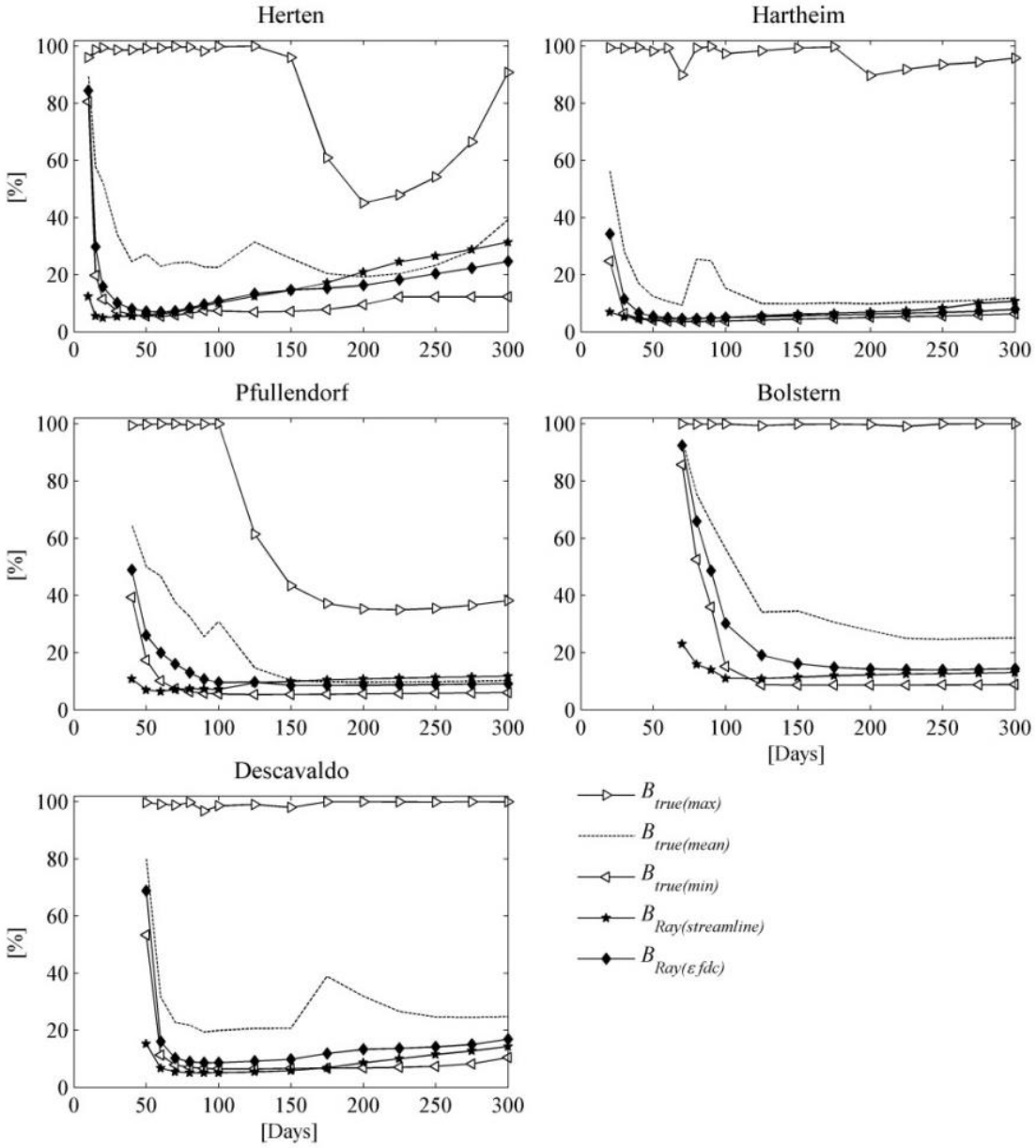

Figure 4.9. Time series comparison of calculated biodegradation based on the conventional Rayleigh equation with dilution corrected enrichment factors ($B_{Ray}(\varepsilon_{fdc})$) and modified Rayleigh streamline approach after Fischer et al. (2007) with a laboratory derived bulk enrichment factor and the range of true intrinsic biodegradation for fully-screened wells at all sites at x = 15m.

estimate of the actual biodegradation. Once upgradient concentrations locally decrease below downgradient concentrations, as caused by a successively depleting non-aqueous phase liquid in highly heterogeneous porous media, $B_{Ray\_streamline}$ may exceed actual biodegradation esti-

mates. Results from short-screened wells show for some screen locations a good agreement with true biodegradation (results not shown), but often also high discrepancies. Depending on the flow path $B_{Ray\_streamline}$ may continuously overestimate biodegradation (Figure 4.10a,b) or underestimate (Figure 4.10c,d).

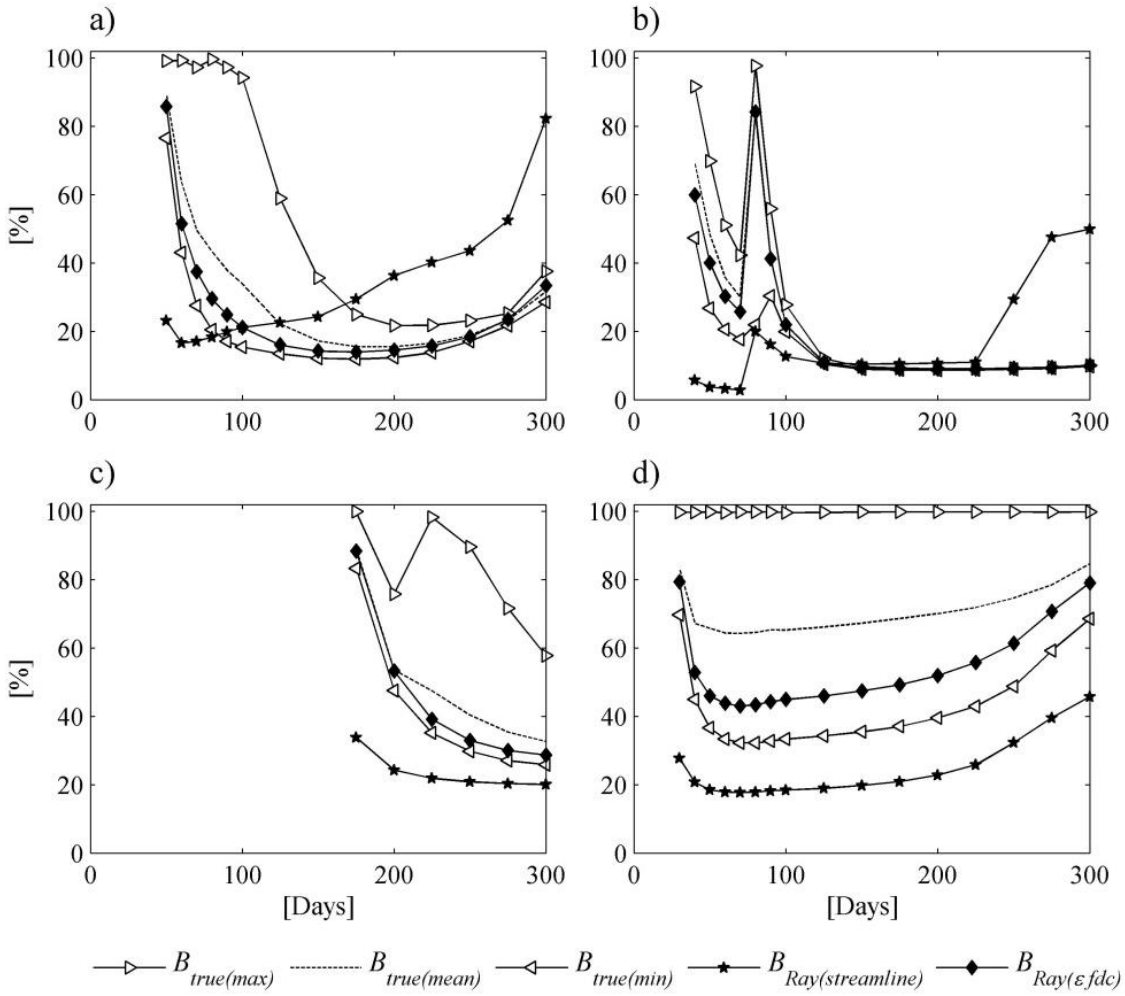

Figure 4.10. Time series comparison of calculated biodegradation based on the conventional Rayleigh equation with dilution corrected enrichment factors ($B_{Ray}(\varepsilon_{fdc})$) and modified Rayleigh streamline approach after Fischer et al. (2007) with a laboratory derived bulk enrichment factor and the range of true intrinsic biodegradation for a) Herten, wells screened z = 4-5 m (source length z = 0-6m), b) Hartheim, wells screened z = 1-2 m (source length z = 0-6m), c) Bolstern, wells screened 1-2 m (source length z = 0-6m), d) Bolstern, wells screened 1-2 m (source length z = 1.5-2.5m).

For the simulated scenarios where the NAPL source occupies only a fraction of the depth of the model domain (e.g., source between z = 1.5 m and z = 2.5 m) the cm-scale heterogeneities cause a pronounced spread of the toluene plumes. These cases, which are the ones

that are most representative of true field conditions, are associated with a continuous underestimation of up to 40% between $B_{Ray\_streamline}$ estimates and $B_{true(mean)}$ (Figure 4.10d).

4.5 Implication of simulation results for employing CSIA in field studies

Understanding of contaminant fate at specific field sites is commonly based on spatially and temporally sparse data sets, relative to the complexity of the subsurface environment and the complexity of the physic-chemical processes. Although field-derived enrichment factors can provide reliable results for the quantification of biodegradation if the dilution/dispersion extent is properly accounted for, the limitation of this method often resides in the difficulty to correctly determine the extent of dilution/dispersion in the field. Only a few compounds can be used as conservative tracers, such as chloride and bromide on landfill sites (Van Breukelen, 2007). In other cases non-degrading organic compounds such as tetrachlorethene (Pooley et al., 2009), 1,2,3-trimethylbenzene (Wiedemeier et al., 1999) and 1,2,3,4-tetrahydronaphthalene (Blum et al., 2009) are occasionally suitable organic tracers to determine dilution. Pooley et al. (2009), for example, observed a decrease of tetrachlorethene (PCE) concentrations downgradient from the source, while $\delta^{13}C$ signatures remained constant indicating the absence of PCE degradation. Under such specific conditions PCE could be used as a tracer to estimate the extent of dilution. However, care must be taken that (1) its release can be unequivocally linked to the same contaminant source as the degradable target compound and (2) sorption is absent or correctly accounted for.

Nevertheless, given the scarcity of laboratory-derived enrichment factors for some compounds, the significant variability of published data, and the fact that the controlling degradation pathways in the field are often uncertain, field-derived enrichment factors corrected for dilution (ε_{fcd}) will still represent a suitable alternative approach. For instance, Van Breukelen (2007) proposed a simplified approach to estimate the enrichment factor for a

given compound based on field data of concomitant contaminants with well constrained enrichment factors. Even if such compounds are present, one should ensure that the selected laboratory-derived enrichment factors are suitable for the redox conditions in the aquifer. It is important to note that even if dilution/dispersion is correctly accounted for as presented in this study, non-destructive isotope fractioning processes such as sorption should also be considered if they are deemed to be relevant for the accurate assessment of contaminant fate (Thullner et al., 2012).

The results of this study elucidate that dilution/dispersion is highly site specific and undergoes significant spatiotemporal variations. Even for aquifers with moderate physical heterogeneities, as found at the Descalvado and Pfullendorf sites ($\delta^2 K$ = 1.91 and 1.66, respectively), biodegradation estimates using the conventional Rayleigh equation are highly uncertain. Our results suggest that a quantification of a systematic bias introduced by the Rayleigh equation for a distinct depositional environment or aquifer type cannot be derived. Hence, conservative transport models can be used to quantify ε_{fcd} and account for dilution/dispersion. Moreover, the quality of the best estimated ε_{fcd} does not depend on the degree of dilution, as stated by Mak et al. (2006), but on the degree of understanding of the aquifer heterogeneities, which is commonly very limited in typical field studies. If a quantification of ε_{fcd} is not possible, the Rayleigh equation streamline approach as proposed by Fischer et al. (2007) and Thullner et al. (2012) with a laboratory derived bulk enrichment factor can provide an alternative for improved assessment of pollutant degradation. It is important to note that the range of redox specific enrichment factors for toluene is narrow (Table 4.4). Thus, uncertainties related to the use of a bulk/average enrichment factor may be acceptable, whereas for compounds with a larger range of enrichment factors for different redox conditions CSIA based biodegradation estimates may be even more challenging. Nev-

ertheless, the use of the Rayleigh equation streamline approach is restricted since the assumption of a constant ratio between dilution/dispersion and degradation rates might often not be fulfilled for aquifers similar to the presented analogs and selected source scenarios. For practical application it should be noted that local values for isotope fractionation strongly depend on small scale heterogeneities, which cannot be accounted for by conventional field investigations. Thus, the high-resolution monitoring that would be required for a correct interpretation of CSIA based results are rarely available at contaminates sites and therefore the successful quantification of local-scale *in situ* biodegradation rates would most likely fail.

The outcome of this study shows that aquifer analogs, combined with reactive transport models, offer an underexplored way to develop generic process understanding and to evaluate monitoring and quantification strategies for complex hydraulic environments. Although the simulation time of the present study covers only 300 days and relatively short distances they are of practical value and can be used to understand field studies, in which a similar sequence of processes is expected to occur, but at longer time-scales. The effects of the simulated dynamics of the source zone on CSIA based biodegradation estimates might be less pronounced depending on the considered scale. Nevertheless, it provides insightful information on effects that might potentially exacerbate CSIA interpretation in highly heterogeneous subsurface settings.

Further work should address (i) 3D simulations, where twisting flow paths enhance dilution (Stauffer, 2007) and reactive mixing, and to identify the magnitude of over- and underestimation under those more complex conditions and (ii) effects of compound-specific diffusion and mixing as recently demonstrated for strongly advection-dominated flow regimes by Rolle et al. (2013).

5 Results and Conclusion

This dissertation investigated and identified the physical and chemical heterogeneities in the Pirambóia Formation of the Guarani aquifer in São Paulo State by constructing an analog model derived from outcrops in an sand pit. The aquifer analog model was translated into a numerical flow and transport model that considered dual heterogeneities to simulate a hypothetical groundwater contamination in the GAS. Further, in a comprehensive numerical experiment this work examined the evolution of carbon isotope signatures during reactive transport of toluene in five different aquifer analogs in order to test the applicability of CSIA based biodegradation estimates of groundwater contaminants in heterogeneous porous media. One can summarize the main findings of this study as follows:

In the second chapter, detailed sedimentological, hydrogeological and hydrochemical investigations were conducted in the GAS in Brazil in order to construct a high-resolution aquifer analog model consisting of three 2D vertical cross-sections of the size of Lx = 28 m and Ly = 7 m and two 2D lateral cross-sections of the size of Lz = 5.8 m and Ly = 7 m. The field investigations were carried out in an open-pit mine near the city of Descalvado (SP) to identify hydraulic properties and sedimentary Fe(III) content in the heterogeneous fluvial-aeolian deposits in the upper Pirambóia Formation. The results deliver a detailed insight into the heterogeneity of the fluvial-aeolian facies association in the upper Pirambóia Formation and provide for the first time a quantitative description of the spatial distribution of hydraulic parameters and sedimentary Fe(III) content in this formation. The study identifies five lithofacies and nine hydrofacies types and describes their spatial distribution and volumetric shares. A particularly relevant outcome of the aquifer analog study is the identification of the horizontally laminated to planar cross-stratified sands (hydrofacies *Sh/Sp,m1* = 1.38×10^{-3} m/s) as the most permeable unit within the examined facies association. This facies is also relatively well connected throughout the entire outcrop, and therefore can serve as preferential

groundwater flow path. Furthermore, the hydraulic investigations revealed higher average conductivity values (K = 2.74 × 10^{-4} m/s) than reported in existing studies for the entire Pirambóia Formation in São Paulo State. Reported K estimates a range from 3.47 × 10^{-5} m/s to 5.78 × 10^{-6} m/s with an average value of K = 2.89 × 10^{-5} m/s in Hirata et al. (2011) and K = 2.19 × 10^{-5} m/s in Araújo et al. (1999). The higher hydraulic conductivity observed in this study suggests higher aquifer vulnerability for areas in São Paulo State, where the fluvial-aeolian deposits of the upper part of the Pirambóia Formation crop out or surface close to the ground. One needs to emphasize that the results reveal more pronounced hydraulic conductivity contrasts compared to the reported values by Hirata et al. (2011) and Araújo et al. (1999), which implies that in the case of contamination this portion of the Pirambóia Formation is more complex to characterize and remediate. Although the presented aquifer analog was only utilized on a local scale it nevertheless provided valuable insight into the heterogeneities of the Pirambóia Formation, and helped to identify possible relevant hydrostratigraphic units. It contributes in particular to an advanced reservoir understanding of GAS segments where little or no site-specific data is available (e.g., for the confined areas).

The outcome of the hydrochemical investigations showed that sedimentary Fe(III) is heterogeneously distributed in the sediments of the upper Pirambóia Foramtion. The laboratory analyses revealed that only crystalline Fe(III) phases are present in the sediments and mainly at low concentrations for most hydrofacies types (< 5 mg Fe(III)/g sediment). Nevertheless, Fe(III) concentrations vary over nearly four orders of magnitude (0.08 – 57.47 mg Fe(III)/g sediment) and correlate inversely on log scale (R = -0.3) with hydraulic conductivity values. The highest concentrations are found in the low permeable facies types.

In the third chapter a 2D cross-section of the aquifer analog - developed in chapter 2 - was employed in a numerical reactive transport simulation. The simulated reaction network incorporates field condition dual heterogeneities (physical and chemical) and visualizes for the first

time the degradation and geochemical evolution during a hypothetical petroleum hydrocarbon contamination in the Guarani aquifer on the field scale. The focus of this study was on the heterogeneous distribution of sediment bound Fe(III) as a solid-phase electron acceptor and its role for the effectiveness of *in situ* bioremediation in the upper Pirambóia Formation of the Guarani aquifer. The results of the reactive transport simulations, assuming goethite as solid-phase electron acceptor, show only a minor impact of a homogeneous/average (scenario 1) versus a heterogeneous (scenario 2) ferric iron distribution on plume concentrations for the chosen set up. This can be attributed to the fact that the assumed solid-phase ferric iron concentrations are based on the weighted mean ($8 \times 10\text{-}5$ mol/L_{bulk}), which is close to the low values present in most parts of the outcrop. The results underscore how vital it is to assess the hydrofacies of immobile electron acceptors in order to gain reliable valuation of microbial natural attenuation potential in aquifers. More specifically, as presented in the case study, an inverse correlation between the hydraulic conductivity and solid-phase ferric iron concentrations implies that electron donor and solid-phase electron acceptor do not co-occur, and hence restricting the natural attenuation potential at the investigated site.

The studies presented in Chapter 2 and 3 provided new insights into the physical and chemical heterogeneities of the upper part of the Pirambóia Formation and demonstrate how the concept of the joint application of outcrop analog models and numerical tools offer a unique way to envision flow and contaminant migration patterns in the recharge zone of the Guarani aquifer, where the Pirambóia Formation potentially crops out. Current initiatives to support sustainable groundwater management of the GAS such as the management framework of the Strategic Action Program (SAP) initiated by the Project for Environmental Protection and Sustainable Development of the Guarani Aquifer System (PGAS) certainly beg for the implementation and development of such mathematical models, the technical capacity building and dissemination of knowledge (OAS, 2009). In this context the successful development

of an aquifer analog model and simulation of a case study as presented in chapter 2 and 3 directly benefit the understanding for an enhanced reservoir and significantly contribute for an integrated and sustainable use of the GAS.

Chapter 4 examines, the applicability of *in situ* biodegradation estimates based on CSIA data in heterogeneous porous aquifers as they were tested in a reactive transport experiment with five high-resolution aquifer analogs, all of them representing different depositional environments. As an outcome of this study, it reveals that dilution/dispersion is highly site-specific and undergoes significant spatiotemporal variations. It demonstrates that biodegradation estimates using the conventional Rayleigh equation not only shows a high degree of uncertainty but also it does not allow a prediction towards a systematic bias for a distinct depositional environment or aquifer type. Instead, the research shows that field-derived enrichment factors can provide reliable results for the accumulated extent of in-situ biodegradation if one correctly accounts for the degree of dilution/dispersion. However, the quantification of dilution/dispersion at a contaminated site creates a challenge since only a few compounds can be used as conservative tracers, such as chloride and bromide on landfill sites (Van Breukelen, 2007), or in some other cases also non-degrading organic compounds such as tetrachlorethene (Pooley et al., 2009), 1,2,3-trimethylbenzene (Wiedemeier et al., 1999) and 1,2,3,4-tetrahydronaphthalene (Blum et al., 2009). Conservative transport models can be used to quantify field-derived enrichment factors corrected for dilution (ε_{fcd}) and account for dilution/dispersion, but as stated by Mak et al. (2006) the best estimated ε_{fcd} does not depend on the degree of dilution but on the correct representation of aquifer heterogeneities. In fact, due to sparse data in typical field studies the reproduction of small-scale heterogeneities - those depicted by the high-resolution aquifer analogs - is strongly limited. An alternative to these constrictions provides the Rayleigh equation streamline

approach as proposed by Fischer et al. (2007) and Thullner et al. (2012). If a quantification of ε_{fcd} is not possible, their approach provides a laboratory derived from bulk enrichment factor for toluene. Using this method, one has to consider that the range of redox specific enrichment factors for toluene stays narrow, and therefore uncertainties related to the use of a bulk/average enrichment factor may be acceptable. For compounds with a bigger range of enrichment factors for different redox conditions, the uncertainties may increase, and as a result, limit the accurate determination of CISA based biodegradation estimates. However, the Rayleigh equation streamline approach assumes a constant ratio between dilution/dispersion and the degradation rates are not always fulfilled for aquifers similar to the presented analogs or determined source scenarios. Given these limitations, the Rayleigh equation seriously presents its own inadequate applicability. As illustrated by simulations of toluene evolution in the aquifer analogs, the local values for isotope fractionation strongly depends on small-scale heterogeneities, which are not captured by conventional monitoring. As a result, a correct quantification of CSIA based *in situ* biodegradation cannot be achieved without a high-resolution monitoring; in fact, it is likely to fail in common practice.

Overall, the three case studies undoubtedly demonstrate the usefulness and effectiveness of aquifer analogs in many aspects. The research shows that (1) the high-resolution quasi-three-dimensional aquifer analog helps to characterize the cm-scale hydrogeologically defined variability of the system in a segment of the recharge area of the GAS in São Paulo State, which in turn enhances the reservoir understanding as well as conceptual model development in general. Secondly (2), the determination of the sediment bound ferric iron content enables the assessment of the sedimentary oxidation capacity in the upper part of the Pirambóia Formation. It also allows simulating the transport and fate of a hypothetical toluene contamination under realistic field conditions, considering both, physical and chemical heterogeneities. Thirdly, (3) the simulations the evolution of carbon isotope signatures during

reactive transport of toluene in different aquifer analogs enables us to examine the applicability of the CSIA-based *in situ* biodegradation estimates in heterogeneous porous aquifers.

Based on the outcome of the presented work, future research should particularly address the extension of the 2D simulations of the constructed aquifer analog into 3D, which would include dual heterogeneities so that one could investigate flow and transport characteristics of those areas where twisting flow channels may enhance dilution (Stauffer, 2007) and reactive mixing. In terms of the applicability of CSIA, the magnitude of over- and underestimation under those conditions could be identified. Furthermore, the first construction and modelling of an aquifer analog from the GAS should initiate and foster similar studies of other stratigraphic units of the GAS. As a result, the implementation of mathematical models would further expand reservoir understanding, and significantly contribute to local and regional groundwater management as demanded by the SAP (OAS, 2009).

References

Abe, Y. and Hunkeler, D., 2006. Does the Rayleigh Equation apply to evaluate field isotope data in contaminant hydrogeology? Environmental Science and Technology, 40(5): 1588-1596.

ABGE, 1981. Ensaios de Permeabilidade em Solos: orientações para a sua execução no campo – 1ª, 4. Associação Brasileira de Geologica de Engenharia, São Paulo.

Aeppli, C., Berg, M., Cirpka, O.A., Holliger, C., Schwarzenbach, R.P. and Hofstetter, T.B., 2009. Influence of Mass-Transfer Limitations on Carbon Isotope Fractionation during Microbial Dechlorination of Trichloroethene. Environmental Science and Technology, 43(23): 8813-8820.

Allen-King, R., R. Halket, D. Gaylord, and M. Robin, 1998. Characterizing the heterogeneity and correlation of perchloroethene sorption and hydraulic conductivity using a facies based approach. Water Resources Research, 34(3): 385-396.

Allen-King, R.M., Divine, D.P., Robin, M.J.L., Alldredge, J.R. and Gaylord, D.R., 2006. Spatial distributions of perchloroethylene reactive transport parameters in the Borden Aquifer. Water Resources Research, 42(1): W01413.

Allen-King, R.M., Grathwohl, P. and Ball, W.P., 2002. New modeling paradigms for the sorption of hydrophobic organic chemicals to heterogeneous carbonaceous matter in soils, sediments, and rocks. Advances in Water Resources, 25(8–12): 985-1016.

Anderson, M.P., 1989. Hydrogeologic facies models to delineate large-scale spatial trends in glacial and glaciofluvial sediments. Geological Society of America Bulletin, 101(4): 501-511.

Anderson, M.P., Aiken, J.S., Webb, E.K. and Mickelson, D.M., 1999. Sedimentology and hydrogeology of two braided stream deposits. Sedimentary Geology, 129(3-4): 187-199.

Anneser, B., Einsiedl, F., Meckenstock, R.U., Richters, L., Wisotzky, F. and Griebler, C., 2008. High-resolution monitoring of biogeochemical gradients in a tar oil-contaminated aquifer. Applied Geochemistry, 23(6): 1715-1730.

Anneser, B., Pilloni, G., Bayer, A., Lueders, T., Griebler, C., Einsiedl, F. and Richters, L., 2010. High Resolution Analysis of Contaminated Aquifer Sediments and Groundwater—What Can be Learned in Terms of Natural Attenuation? Geomicrobiology Journal, 27(2): 130-142.

Appelo, C.A.J. and Postma, D., 2005. Geochemistry, groundwater and pollution. A.A. Balkema Publishers, Leiden, The Netherlands: Taylor &Francis Group plc.

Araújo, L.M., França, A.B. and Potter, P.E., 1999. Hydrogeology of the Mercosul aquifer system in the Paraná and Chaco-Paraná Basins, South America, and comparison with the Navajo-Nugget aquifer system, USA. Hydrogeology Journal, 7(3): 317-336.

Assine, M.L., Piranha, J.M. and Carneiro, C.D.R., 2004. Os paleodesertos Pirambóia e Botucatu. In: Mantesso-Neto, V., Batorelli, A., Carneiro, C.D.R., Brito-Neves,

B.B.(Eds.), Geologia do Continente Sul-Americano: Evolução da obra de Fernando Flávio Marques de Almeida. Editora Beca, São Paulo: 77-92.

ATSDR, 2000. Agency for toxic substances and disease registry. Toxicological profile for toluene. U.S. Public Health Service, U.S. department of health and human services, Atlanta, GA.

Atteia, O., Franceschi, M. and Dupuy, A., 2008. Validation of Reactive Model Assumptions with Isotope Data: Application to the Dover Case. Environmental Science and Technology, 42(9): 3289-3295.

Bauer, R.D., Rolle, M., Bauer, S., Eberhardt, C., Grathwohl, P., Kolditz, O., Meckenstock, R.U. and Griebler, C., 2009. Enhanced biodegradation by hydraulic heterogeneities in petroleum hydrocarbon plumes. Journal of Contaminant Hydrology, 105(1–2): 56-68.

Bayer, P., Huggenberger, P., Renard, P. and Comunian, A., 2011. Three-dimensional high resolution fluvio-glacial aquifer analog: Part 1: Field study. Journal of Hydrology, 405(1-2): 1-9.

Bersezio, R., 2007. Aquifer Analogues. Mem. Descr. Carta Geol. d'It.: 39-50.

Bersezio, R., Bini, A. and Giudici, M., 1999. Effects of sedimentary heterogeneity on groundwater flow in a Quaternary pro-glacial delta environment: joining facies analysis and numerical modelling. Sedimentary Geology, 129(3-4): 327-344.

Bersezio, R., Felletti, F., Giudici, M., Miceli, A. and Zembo, I., 2007. Aquifer Analogues to Assist Modeling of Groundwater Flow: the Pleistocene Aquifer Complex of the Agri Valley (Basilicata). Mem. Descr. Carta Geol. d'It.: 51-66.

Bersezio, R., Pavia, F., Baio, M., Bini, A., Felletti, F. and Rodondi, C., 2004. Aquifer architecture of the Quaternary alluvial succession of the southern lambro basin (Lombardy-Italy). Quaternario, 17(2/1): 361-378.

Blum, P., Hunkeler, D., Weede, M., Beyer, C., Grathwohl, P. and Morasch, B., 2009. Quantification of biodegradation for o-xylene and naphthalene using first order decay models, Michaelis–Menten kinetics and stable carbon isotopes. Journal of Contaminant Hydrology, 105(3–4): 118-130.

BMBF, 2010. Bundesministerium für Bildung und Forschung. Science for Sustainability - The Potential for German - Brazilian Cooperation, Proceedings of the 1st German - Brazilian Conference on Research for Sustainability, São Paulo.

Bombach, P., Richnow, H., Kästner, M. and Fischer, A., 2010. Current approaches for the assessment of in situ biodegradation. Applied Microbiology and Biotechnology, 86(3): 839-852.

Bonneville, S., Behrends, T. and Van Cappellen, P., 2009. Solubility and dissimilatory reduction kinetics of iron(III) oxyhydroxides: A linear free energy relationship. Geochimica Cosmochimica Acta, 73(18): 5273-5282.

Bonotto, D., 2012. A comparative study of aquifer systems occurring at the Paraná sedimentary basin, Brazil: major hydrochemical trends. Environmental Earth Sciences, 67(8): 2285-2300.

Bonotto, D.M., 2013. A comparative study of aquifer systems occurring at the Paraná sedimentary basin, Brazil: U-isotopes contribution. Environmental Earth Sciences, 68(5): 1405-1418.

Bouchard, D., Höhener, P. and Hunkeler, D., 2008. Carbon Isotope Fractionation During Volatilization of Petroleum Hydrocarbons and Diffusion Across a Porous Medium: A Column Experiment. Environmental Science and Technology, 42(21): 7801-7806.

Braeckevelt, M., Fischer, A. and Kästner, M., 2012. Field applicability of Compound-Specific Isotope Analysis (CSIA) for characterization and quantification of in situ contaminant degradation in aquifers. Applied Microbiology and Biotechnology, 94(6): 1401-1421.

Caetano-Chang, M.R. and Wu, F.T., 2006. Arenitos flúvio-eólicos da porção superior da Formação Pirambóia no centro-leste paulista. Revista Brasileira de Geociências, 36(2): 296-304.

Cardenas, M.B. and Zlotnik, V.A., 2003. Three-dimensional model of modern channel bend deposits. Water Resources Research, 39(6): 1141.

Carrier, W.D., 2003. Goodbye, Hazen; Hello, Kozeny-Carman. Journal of Geotechnical and Geoenvironmental Engineering, 129(11): 1054-1056.

Childers, S.E., Ciufo, S. and Lovley, D.R., 2002. *Geobacter metallireducens* accesses insoluble Fe(III) oxide by chemotaxis. Nature, 416(6882): 767-769.

Christensen, T.H., Bjerg, P.L., Banwart, S.A., Jakobsen, R., Heron, G. and Albrechtsen, H.-J., 2000. Characterization of redox conditions in groundwater contaminant plumes. Journal of Contaminant Hydrology, 45(3–4): 165-241.

Cirpka, O.A., Frind, E.O. and Helmig, R., 1999. Numerical simulation of biodegradation controlled by transverse mixing. Journal of Contaminant Hydrology, 40(2): 159-182.

Comunian, A., Renard, P., Straubhaar, J. and Bayer, P., 2011. Three-dimensional high resolution fluvio-glacial aquifer analog – Part 2: Geostatistical modeling. Journal of Hydrology, 405(1-2): 10-23.

Cornell, R.M. and Schwertmann, U., 2003. The Iron Oxides: Structure, Properties, Reactions, Occurences and Uses. Wiley, Weinheim, Germany.

Cozzarelli, I.M., Bekins, B.A., Baedecker, M.J., Aiken, G.R., Eganhouse, R.P. and Tuccillo, M.E., 2001. Progression of natural attenuation processes at a crude-oil spill site: I. Geochemical evolution of the plume. Journal of Contaminant Hydrology, 53(3–4): 369-385.

Cunningham, J.A. and Fadel, Z.J., 2007. Contaminant degradation in physically and chemically heterogeneous aquifers. Journal of Contaminant Hydrology, 94(3-4): 293-304.

D'Affonseca, F.M., Blum, P., Finkel, M., Melzer, R. and Grathwohl, P., 2008. Field scale characterization and modeling of contaminant release from a coal tar source zone. Journal of Contaminant Hydrology, 102(1–2): 120-139.

D'Affonseca, F.M., Prommer, H., Finkel, M., Blum, P. and Grathwohl, P., 2011. Modeling the long-term and transient evolution of biogeochemical and isotopic signatures in coal tar-contaminated aquifers. Water Resoures Research, 47(5): W05518.

Dantas, A.D., Paschoalato, C.F.R., Martinez, M.S., Ballejo, R.R. and Di Bernardo, L., 2011. Removal of diuron and hexazinone from Guarany aquifer groundwater. Brazilian Journal of Chemical Engineering, 28(3): 415-424.

Dentz, M., Le Borgne, T., Englert, A. and Bijeljic, B., 2011. Mixing, spreading and reaction in heterogeneous media: A brief review. Journal of Contaminant Hydrology, 120–121(0): 1-17.

Dethlefsen, F., Bliss, F., Wachter, T. and Dahmke, A., 2004. Reaktive Tracer zur Bestimmung der sedimentären Aquifer-Oxidationskapazität im Labor- und Feldversuch. Grundwasser, 9(1): 12-20.

Dias, K.D.N. and Scherer, C.M.S., 2008. Cross-bedding set thickness and stratigraphic architecture of aeolian systems: An example from the Upper Permian Pirambóia Formation (Paraná Basin), southern Brazil. Journal of South American Earth Sciences, 25(3): 405-415.

DIN EN ISO 14688-1, 2002. Geotechnical Investigation and testing - Identification and classification of soil - Part 1: Identification and description (ISO 14688-1:2002); German version EN ISO 14688-1:2002.

Donatti, L.M., Sawakuchi, A.O., Giannini, P.C.F. and Fernandes, L.A., 2001. The Pirambóia-Botucatu Succession (Late Permian - Early Cretaceous, Paraná basin, São Paulo and Paraná states): Two contrasting eaolian systems. Academia Brasileira de Ciências, 73(3): 465.

Eckert, D., Qiu, S., Elsner, M. and Cirpka, O.A., 2013. Model complexity needed for quantitative analysis of high resolution isotope and concentration data from a toluene-pulse experiment. Environmental Science and Technology, 47(13): 6900-6907.

Eckert, D., Rolle, M. and Cirpka, O.A., 2012. Numerical simulation of isotope fractionation in steady-state bioreactive transport controlled by transverse mixing. Journal of Contaminant Hydrology, 140–141(0): 95-106.

Elsner, M., 2010. Stable isotope fractionation to investigate natural transformation mechanisms of organic contaminants: principles, prospects and limitations. Journal of Environmental Monitoring, 12(11): 2005-2031.

Elsner, M., Zwank, L., Hunkeler, D. and Schwarzenbach, R.P., 2005. A new concept linking observable stable isotope fractionation to transformation pathways of organic pollutants. Environmental Science and Technology, 39(18): 6896-6916.

Felletti, F., Bersezio, R. and Giudici, M., 2006. Geostatistical simulation and numerical upscaling, to model ground-water flow in a sandy-gravel, braided river, aquifer analogue. Journal of Sedimentary Research, 76(11-12): 1215-1229.

Fetter, C.W., 2001. Applied Hydrogeology. Prentice-Hall, Inc., New Jersey, 598 pp.

Fischer, A., Bauer, J., Meckenstock, R.U., Stichler, W., Griebler, C., Maloszewski, P., Kästner, M. and Richnow, H.H., 2006. A multitracer test proving the reliability of Rayleigh equation-based approach for assessing biodegradation in a BTEX contaminated aquifer. Environmental Science and Technology, 40(13): 4245-4252.

Fischer, A., Theuerkorn, K., Stelzer, N., Gehre, M., Thullner, M. and Richnow, H.H., 2007. Applicability of Stable Isotope Fractionation Analysis for the Characterization of Benzene Biodegradation in a BTEX-contaminated Aquifer. Environmental Science and Technology, 41(10): 3689-3696.

Flint, S.S. and Bryant, I.D., 1993. Quantitative clastic reservoir geological modelling; problems and perspectives. The Geological Modelling of Hydrocarbon Reservoirs and Outcrop Analogues. Special Publication of the International Association of Sedimentologists, 15: 3-20.

Foster, S., Hirata, R., Vidal, A., Schmidt, G. and Garduño, H., 2009. The Guaraní aquifer initiative - towards realistic groundwater management in a transboundary context, GW-MATE (The Groundwater Management Advisory Team) case profile collection No. 9; The World Bank. http://siteresources.worldbank.org/INTWAT/Resources/GWMATE_English_CP_09.pdf

Fure, A.D., Jawitz, J.W. and Annable, M.D., 2006. DNAPL source depletion: Linking architecture and flux response. Journal of Contaminant Hydrology, 85(3–4): 118-140.

Gastmans, D., Veroslavsky, G., Kiang Chang, H., Caetano-Chang, M.R. and Nogueira Pressinott, M.M., 2012. Modelo hidrogeológico conceptual del Sistema Acuífero Guaraní (SAG): una herramienta para la gestión. Boletín Geológico y Minero, 123(3): 249-265.

Goldemberg, J., Coelho, S.T. and Guardabassi, P., 2008. The sustainability of ethanol production from sugarcane. Energ Policy, 36(6): 2086-2097.

Grammer, M.G., Harris, P.M. and Eberli, G.P., 2004. Integration of outcrop and modern analogs in reservoir modeling. AAPG Memoir 80. American Association of Petroleum Geologist, Tulsa, Oklahoma.

Grathwohl, P., Rügner, H., Wöhling, T., Osenbrück, K., Schwientek, M., Gayler, S., Wollschläger, U., Selle, B., Pause, M., Delfs, J.-O., Grzeschik, M., Weller, U., Ivanov, M., Cirpka, O., Maier, U., Kuch, B., Nowak, W., Wulfmeyer, V., Warrach-Sagi, K., Streck, T., Attinger, S., Bilke, L., Dietrich, P., Fleckenstein, J., Kalbacher, T., Kolditz, O., Rink, K., Samaniego, L., Vogel, H.-J., Werban, U. and Teutsch, G., 2013. Catchments as reactors: a comprehensive approach for water fluxes and solute turnover. Environmental Earth Sciences, 69(2): 317-333.

Green, C.T., Böhlke, J.K., Bekins, B.A. and Phillips, S.P., 2010. Mixing effects on apparent reaction rates and isotope fractionation during denitrification in a heterogeneous aquifer. Water Resources Research, 46(8): W08525.

Griebler, C., Safinowski, M., Vieth, A., Richnow, H.H. and Meckenstock, R.U., 2004. Combined application of stable carbon isotope analysis and specific metabolites determination for assessing in situ degradation of aromatic hydrocarbons in a tar oil-contaminated aquifer. Environmental Science and Technology, 38(2): 617-631.

Halford, K.J. and Hanson, R.T., 2002. User Guide for the drawdown-limited, multi-node well (MNW) package for the U.S. Geological Survey's modular three-dimensional finite-difference ground-water flow model, versions MODFLOW-96 and MODFLOW-2000. USGS Open-File Report 00-293.

Harbaugh, A.W., Banta, E.R., Hill, M.C. and McDonald, M.G., 2000. MODFLOW-2000, The U.S. Geological Survey modular ground-water model - user guide to modularization concepts and the ground-water flow process. USGS Open-File Report 00-92.

Heinz, J., 2001. Sedimentary Geology of Glacial and Periglacial Gravel Bodies (SW-Germany): Dynamic Stratigraphy and Aquifer Sedimentology. PhD Thesis, Eberhard Karls Universität Tübingen, Tübingen (Germany), 102 pp.

Heinz, J. and Aigner, T., 2003. Hierarchical dynamic stratigraphy in various Quaternary gravel deposits, Rhine glacier area (SW Germany): implications for hydrostratigraphy. International Journal of Earth Sciences, 92: 923–938.

Heinz, J., Kleineidam, S., Teutsch, G. and Aigner, T., 2003. Heterogeneity patterns of Quaternary glaciofluvial gravel bodies (SW-Germany): application to hydrogeology. Sedimentary Geology, 158(1-2): 1-23.

Hirata, R., Gesicki, A., Sracek, O., Bertolo, R., Giannini, P.C. and Aravena, R., 2011. Relation between sedimentary framework and hydrogeology in the Guarani Aquifer System in São Paulo state, Brazil. Journal of South American Earth Sciences, 31(4): 444-456.

Höhener, P. and Atteia, O., 2010. Multidimensional analytical models for isotope ratios in groundwater pollutant plumes of organic contaminants undergoing different biodegradation kinetics. Advances in Water Resources, 33(7): 740-751.

Höhener, P. and Yu, X., 2012. Stable carbon and hydrogen isotope fractionation of dissolved organic groundwater pollutants by equilibrium sorption. Journal of Contaminant Hydrology, 129–130(0): 54-61.

Hornung, J. and Aigner, T., 1999. Reservoir and aquifer characterization of fluvial architectural elements: Stubensandstein, Upper Triassic, southwest Germany. Sedimentary Geology, 129(3–4): 215-280.

Höyng, D., D'Affonseca, F., Bayer, P., Oliveira, E., Perinotto, J., Reis, F., Weiß, H. and Grathwohl, P., 2014. High-resolution aquifer analog of fluvial–aeolian sediments of the Guarani aquifer system. Environmental Earth Sciences, 71(7): 3081-3094.

Huggenberger, P. and Aigner, T., 1999. Introduction to the special issue on aquifer-sedimentology: problems, perspectives and modern approaches. Sedimentary Geology, 129(3-4): 179-186.

ITRC, 2010. Use and measurement of mass flux and mass discharge. Interstate Technology & Regulatory Council, Washington, D.C, Integrated DNAPL Site Strategy Team.

Jakobsen, R. and Postma, D., 1999. Redox zoning, rates of sulfate reduction and interactions with Fe-reduction and methanogenesis in a shallow sandy aquifer, Rømø, Denmark. Geochimica et Cosmochimica Acta, 63(1): 137-151.

Kasenow, M., 2002. Determination of Hydraulic Conductivity from Grain Size Analysis. Water Resources Publications, Littleton, Colorado.

Kessler, T.C., Comunian, A., Oriani, F., Renard, P., Nilsson, B., Klint, K.E. and Bjerg, P.L., 2013. Modeling Fine-Scale Geological Heterogeneity—Examples of Sand Lenses in Tills. Groundwater, 51(5): 692-705.

Klingbeil, R., Kleineidam, S., Asprion, U., Aigner, T. and Teutsch, G., 1999. Relating lithofacies to hydrofacies: outcrop-based hydrogeological characterisation of Quaternary gravel deposits. Sedimentary Geology, 129(3-4): 299-310.

Koltermann, C.E. and Gorelick, S.M., 1996. Heterogeneity in Sedimentary Deposits: A Review of Structure-Imitating, Process-Imitating, and Descriptive Approaches. Water Resources Research, 32(9): 2617-2658.

Kopinke, F.D., Georgi, A., Voskamp, M. and Richnow, H.H., 2005. Carbon isotope fractionation of organic contaminants due to retardation on humic substances: Implications for natural attenuation studies in aquifers. Environmental Science and Technology, 39(16): 6052-6062.

Kostic, B., Becht, A. and Aigner, T., 2005. 3-D sedimentary architecture of a Quaternary gravel delta (SW-Germany): Implications for hydrostratigraphy. Sedimentary Geology, 181(3-4): 147-171.

Kuder, T., Philp, P. and Allen, J., 2009. Effects of Volatilization on Carbon and Hydrogen Isotope Ratios of MTBE. Environmental Science and Technology, 43(6): 1763-1768.

LaBolle, E.M., Fogg, G.E., Eweis, J.B., Gravner, J. and Leaist, D.G., 2008. Isotopic fractionation by diffusion in groundwater. Water Resources Research, 44(7): W07405.

Lago, A., Elis, V., Borges, W. and Penner, G., 2009. Geophysical investigation using resistivity and GPR methods: a case study of a lubricant oil waste disposal area in the city of Ribeirão Preto, São Paulo, Brazil. Environmental Geology, 58(2): 407-417.

Lovley, D., Coates, J.D., Blunt-Harris, E.L., Phillips, E.J.P. and Woodward, J.C., 1996. Humic substances as electron acceptors for microbial respiration. Nature, 382: 445-448.

Lyngkilde, J. and Christensen, T.H., 1992. Redox zones of a landfill leachate pollution plume (Vejen, Denmark). Journal of Contaminant Hydrology, 10(4): 273-289.

MacDonald, J.A., 2000. Peer reviewed: evaluating natural attenuation for groundwater cleanup. Environmental Science and Technology, 34(15): 346A-353A.

Maier, U., Becht, A., Kostic, B., Bürger, C., Bayer, P., Teutsch, G. and Dietrich, P., 2005. Characterisation of Quarterny gravel aquifers and their implementation in hydrogeolocigal models. IAHS Publication, 297: 159-168.

Maji, R. and Sudicky, E.A., 2008. Influence of mass transfer characteristics for DNAPL source depletion and contaminant flux in a highly characterized glaciofluvial aquifer. Journal of Contaminant Hydrology, 102(1-2): 105-119.

Mak, K.S., Griebler, C., Meckenstock, R.U., Liedl, R. and Peter, A., 2006. Combined application of conservative transport modelling and compound-specific carbon isotope analyses to assess in situ attenuation of benzene, toluene, and o-xylene. Journal of Contaminant Hydrology, 88(3–4): 306-320.

Marimon, M., Roisenberg, A., Viero, A., Oliveira Camargo, F. and Suhogusoff, A., 2013. Evaluation of the potential impact of fluorine-rich fertilizers on the Guarani Aquifer System, Rio Grande do Sul, Southern Brazil. Environmental Earth Sciences, 69(1): 77-84.

Meckenstock, R.U., Morasch, B., Griebler, C. and Richnow, H.H., 2004. Stable isotope fractionation analysis as a tool to monitor biodegradation in contaminated acquifers. Journal of Contaminant Hydrology, 75(3-4): 215-255.

Meckenstock, R.U., Morasch, B., Warthmann, R., Schink, B., Annweiler, E., Michaelis, W. and Richnow, H.H., 1999. 13C/12C isotope fractionation of aromatic hydrocarbons during microbial degradation. Environmental Microbiology, 1(5): 409-414.

Miall, A.D., 1978. Fluvial Sedimentology. In: A.D.e. Miall (Editor), Lithofacies types and vertical profile models in braided river deposits: a summary. Mem. Can. Soc. Petrol. Geol., pp. 597– 604.

Miall, A.D., 2010. The Geology of Fluvial Deposits: Sedimentary Facies, Basin Analysis, and Petroleum Geology, Springer.

Milani, E.J., Faccini, U.F., Scherer, C.M., Araujo, L.M. and Cupertino, J.A., 1998. Sequences and stratigraphic hierarchy of the Paraná basin (Ordovician to Cretaceous), Southern Brazil. Boletim IG USP, Série Científica, 29: 126-173.

Morales, N., D'Affonseca, F.M. and Perinotto, J.A.J., 1997. Utilização de ortofotografia terrestre em geologia, exemplificada pelo estudo de afloramentos da formação Tatuí. VII Simpósio de quantificação em geociências, Rio Claro (SP).

Morasch, B., Richnow, H.H., Schink, B., Vieth, A. and Meckenstock, R.U., 2002. Carbon and hydrogen stable isotope fractionation during aerobic bacterial degradation of aromatic hydrocarbons. Applied and Environmental Microbiology, 68: 5191-5194.

Nevin, K.P. and Lovley, D., 2002. Mechanisms for accessing insoluble Fe(III) oxide during dissimilatory Fe(III) reduction by Geothrix fermentans. Applied and Environmental Microbiology, 68(5).

OAS, 2009. Organization of American States, Guarani Aquifer: strategic action program = Acuífero Guaraní: programa estatégico de acción.– Bilingual edition.– Brazil; Argentina; Paraguay; Uruguay. p. 224.

Oliveira, E.G., 2000. Hidrogeoquímica aplicada na avaliação do impacto ambiental em áreas de lavra de areia. Ph.D. Thesis Thesis, University of São Paulo State (UNESP), Rio Claro.

Parker, B.L., Chapman, S.W. and Guilbeault, M.A., 2008. Plume persistence caused by back diffusion from thin clay layers in a sand aquifer following TCE source-zone hydraulic isolation. Journal of Contaminant Hydrology, 102(1-2): 86-104.

Parkhurst, D.L. and Appelo, C.A.J., 1999. User's guide to PHREEQC – A computer program for speciation, reaction-path, 1D-transport, and inverse geochemical calculations, Technical Report 99-4259, US Geol. Survey Water-Resources Investigations Report, 1999.

Poeter, E. and Gaylord, D.R., 1990. Influence of Aquifer Heterogeneity on Contaminant Transport at the Hanford Site. Ground Water, 28(6): 900-909.

Pooley, K.E., Blessing, M., Schmidt, T.C., Haderlein, S.B., MacQuarrie, K.T.B. and Prommer, H., 2009. Aerobic biodegradation of chlorinated ethenes in a fractured bedrock aquifer: Quantitative assessment by compound-specific isotope analysis (CSIA) and reactive transport modeling. Environmental Science and Technology, 43(19): 7458-7464.

Pringle, J.K., Howell, J.A., Hodgetts, D., Westerman, A.R. and Hodgson, D.M., 2006. Virtual outcrop models of petroleum reservoir analogues: a review of the current state-of-the-art. First Break, 24: 33-42.

Prommer, H., Anneser, B., Rolle, M., Einsiedl, F. and Griebler, C., 2009. Biogeochemical and isotopic gradients in a BTEX/PAH contaminant plume: Model-based interpretation of a high-resolution field data set. Environmental Science and Technology, 43(21): 8206-8212.

Prommer, H., Barry, D.A. and Zheng, C., 2003a. MODFLOW/MT3DMS-based reactive multicomponent transport modeling. Ground Water, 41(2): 247-257.

Prommer, H., Davis, G.B., Barry, D.A. and Miller, C.T., 2003b. Modelling the fate of petroleum hydrocarbons in groundwater. Proceedings of the Fifth National Workshop on the Assessment of Site Contamination,13-15 May 2002, Adelaide,, Australian Environmental Protection and Heritage Council (EPHC) incorporating the National Environmental Protection Council (NEPC): 21-45.

Puri, S., Appelgren, B., Arnold, G., Aureli, A., Burchi, S., Burke, J., Margat, J. and Pallas, P., 2001. Internationally shared (transboundary) aquifer resources management, their significance and sustainable management: a framework document. IHP-VI, Int. Hydrol. Program, Non Ser. Publ. Hydrol. 40. Paris: UNESCO.

Qiu, S., Eckert, D., Cirpka, O.A., Huenniger, M., Knappett, P., Maloszewski, P., Meckenstock, R.U., Griebler, C. and Elsner, M., 2013. Direct experimental evidence of

non-first order degradation kinetics and sorption-induced isotopic fractionation in a mesoscale aquifer: 13C/12C analysis of a transient toluene pulse. Environmental Science and Technology, 47(13): 6892-6899.

Rabelo, J. and Wendland, E., 2009. Assessment of groundwater recharge and water fluxes of the Guarani Aquifer System, Brazil. Hydrogeology Journal, 17(7): 1733-1748.

Ritzi, R.W., Huang, L., Ramanathan, R. and Allen-King, R.M., 2013. Horizontal spatial correlation of hydraulic and reactive transport parameters as related to hierarchical sedimentary architecture at the Borden research site. Water Resources Research, 49(4): 1901-1913.

Rolle, M., Chiogna, G., Bauer, R., Griebler, C. and Grathwohl, P., 2010. Isotopic fractionation by transverse dispersion: Flow-through microcosms and reactive transport modeling study. Environmental Science and Technology, 44(16): 6167-6173.

Rolle, M., Chiogna, G., Hochstetler, D.L. and Kitanidis, P.K., 2013. On the importance of diffusion and compound-specific mixing for groundwater transport: An investigation from pore to field scale. Journal of Contaminant Hydrology, 153(0): 51-68.

Rolle, M., Eberhardt, C., Chiogna, G., Cirpka, O.A. and Grathwohl, P., 2009. Enhancement of dilution and transverse reactive mixing in porous media: Experiments and model-based interpretation. Journal of Contaminant Hydrology, 110(3–4): 130-142.

Ronen, D., Sorek, S. and Gilron, J., 2012. Rationales Behind Irrationality of Decision Making in Groundwater Quality Management. Ground Water, 50(1): 27-36.

Scheibe, T.D., Fang, Y., Murray, C.J., Roden, E.E., Chen, J., Chien, Y.-J., Brooks, S.C. and Hubbard, S.S., 2006. Transport and biogeochemical reaction of metals in a physically and chemically heterogeneous aquifer. Geosphere, 2(4): 220-235.

Schmidt, G. and Vassolo, S., 2011. Untersuchungen zu einem der größten Grundwasservorkommen Südamerikas: Der Guaraní-Aquifer in Paraguay. Grundwasser, 16(3): 187-194.

Soares, A.P., Soares, P.C. and Holz, M., 2008. Heterogeneidades hidroestratigráficas no Sistema Aqüífero Guarani. Revista Brasileira de Geociências, 38(4): 598-617.

Stauffer, F., 2007. Impact of highly permeable sediment units with inclined bedding on solute transport in aquifers. Advances in Water Resources, 30(11): 2194-2201.

Stookey, L.L., 1970. Ferrozine - a new spectrophotometric reagent for iron. Analytical Chemistry, 42(7): 779-781.

Stumm, W. and Morgan, J.J., 1996. Aquatic Chemistry. John Wiley & Sons Inc, New York.

Sweet, M.L., Blewden, C.J., Carter, A.M. and Mills, C.A., 1996. Modeling Heterogeneity in a Low-Permeability Gas Reservoir Using Geostatistical Techniques, Hyde Field, Southern North Sea. AAPG Bulletin, 80(11): 1719-1735.

Thullner, M., Centler, F., Richnow, H.-H. and Fischer, A., 2012. Quantification of organic pollutant degradation in contaminated aquifers using compound specific stable isotope analysis – Review of recent developments. Organic Geochemistry, 42(12): 1440-1460.

Thullner, M., Fischer, A., Richnow, H.-H. and Wick, L., 2013. Influence of mass transfer on stable isotope fractionation. Applied Microbiology and Biotechnology, 97(2): 441-452.

Tuccillo, M.E., Cozzarelli, I.M. and Herman, J.S., 1999. Iron reduction in the sediments of a hydrocarbon-contaminated aquifer. Applied Geochemistry, 14(5): 655-667.

UN, 2009. The 3rd United Nations World Water Development Report: Water in Changing World, United Nations, p. 349.

USEPA, 2004. U.S. Environmental Protection Agency. How to evaluate alternative cleanup technologies for underground storage tank sites: A guide for corrective action plan reviewers. Chapter IX: Monitored Natural Attentuation. EPA report 510-R-04-002,Washington, DC.

USEPA, 2008. A Guide for Assessing Biodegradation and Source Identification of Organic Ground Water Contaminants using Compound Specific Isotope Analysis (CSIA). EPA 600/R-08/148, National Risk Management Research Laboratory, Ada, Oklahoma, USA.

Van Breukelen, B.M., 2007. Quantifying the degradation and dilution contribution to natural attenuation of contaminants by means of an open system Rayleigh equation. Environmental Science and Technology, 41(14): 4980-4985.

Van Breukelen, B.M., Hunkeler, D. and Volkering, F., 2005. Quantification of sequential chlorinated ethene degradation by use of a reactive transport model incorporating isotope fractionation. Environmental Science and Technology, 39(11): 4189-4197.

Van Breukelen, B.M. and Prommer, H., 2008. Beyond the Rayleigh Equation: Reactive Transport Modeling of Isotope Fractionation Effects to Improve Quantification of Biodegradation. Environmental Science and Technology, 42(7): 2457-2463.

Van Breukelen, B.M. and Rolle, M., 2012. Transverse Hydrodynamic Dispersion Effects on Isotope Signals in Groundwater Chlorinated Solvents' Plumes. Environmental Science and Technology, 46(14): 7700-7708.

Van Keer, I., Bronders, J., Verhack, J., Schwarzbauer, J. and Swennen, R., 2012. Limitations in the use of compound-specific stable isotope analysis to understand the behaviour of a complex BTEX groundwater contamination near Brussels (Belgium). Environmental Earth Sciences, 66(2): 457-470.

Vencelides, Z., Sracek, O. and Prommer, H., 2007. Modelling of iron cycling and its impact on the electron balance at a petroleum hydrocarbon contaminated site in Hnevice, Czech Republic. Journal of Contaminant Hydrology, 89(3–4): 270-294.

Vogt, C., Cyrus, E., Herklotz, I., Schlosser, D., Bahr, A., Herrmann, S., Richnow, H.-H. and Fischer, A., 2008. Evaluation of Toluene Degradation Pathways by Two-Dimensional Stable Isotope Fractionation. Environmental Science and Technology, 42(21): 7793-7800.

Vukovic, M. and Soro, A., 1992. Determination of Hydraulic Conductivity of Porous Media from Grain-size Composition. Water Resources Publications, Littleton, Colorado.

Weber, K.A., Achenbach, L.A. and Coates, J.D., 2006. Microorganisms pumping iron: anaerobic microbial iron oxidation and reduction. Nature Reviews Microbiology, 4(10): 752-764.

Weissmann, G.S., Carle, S.F. and Fogg, G.E., 1999. Three-dimensional hydrofacies modeling based on soil surveys and transition probability geostatistics. Water Resources Research, 35(6): 1761-1770.

Weissmann, G.S. and Fogg, G.E., 1999. Multi-scale alluvial fan heterogeneity modeled with transition probability geostatistics in a sequence stratigraphic framework. Journal of Hydrology, 226(1–2): 48-65.

Wendland, E., Barreto, C. and Gomes, L.H., 2007. Water balance in the Guarani Aquifer outcrop zone based on hydrogeologic monitoring. Journal of Hydrology, 342(3-4): 261-269.

Werth, C.J., Cirpka, O.A. and Grathwohl, P., 2006. Enhanced mixing and reaction through flow focusing in heterogeneous porous media. Water Resources Research, 42(12): W12414.

Whittaker, J. and Teutsch, G., 1999. Numerical simulation of subsurface characterization methods: application to a natural aquifer analogue. Advances in Water Resources, 22(8): 819-829.

Wiedemeier, T.H., Rifai, H.S., Newell, C.J. and Wilson, J.T., 1999. Natural Attenuation of Fuels and Chlorinated Solvents in the Subsurface. John Wiley and Sons, New York.

Wolf, A.T., 2007. Shared Waters: Conflict and Cooperation. Annual Review of Environment and Resources, 32(1): 241-269.

Zappa, G., Bersezio, R., Felletti, F. and Giudici, M., 2006. Modeling heterogeneity of gravel-sand, braided stream, alluvial aquifers at the facies scale. Journal of Hydrology, 325(1-4): 134-153.

Zheng, C. and Wang, P.P., 1999. MT3DMS: A modular three-dimensional multispecies transport model for simulation of advection, dispersion, and chemical reactions of contaminants in groundwater systems; documentation and user's guide. Report SERDP-99-1, Vicksburg, MS.

Zuquette, L., Palma, J. and Pejon, O., 2009. Methodology to assess groundwater pollution conditions (current and pre-disposition) in the São Carlos and Ribeirão Preto regions, Brazil. Bulletin of Engineering Geology and the Environment, 68(1): 117-136.

Acknowledgements

First and foremost, I would like to express my explicit gratitude to my supervisors Prof. Dr. Peter Grathwohl (University Tübingen), Prof. Dr. Holger Weiß (Centre for Environmental Research - UFZ Leipzig), Dr. Fernando Mazo D´Affonseca (University Tübingen) and Dr. Peter Bayer (ETH Zurich), who provided excellent support and expert guidance throughout the years to successfully accomplish my dissertation. I greatly appreciate the helpful scientific discussions with Prof. Dr. Henning Prommer (CSIRO Land and Water) and thoughtful review of the third chapter of this work. I am also indebted to Jun.- Prof. Dr. habil. Philipp Blum (KIT) for his support, ideas and cooperativeness.

I wish to express my sincere thanks to the board of examiners members Prof. Dr. Peter Grathwohl, Prof. Dr. Holger Weiß, Prof. Dr. Christian Zwiener, and Dr. Massimo Rolle.

Special recognition is given to the Institute of Geosciences of the São Paulo State Univeristy (UNESP) in Rio Claro (Brazil) for the bilateral cooperation and in particular to Prof. Dr. José Alexandre J. Perinotto and Prof. Dr. Fábio Reis for their support and assistance during my research stay in Rio Claro. A special thanks goes to Prof. Dr. Edson Gomes de Oliveira († 2013) for his unconditional support, encouragement and helpful ideas during the field- and laboratory work in Rio Claro. I would like to thank Prof. Dr. Andreas Kappler for the opportunity and assistance to conduct iron extraction analysis at his laboratory.

I would like to further gratefully acknowledge all members of the Department of Geosciences of the University of Tübingen and the great working atmosphere, especially Dr. Wolfgang Bott, Dr. Peter Merkel and Monika Jekelius for their help in all administration matters.

In the end I must thank my family and friends who continuously supported me in any regard during the last years.

The research funding for this work comes from the German Federal Ministry for Education and Research (BMBF) scholarship program for International Postgraduate Studies in Water Technologies (IPSWaT) and is gratefully acknowledged.

Ergänzungsblatt zur Eigenleistung

Erklärung über den Rahmen gemeinschaftlicher Arbeit:

Das Kapitel 2 der Dissertation enthält Anteile von gemeinschaftlicher Arbeit.
Die Eigenanteile des Kandidaten für Kapitel 2 sind in Prozent (%) in folgender Tabelle angegeben:

Idee und Fragenstellung	Planung, Organisation (Brasilien)	Geländearbeit (Brasilien)	Laborarbeit (I): Unesp (Brasilien)	Laborarbeit (II): Uni Tübingen	Auswertung, Interpretation	Kapitel-erstellung
70	90	95	95	100	90	100

Folgende Personen haben folgende Anteile in Prozent (%) am Kapitel 2:

Mitarbeiter	Idee, Fragen-stellung	Planung, Organisation (Brasilien)	Geländearbeit (Brasilien)	Laborarbeit (I): Unesp (Brasilien)	Auswertung, Interpretation
Dr. F. Mazo D´Affonseca	10	5			2,5
Dr. P. Bayer	10				2,5
Prof. Dr. F. Reis		2,5	2,5		
Prof. Dr. A. Perinotto		2,5			2,5
Prof. Dr. E. Gomes			2,5	5	2,5
Prof. Dr. H. Weiß	5				
Prof. Dr. P. Grathwohl	5				

Der Kandidat hat Teilergebnisse der Dissertation in folgendem Fachartikel veröffentlicht:
Höyng, D., D´Affonseca F.M., Bayer, P., de Oliveira, E.G., Perinotto, J.A.J., Reis, F., Weiß, H., Grathwohl, P. (2014), High-resolution aquifer analog of fluvial-aeolian sediments of the Guarani aquifer system. *Environmental Earth Sciences*, 71: 3081-3094.

Appendix A: 3D realization of the aquifer analog

This appendix provides an explanation of the file format and the files (attached on CD-ROM) which were used for the generation of a three-dimensional realization of the aquifer analog.

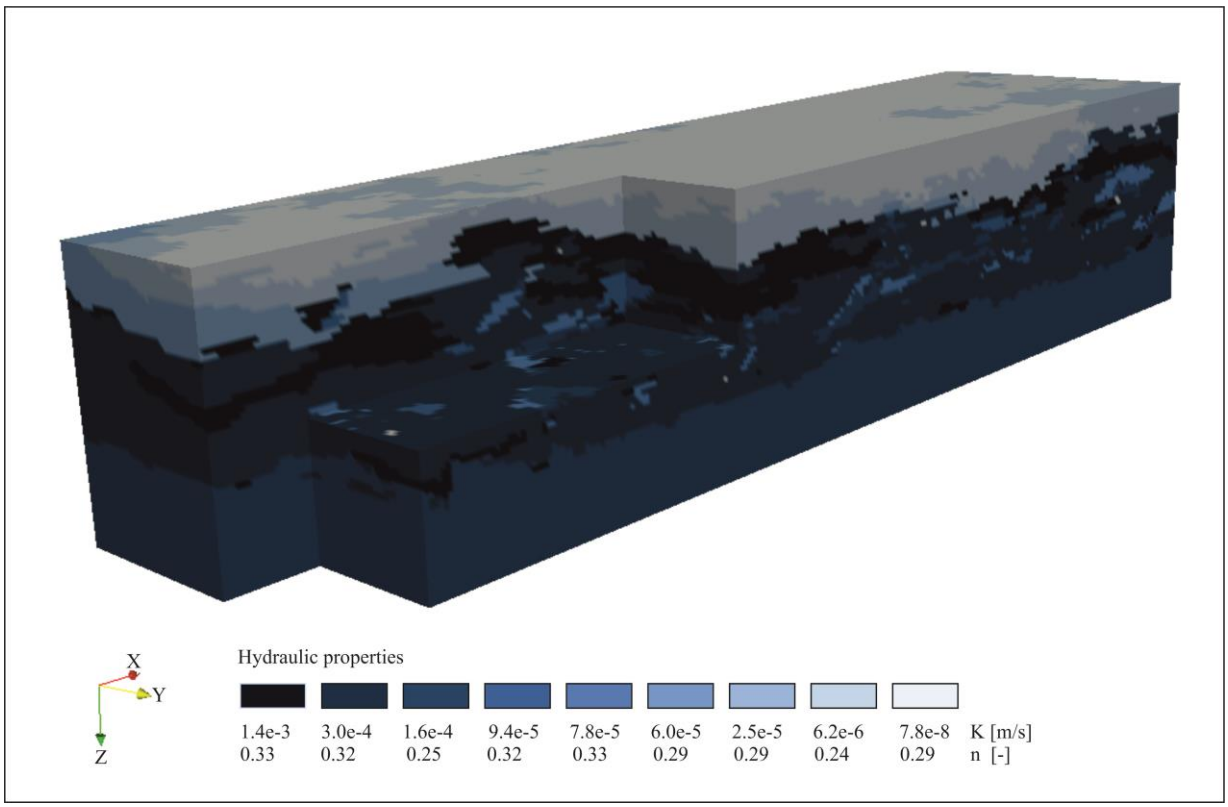

3D realization of the aquifer analog obtained from one multiple-point simulation.

Outcrop analog profiles

Three vertical (x = 28 m, z = 5.8 m) and two lateral (y = 7 m, z = 5.8 m) outcrop analog profiles were discretized to a grid size of 0.1 m. They provide the digitalized hydrofacies distribution as presented in Figure 2.6. The profiles 1, 2 and 3 (*profile_1.txt, profile_2.txt, profile_3.txt*) refer to the sections A-A´, B-B´and C-C´ (Figure 2.5, Figure 2.6). The lateral profiles (*profile_left.txt, profile_right.txt*) refer to the sections A-C and A´-C´ (Figure 2.5).

The profile files (ASCII format) contain integers from 1-9 for the nine different hydrofacies types. The corresponding hydraulic properties (*K*, *n*) are listed in the file *hydr_prop_code.txt*.

3D realization and visualization

The three vertical (XZ) and two lateral (YZ) 2D outcrop analog profiles were used as training images for one 3D multiple-point simulation. No conditioning data is considered and the z location is used as an auxiliary variable describing the non-stationarity. The realization is saved in a VTK structured grid format (*realization01.vtk*). The header of the VTK file contains information about the dimension, origin, spacing (resolution) and total number of point data. The point data are written successively. They fill the index along x-axis, along the y-axis, and then along the z-axis. Detailed information about the VTK file format can be found in the VTK User´s Guide[1]. The code in the VTK file corresponds to the same code for the hydraulic properties as in the outcrop profile files. The VTK file can be open with the open-source visualization application Paraview[2].

References:

[1]VTK file formats (for VTK Version 4.2, taken from the VTK User's Guide, Kitware, Inc.) www.vtk.org/VTK/img/file-formats.pdf

[2]Paraview, an open-source, multi-platform data analysis and visualization application. http://www.paraview.org/

Appendix B: Springer License Terms and Conditions

This is a License Agreement between Dominik Höyng ("You") and Springer ("Springer") provided by Copyright Clearance Center ("CCC"). The license consists of your order details, the terms and conditions provided by Springer, and the payment terms and conditions.

All payments must be made in full to CCC. For payment instructions, please see information listed at the bottom of this form.

License Number	3364750203783
License date	Apr 09, 2014
Licensed content publisher	Springer
Licensed content publication	Environmental Earth Sciences
Licensed content title	High-resolution aquifer analog of fluvial–aeolian sediments of the Guarani aquifer system
Licensed content author	Dominik Höyng
Licensed content date	Jan 1, 2013
Volume number	71
Issue number	7
Type of Use	Thesis/Dissertation
Portion	Full text
Number of copies	15
Author of this Springer article	Yes and you are the sole author of the new work
Order reference number	
Title of your thesis / dissertation	Development and modeling of a high-resolution aquifer analog in the Guarani Aquifer (Brazil)
Expected completion date	Apr 2014
Estimated size(pages)	120
Total	0.00 USD

Terms and Conditions

Introduction

The publisher for this copyrighted material is Springer Science + Business Media. By clicking "accept" in connection with completing this licensing transaction, you agree that the following terms and conditions apply to this transaction (along with the Billing and Payment terms and conditions established by Copyright Clearance Center, Inc. ("CCC"), at the time that you opened your Rightslink account and that are available at any time at http://myaccount.copyright.com).

Limited License

With reference to your request to reprint in your thesis material on which Springer Science and Business Media control the copyright, permission is granted, free of charge, for the use

indicated in your enquiry.

Licenses are for one-time use only with a maximum distribution equal to the number that you identified in the licensing process.

This License includes use in an electronic form, provided its password protected or on the university's intranet or repository, including UMI (according to the definition at the Sherpa website: http://www.sherpa.ac.uk/romeo/). For any other electronic use, please contact Springer at (permissions.dordrecht@springer.com or permissions.heidelberg@springer.com).

The material can only be used for the purpose of defending your thesis, and with a maximum of 100 extra copies in paper.

Although Springer holds copyright to the material and is entitled to negotiate on rights, this license is only valid, subject to a courtesy information to the author (address is given with the article/chapter) and provided it concerns original material which does not carry references to other sources (if material in question appears with credit to another source, authorization from that source is required as well).

Permission free of charge on this occasion does not prejudice any rights we might have to charge for reproduction of our copyrighted material in the future.

Altering/Modifying Material: Not Permitted
You may not alter or modify the material in any manner. Abbreviations, additions, deletions and/or any other alterations shall be made only with prior written authorization of the author(s) and/or Springer Science + Business Media. (Please contact Springer at (permissions.dordrecht@springer.com or permissions.heidelberg@springer.com)

Reservation of Rights
Springer Science + Business Media reserves all rights not specifically granted in the combination of (i) the license details provided by you and accepted in the course of this licensing transaction, (ii) these terms and conditions and (iii) CCC's Billing and Payment terms and conditions.

Copyright Notice:Disclaimer
You must include the following copyright and permission notice in connection with any reproduction of the licensed material: "Springer and the original publisher /journal title, volume, year of publication, page, chapter/article title, name(s) of author(s), figure number(s), original copyright notice) is given to the publication in which the material was originally published, by adding; with kind permission from Springer Science and Business Media"

Warranties: None

Example 1: Springer Science + Business Media makes no representations or warranties with respect to the licensed material.

Example 2: Springer Science + Business Media makes no representations or warranties with

respect to the licensed material and adopts on its own behalf the limitations and disclaimers established by CCC on its behalf in its Billing and Payment terms and conditions for this licensing transaction.

Indemnity
You hereby indemnify and agree to hold harmless Springer Science + Business Media and CCC, and their respective officers, directors, employees and agents, from and against any and all claims arising out of your use of the licensed material other than as specifically authorized pursuant to this license.

No Transfer of License
This license is personal to you and may not be sublicensed, assigned, or transferred by you to any other person without Springer Science + Business Media's written permission.

No Amendment Except in Writing
This license may not be amended except in a writing signed by both parties (or, in the case of Springer Science + Business Media, by CCC on Springer Science + Business Media's behalf).

Objection to Contrary Terms
Springer Science + Business Media hereby objects to any terms contained in any purchase order, acknowledgment, check endorsement or other writing prepared by you, which terms are inconsistent with these terms and conditions or CCC's Billing and Payment terms and conditions. These terms and conditions, together with CCC's Billing and Payment terms and conditions (which are incorporated herein), comprise the entire agreement between you and Springer Science + Business Media (and CCC) concerning this licensing transaction. In the event of any conflict between your obligations established by these terms and conditions and those established by CCC's Billing and Payment terms and conditions, these terms and conditions shall control.

Jurisdiction
All disputes that may arise in connection with this present License, or the breach thereof, shall be settled exclusively by arbitration, to be held in The Netherlands, in accordance with Dutch law, and to be conducted under the Rules of the 'Netherlands Arbitrage Instituut' (Netherlands Institute of Arbitration).*OR:*

All disputes that may arise in connection with this present License, or the breach thereof, shall be settled exclusively by arbitration, to be held in the Federal Republic of Germany, in accordance with German law.

Other terms and conditions:

v1.3
If you would like to pay for this license now, please remit this license along with your payment made payable to "COPYRIGHT CLEARANCE CENTER" otherwise you will be invoiced within 48 hours of the license date. Payment should be in the form of a check or money order referencing your account number and this invoice number RLNK501273819.

Once you receive your invoice for this order, you may pay your invoice by credit card. Please follow instructions provided at that time.

Make Payment To:
Copyright Clearance Center
Dept 001
P.O. Box 843006
Boston, MA 02284-3006

For suggestions or comments regarding this order, contact RightsLink Customer Support: customercare@copyright.com or +1-877-622-5543 (toll free in the US) or +1-978-646-2777.

Gratis licenses (referencing $0 in the Total field) are free. Please retain this printable license for your reference. No payment is required.